JOURNAL OF THE AMERICAN CERAMIC SOCIETY

RECEIVED
OCT 6 1933

A MONTHLY JOURNAL DEVOTED TO THE ARTS AND SCIENCES RELATED TO THE SILICATE INDUSTRIES

VOLUME 16 OCTOBER 1933 NUMBER 10

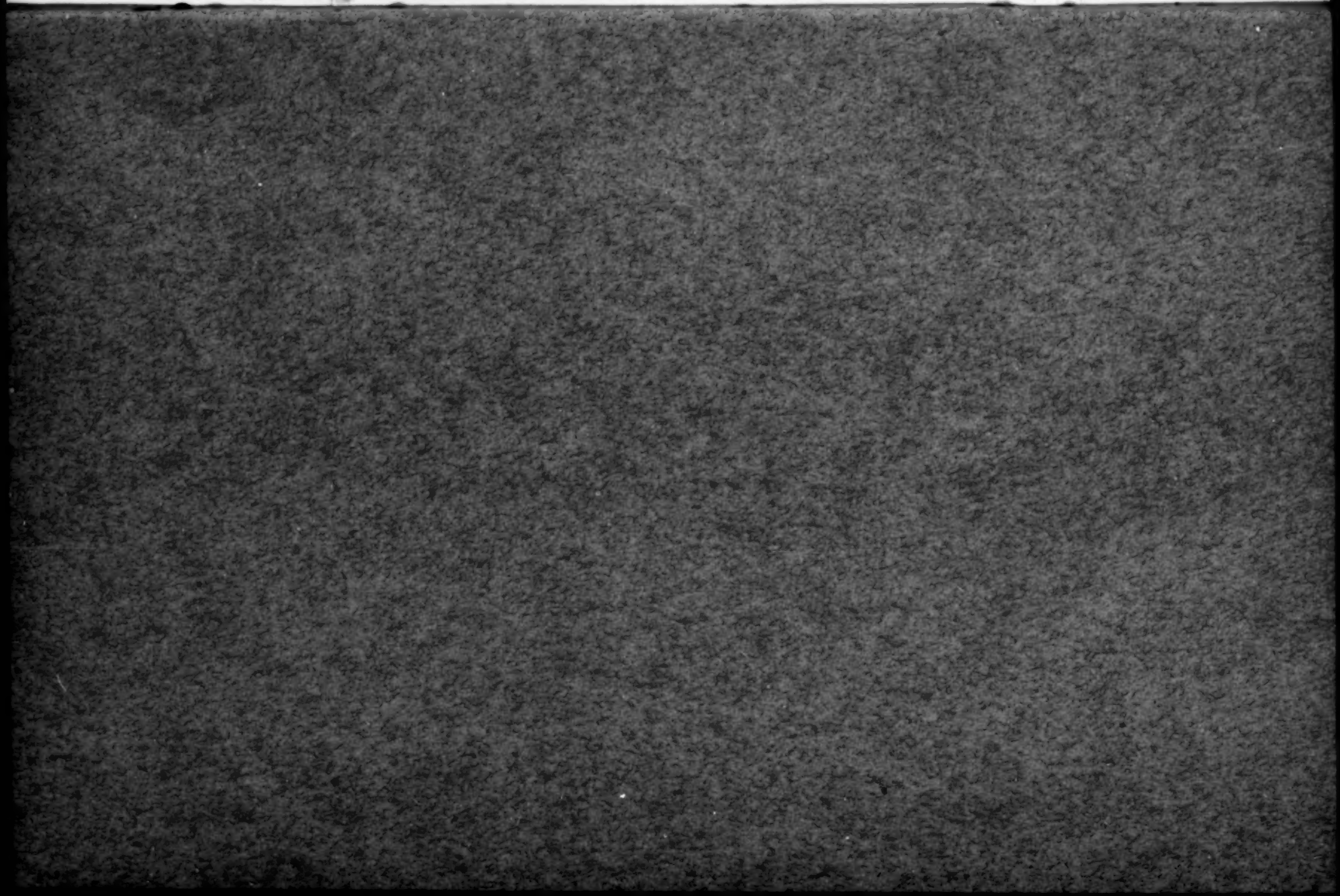

A COMPILATION OF PHASE-RULE DIAGRAMS OF INTEREST TO THE CERAMIST AND SILICATE TECHNOLOGIST

By F. P. Hall and Herbert Insley

Issued as the October, 1933, number of *The Journal of the American Ceramic Society*

Publication Office: 20th & Northampton Sts., Easton, Pa.
Editorial and Advertising Offices: 2525 N. High St., Columbus, Ohio.
Executive Office: 2525 N. High St., Columbus, Ohio.
Committee on Publications: L. Navias, *Chairman;* L. J. Trostel, M. F. Beecher, R. M. King, Ross C. Purdy.
Entered as second-class matter at the post office at Easton, Pa., under the Act of March 3, 1879.
(*Copyright 1933, American Ceramic Society*)
Subscription twelve dollars a year. Single numbers one dollar
(*Foreign and Canadian postage, 50c additional on subscriptions*)

Table of Contents

	Page
I. Introduction	463
II. General Discussion of Phase-Rule Diagrams	463
(A) Definitions	463
(B) Methods for the Study of High-Temperature Heterogeneous Equilibrium	465
(1) Cooling Curves	465
(2) Heating Curves Combined with Optical Examination	466
(3) Quenching Method	466
(4) Cone Deformation Method	467
(C) One-Component Systems	467
(D) Two-Component Systems	468
(1) Two-Component Systems without Solid Solutions	468
(*a*) Isoplethal Studies	468
(*b*) Isothermal Studies	470
(2) Two-Component Systems with Compounds Present	471
(3) Two-Component Systems with Solid Solutions Present	471
(*a*) A Single Solid Solution	471
(*b*) Two Solid Solutions Present	472
(4) Two-Component Systems with Two Liquid Phases	472
(E) Three-Component Systems	473
(1) Three-Component Systems without Solid Solution	473
(*a*) Three-Component Systems without Solid Solutions	474
(*b*) Crystallization in Ternary Systems without Solid Solutions	475
(*c*) Summary Relating to Crystallization within Ternary Systems Not Containing Solid Solutions	479
(2) Three-Component Systems with Solid Solutions	480
(*a*) Methods of Determination of the Three-Phase Boundaries	484
III. Comments on Diagrams	485
IV. List of Diagrams	459
Part I. General Diagrams	467–84
Part II. Specific Diagrams	
(1) One-Component System (SiO_2)	486–87
(2) Two-Component Systems	
(*a*) Both Components Simple Oxides	487–98
(*b*) One Simple Oxide and a Binary Compound of Two Oxides	499–501
(*c*) One Simple Oxide and a Ternary Compound	501–502
(*d*) Both Components Binary Compounds	502–504
(*e*) Two Ternary Compounds	505–508
(3) Three-Component Systems	
(*a*) All Components Simple Oxides	508–527
(*b*) One Component a Binary or Higher Compound	528–30
(4) Sections of Three-Component Systems	
(*a*) System K_2O–CaO–SiO_2	530–31
(*b*) System Na_2O–CaO–SiO_2	531–32
(*c*) System Na_2O–Fe_2O_3–SiO_2	532–34
(*d*) System CaO–MgO–SiO_2	534–37
(*e*) System CaO–Al_2O_3–Fe_2O_3	538
(*f*) System CaO–Al_2O_3–SiO_2	539–40
(5) Relation of Optical Properties to Chemical Composition	540–54
(6) Cone Deformation Diagrams	555–57
(7) Melting Diagrams	558–67

CONTRIBUTION ACKNOWLEDGMENTS

For the financing of this Compilation of Phase-Rule Diagrams the following contributions have been received:

The Fellows of the American Ceramic Society	$ 700
Pittsburgh Section	300
Baltimore-Washington Section	100
The Hartford-Empire Company	150
	$1250

LIST OF ILLUSTRATIONS

Part I. General Diagrams

Fig. 1.—Phase relations in a one-component system.

Fig. 2.—A two-component system without intermediate compounds or solid solutions.

Fig. 3.—Variations in relative amounts of liquid and solid phases.

Fig. 4.—Two-component systems with compounds present.

Fig. 5.—Complete solid solution without maximum or minimum in a binary system.

Fig. 6.—Binary systems with a single solid solution.

Fig. 7.—Vapor pressure of component *A* in solid and liquid phases.

Fig. 8— Solid solutions showing conjugate relationships.

Fig. 9.—Conjugate liquid phases.

Fig. 10.—Six typical cases of three-component systems.

Fig. 11.—Three-component system, CaO–Al_2O_3–SiO_2, showing boundary curves and composition lines.

Fig. 12.—The course of crystallization in a ternary system.

Fig. 13.—A ternary system with a binary compound of two components which does not form a binary system with the third component.

Fig. 14.—A ternary system containing a binary compound unstable at its melting point.

Fig. 15.—Recurrent crystallization in a ternary system.

Fig. 16.—Diagrams of a three-component system in which one of the binary systems has solid solutions.

Fig. 17.—Course of crystallization in a ternary system where one of the binary systems is a complete solid solution series.

Fig. 18.—A ternary system containing a binary compound of two components stable at its melting point which forms a complete series of solid solutions with the third component.

Fig. 19.—A ternary system containing a binary compound of two components unstable at its melting point which forms a series of solid solutions with the third component.

Fig. 20.—Determination of the position of the three-phase boundary.

Part II. Specific Diagrams*

(1) One-Component System (SiO_2)

Fig. 21.—Stability relations of silica minerals (McDowell).

Fig. 22.—Stability relations of silica minerals (Fenner).

Fig. 23.—Thermal expansion of quartz (Day, Sosman, and Hostetter).

---

* The major subdivisions with headings given below follow, in general, the arrangement used in the International Critical Tables. Within these subdivisions the systems and components are so arranged that an ascending valence order is followed from left to right and from top to bottom. Within a group of oxides having the same valence, an alphabetical arrangement is followed. Temperatures are given in degrees Centigrade and compositions in weight percentage unless otherwise stated on the individual diagrams.

(2) Two-Component Systems

(a) Both components simple oxides

Fig.

24 CaO–MgO
25 NaF–AlF_3
26 CaF_2–Al_2O_3
27 CaO–Al_2O_3
28 CaO–B_2O_3
29 MgO–αAl_2O_3
30 ZnO–Al_2O_3
31 Cr_2O_3–Al_2O_3
32 CaO–Fe_2O_3
33 K_2SiO_3–SiO_2
34 Li_2O–SiO_2
35 Na_2O–SiO_2
36 BaO–SiO_2
37 CaO–SiO_2
38 FeO–SiO_2
39 MgO–SiO_2
40 MnO–SiO_2
41 PbO–SiO_2
42 SrO–SiO_2
43 ZnO–SiO_2
44 CaO–ZrO_2
45 Al_2O_3–SiO_2
46 Al_2O_3–TiO_2
47 ZrO_2–SiO_2
48 SiO_2–TiO_2
49 ZrO_2–ThO_2

(b) One simple oxide and a binary compound of two oxides

Fig.

50 CaF_2–$3NaF{\cdot}AlF_3$
51 Al_2O_3–$3NaF{\cdot}AlF_3$
52 Al_2O_3–$3NaF{\cdot}AlF_3$
53 $Na_2O{\cdot}SiO_2$–ZrO_2

(c) One simple oxide and a ternary compound

54 $K_2O{\cdot}Al_2O_3{\cdot}4SiO_2$–$SiO_2$
55 K_2SiO_3–Na_2SiO_3
56 $K_2Si_2O_5$–$Na_2Si_2O_5$

(d) Both components binary compounds

57 $2Li_2O{\cdot}SiO_2$–$2CaO{\cdot}SiO_2$
58 $2CaO{\cdot}SiO_2$–$2FeO{\cdot}SiO_2$
59 $BaO{\cdot}SiO_2$–$CaO{\cdot}SiO_2$
60 $CaO{\cdot}SiO_2$–$SrO{\cdot}SiO_2$
61 $CaO{\cdot}SiO_2$–$CaO{\cdot}TiO_2$
62 $MnO{\cdot}SiO_2$–$MnO{\cdot}TiO_2$

(e) Two ternary compounds

63 $Na_2O{\cdot}Al_2O_3{\cdot}2SiO_2$–$K_2O{\cdot}Al_2O_3{\cdot}2SiO_2$
64 $K_2O{\cdot}Al_2O_3{\cdot}4SiO_2$–$CaO{\cdot}MgO{\cdot}2SiO_2$
65 $Na_2O{\cdot}Al_2O_3{\cdot}2SiO_2$–$CaO{\cdot}MgO{\cdot}2SiO_2$ (pseudo-binary)
66 $Na_2O{\cdot}Al_2O_3{\cdot}6SiO_2$–$CaO{\cdot}MgO{\cdot}2SiO_2$
67 $Na_2O{\cdot}Al_2O_3{\cdot}2SiO_2$–$CaO{\cdot}Al_2O_3{\cdot}2SiO_2$
68 $Na_2O{\cdot}Al_2O_3{\cdot}6SiO_2$–$CaO{\cdot}Al_2O_3{\cdot}2SiO_2$
69 $CaO{\cdot}MgO{\cdot}2SiO_2$–$CaO{\cdot}Al_2O_3{\cdot}2SiO_2$
70 $2CaO{\cdot}MgO{\cdot}2SiO_2$–$2CaO{\cdot}Al_2O_3{\cdot}SiO_2$

(3) Three-Component Systems

(a) All components simple oxides

Fig.

71 NaF–CaF_2–AlF_3
72 K_2SiO_3–Na_2SiO_3–SiO_2
73 K_2O–CaO–Al_2O_3
74 Na_2O–CaO–Al_2O_3
75 K_2O–CaO–SiO_2
76 K_2O–CaO–SiO_2
77 Na_2O–CaO–SiO_2
78 Na_2O–CaO–SiO_2
79 Na_2O–Fe_2O_3–SiO_2
80 Na_2O–Fe_2O_3–SiO_2
81 Na_2O–Fe_2O_3–SiO_2
82 Na_2O–Fe_2O_3–SiO_2
83 Na_2O–Fe_2O_3–SiO_2
84 Na_2O–ZrO_2–SiO_2

Fig.

85 CaO–MgO–Al_2O_3
86 MgO–FeO–Fe_2O_3
87 MgO–FeO–Fe_2O_3
88 CaO–MgO–SiO_2
89 CaO–MgO–SiO_2
90 CaO–Al_2O_3–Fe_2O_3
91 CaO–Al_2O_3–Fe_2O_3
92 CaO–Al_2O_3–SiO_2
93 CaO–Fe_2O_3–SiO_2
94 MgO–Al_2O_3–SiO_2
95 ZnO–Al_2O_3–SiO_2
96 Fe_2O_3–Fe_3O_4–O_2
97 Fe_2O_3–Fe_3O_4–O_2

(3) Three-Component Systems *(continued)*

(b) At least one component a binary or higher compound

98 CaF_2–Al_2O_3–3NaF·AlF_3
99 CaO·Al_2O_3·2SiO_2–2MgO·SiO_2–SiO_2
100 Na_2O·Al_2O_3·6SiO_2–CaO·MgO·2SiO_2–CaO·Al_2O_3·2SiO_2
101 90%[3CaO·Al_2O_3·3SiO_2] 10%[3Na_2O·Al_2O_3·3SiO_2] –2CaO·MgO·2SiO_2–2CaO·Al_2O_3·SiO_2
102 2CaO·MgO·2SiO_2–2CaO·Al_2O_3·SiO_2–3CaO·Al_2O_3·3SiO_2

(4) Sections of Three-Component Systems

(a) The system K_2O–CaO–SiO_2

Fig.

103 K_2O·SiO_2–CaO·SiO_2
104 K_2O·2SiO_2–30%CaO·70%SiO_2
105 K_2O·4SiO_2–CaO·SiO_2
106 K_2O·2SiO_2–K_2O·CaO·SiO_2

(b) The system Na_2O–CaO–SiO_2

107 Na_2O·SiO_2–CaO·SiO_2
108 Na_2O·2CaO·3SiO_2–Na_2O·2SiO_2

(c) The system Na_2O–Fe_2O_3–SiO_2

109 Na_2O·SiO_2–Fe_2O_3
110 Na_2O·Fe_2O_3·4SiO_2–Na_2O·2SiO_2
111 Na_2O·Fe_2O_3·4SiO_2–Na_2O·SiO_2
112 Na_2O·FeO_3·4SiO_2–Fe_2O_3
113 Na_2O·Fe_2O_3·4SiO_2–Na_2O·4SiO_2
114 5Na_2O·Fe_2O_3·8SiO_2–Fe_2O_3
115 5Na_2O·Fe_2O_3·8SiO_2– Na_2O·2SiO_2

(d) The system CaO–MgO–SiO_2

Fig.

116 CaO·MgO·2SiO_2–SiO_2
117 CaO·MgO·2SiO_2–CaO·SiO_2
118 CaO·MgO·2SiO_2–2MgO·SiO_2
119 2CaO·MgO·2SiO_2–CaO·SiO_2
120 2CaO·MgO·2SiO_2–2CaO·SiO_2
121 CaO·MgO·2SiO_2–2CaO·MgO·2SiO_2
122 CaO·MgO·2SiO_2–2MgO·SiO_2–SiO_2

(e) The system CaO–Al_2O_3–Fe_2O_3

123 4CaO·Al_2O_3·Fe_2O_3–CaO
124 CaO·Al_2O_3–CaO·Fe_2O_3
125 4CaO·Al_2O_3·Fe_2O_3–2CaO·Fe_2O_3
126 4CaO·Al_2O_3·Fe_2O_3–5CaO·3Al_2O_3

(f) The system CaO–Al_2O_3–SiO_2

127 CaO·Al_2O_3·2SiO_2–Al_2O_3
128 CaO·Al_2O_3·2SiO_2–SiO_2
129 CaO·Al_2O_3–CaO·SiO_2
130 5CaO·3Al_2O_3–2CaO·SiO_2
131 2CaO·Al_2O_3·SiO_2–3CaO·5Al_2O_3
132 2CaO·Al_2O_3·SiO_2–2CaO·SiO_2
133 CaO·Al_2O_3·2SiO_2–CaO·SiO_2
134 CaO·Al_2O_3·2SiO_2–2CaO·Al_2O_3·SiO_2

(5) Diagrams Showing Relation of Optical Properties to Chemical Composition

135 Effect of TiO_2 and Fe_2O_3 on refractive index of mullite. Variation in optical properties of solid solutions
136 Na_2O·Al_2O_3·6SiO_2–CaO·Al_2O_3·2SiO_2
137 Na_2O·Al_2O_3·4SiO_2–Na_2O·Fe_2O_3·4SiO_2–CaO·Fe_2O_3·2SiO_2–CaO·MgO·2SiO_2
138 Na_2SiO_3–Fe_2O_3–SiO_2
139 90%[3CaO·Al_2O_3·3SiO_2] 10%[3Na_2O·Al_2O_3·3SiO_2] –2CaO·MgO·2SiO_2–2CaO·Al_2O_3·SiO_2
140 BaO·2SiO_2–2BaO·3SiO_2
141 CaO·SiO_2–SrO·SiO_2
142 2CaO·SiO_2–2FeO·SiO_2
143 MgO·SiO_2–FeO·SiO_2
144 MgO·SiO_2–CaO·MgO·2SiO_2
145 CaO·FeO·2SiO_2–CaO·MgO·2SiO_2
146 2CaO·Fe_2O_3–4CaO·Al_2O_3·Fe_2O_3
147 2CaO·Al_2O_3·SiO_2–2CaO·MgO·2SiO_2
148 2CaO·Al_2O_3·SiO_2–2CaO·MgO·2SiO_2–3CaO·Al_2O_3·3SiO_2
149–156 Garnet groups

(6) Cone Deformation Diagrams

157 $Al_2O_3 \cdot 2SiO_2$–CaO
158 $Al_2O_3 \cdot 2SiO_2$–MgO
159 $Al_2O_3 \cdot 2SiO_2$–FeO
160 $Al_2O_3 \cdot 2SiO_2$–potash feldspar
161 Microcline–steatite
162 Microcline–albite
163 Orthoclase–CaO
164 Orthoclase–MgO
165 Albite–CaO
166 Albite–MgO
167 Feldspar–flint–kaolin

(7) Melting Diagrams

168 MgO–NiO, CoO, Al_2O_3, Cr_2O_3, Fe_3O_4, Mn_3O_4, SiO_2, TiO_2, and ZrO_2
169 MgO–Cu_2O, CaO, BaO, SrO, BeO, and CeO_2
170 Al_2O_3–CaO, BaO, SrO, MgO, NiO, CoO, TiO_2, and SiO_2
171 Al_2O_3–BeO, Cu_2O, ZrO_2, ThO_2, CeO_2, La_2O_3, Mn_3O_4, Fe_3O_4, Ga_2O_3, and Cr_2O_3
172 ZrO_2–CaO, SrO, and BaO
173 ZrO_2–BeO and MgO
174 ZrO_2–ZnO, NiO, CoO, Al_2O_3, Cr_2O_3, Fe_2O_3, Mn_3O_4, and (CeO, Ce_2O_3)
175 ZrO_2–BeO–CaO
176 ZrO_2–BeO–CeO_2
177 ZrO_2–ThO_2–CaO
178 ZrO_2–ThO_2–MgO

A COMPILATION OF PHASE-RULE DIAGRAMS OF INTEREST TO THE CERAMIST AND SILICATE TECHNOLOGIST*

By F. P. Hall and Herbert Insley

ABSTRACT

This paper is a compilation of phase-rule diagrams, principally of silicates and the refractory oxides, that may be useful to the ceramist and the silicate technologist. The text of the paper includes definitions of terms used in discussion of the Phase Rule, a description of methods used in the study of systems at high temperatures, and an interpretation of Phase-Rule diagrams for systems with one or more components.

I. Introduction

It is the purpose of this paper to present a compilation of equilibrium diagrams and data related to systems with nonmetallic components which react at high temperatures. Such systems are of interest to workers in the fields of ceramics, cements, and related materials and it is hoped that a compilation such as this will give a better understanding of the melting and crystallization processes encountered in manufacture.

Work of this nature has been guided by the application of the Phase Rule of Willard Gibbs[1] which was later greatly elucidated by Roozeboom[2] in his monograph on heterogeneous equilibrium.

Great strides have been made during the last twenty years in the investigation of the phase relationships in ceramic systems. During this time the principal contributions to the study of heterogeneous equilibria in such systems have been made by members of the staff of the Geophysical Laboratory of the Carnegie Institution of Washington.

II. General Discussion of Phase-Rule Diagrams

(A) Definitions

To be able correctly to interpret phase-equilibrium diagrams and the following discussions it is necessary to have a thorough understanding of the Phase Rule and the terms used. The Phase Rule may be expressed by the equation

$$F + P = C + 2$$

Where C = number of components of system.
P = number of phases present at equilibrium.
F = variance of system.

---

* Publication approved by the Director of the Bureau of Standards of the U. S. Department of Commerce. Received January 7, 1931. Final approved copy received August 2, 1933.

[1] (*a*) *Trans. Conn. Acad. Sci.*, **3**, 228 (1876); (*b*) The Collected Works of J. Willard Gibbs, Vol. I (1928).

[2] Die heterogenen Gleichgewichte, 1901–1918 (6 vol.).

The terms used are defined[3] as follows:

(1) System Any portion of the material universe which we choose to separate in thought from the rest of the universe for the purpose of considering and discussing the various changes which may occur within it under various conditions is called a system.

(2) Phase The physically homogeneous but mechanically separable portions of the system are called its phases.

(3) Components The number of components of a system at equilibrium is defined as the smallest number of independently variable constituents by means of which the composition of each phase may be quantitatively expressed.

(4) Variance of a System (Degree of Freedom) In the application of the Phase Rule to the type of systems under consideration, the independently variable conditions which are usually taken into consideration are temperature, pressure, and concentration. The number of these variables, which must be arbitrarily fixed to define the system completely, is called the variance or degree of freedom of that system.

(5) Equilibrium An equilibrium exists in any system under a fixed set of conditions when the parts of the system do not undergo any change of properties with the passage of time and provided the parts of the system have the same properties when the same conditions are again arrived at by a different procedure.

(6) Melting Point The temperature of transition of solid to liquid state at atmospheric pressure in which the liquid phase is of the same composition as the solid phase is known as the congruent melting point of the solid phase. This is in contradistinction to the transition of one solid phase into a second solid phase with the liberation of liquid of a different composition; the latter is called an incongruent melting point.

(7) Solid Solution In certain cases two solids may form physical mixtures that are homogeneous and therefore must be classed as solutions.

(8) Polymorphism Polymorphism is the property that a substance may possess of existing in more than one crystal form. Polymorphic solids are solid phases of the same ultimate composition differing in crystalline form and physical properties but yielding identical liquid or gaseous phases upon fusion or evaporation.

(9) Transition Point When the pressure is the atmospheric pressure, the temperature at which two solid phases can

[3] The definitions are those found in standard textbooks on physical chemistry such as (*a*) Principles of Physical Chemistry by E. W. Washburn, (*b*) A Treatise on Physical Chemistry by H. S. Taylor and collaborators, and (*c*) The Phase Rule by Alexander Findlay.

coexist and at which the relative stability of the two forms undergoes change is known as the transition point.

(10) Enantiotropic Forms Polymorphic forms which possess a transition point at which they are in equilibrium are known as enantiotropic forms.

(11) Monotropic Forms In certain instances of polymorphism the vapor-pressure curves of the two forms do not meet below the melting point. They therefore lack a stable transition point, and one form is metastable with respect to the other at all temperatures below the melting point. Such forms are called monotropic.

Other terms will be defined as encountered in the discussions.

(B) Methods Used for Study of High-Temperature Heterogeneous Equilibrium

The diagrams presented refer only to systems which are in equilibrium for the temperatures (and pressures) specified. They give no information as to the velocity of reactions but they do define the relative amounts of crystalline and liquid phases present at any temperature and composition provided the time has been sufficient for equilibrium to be attained. Most ceramic and related processes are incomplete chemical reactions and the results obtained are dependent upon the time element as well as upon the temperature. In applying equilibrium diagrams to manufacturing processes due consideration must be given this difference between the ideal and the practical conditions. Moreover, equilibrium diagrams portray reactions between pure components, while frequently in the heat treatments of ceramic materials small amounts of impurities are present which may profoundly affect the equilibrium relations of the major components. Thus in the heat treatment of kaolin at high temperatures the result of the reactions taking place may be predicted from a study of the Al_2O_3-SiO_2 equilibrium diagram, providing sufficient heating time has been allowed and providing the kaolin is absolutely pure. If, however, small amounts of alkalis, lime, or other impurities are present, the system is no longer a simple binary one, the eutectic and liquidus temperatures may be lowered very considerably, and the ratios of Al_2O_3 to SiO_2 may be altered at eutectics and transition points.

(1) Cooling Curves This method has been used extensively in the study of metals but, because of the high viscosity and resultant undercooling in silicate systems, its use in their study has not usually been successful. It is evident that if a system is allowed to cool with a constant outside temperature environment the time-temperature curve obtained for the system will depend upon the heat radiation of the system and the energy changes occurring within the system as a result of alteration in the chemical equilibrium with the temperature. If the

time-temperature cooling curve is plotted, it will reveal certain "arrests" indicating temperatures pertinent to the study of the system and will enable the construction of a temperature-composition diagram which, when properly interpreted, will show the phase relations in the system at various temperatures and compositions.

(2) Heating Curves Combined with Optical Examinations In metals and easily crystallizable salts the time-temperature heating curve shows a sharp break both at the beginning and end of melting and usually a flat portion between. In the case of silicate minerals the heating curve is rarely sharply broken and often is oblique. The use of the heating curves is made difficult by the same sluggishness that is present in the cooling curve experiments. The heating curves, however, are more reliable and have been much more widely used than the cooling curves.

Morey[4] makes the following statement:

> It is well recognized both in theory and practice that the melting point of a substance of the latter class (silicates) is more accurately determinable by the quenching method. Taking the melting point determination by this method as the standard, it is shown that the true melting point lies on the more rapidly rising end portion of the heating curve. As usually interpreted, therefore, the heating curve method tends to give a melting point which is too low.

(3) Quenching Method[5] Before the actual quenching is done it is necessary to be certain that the charge is uniform in composition throughout. This may be accomplished by sintering and grinding the charge several times. Complete melting, repeated with intermediate grinding if necessary, is even more effective in making the charge homogeneous.

In the quenching operation a charge of the composition to be investigated is wrapped in platinum foil, for example, and suspended in a furnace frequently of the platinum resistance type. The charge is brought to the desired temperature, T, and held for a suitable length of time. By fusion of the wire holding the foil or by some other method which instantaneously releases the charge it is dropped from the furnace into a vessel containing mercury or some other liquid which does not react with the sample. In this manner the charge is "frozen" and a microscopic examination of the charge after it is quenched reveals the phases present at the temperature, T.

If it is found that the charge contains more than one crystalline phase, a charge of the same composition is heated to a higher temperature, T,

[4] George W. Morey, "A Comparison of the Heating Curve and Quenching Method of Melting Point Determinations," *Jour. Wash. Acad. Sci.*, **13** [14], 326–29 (1923).

[5] E. S. Shepherd, G. A. Rankin, and F. E. Wright, "Binary Systems of Alumina with Silica, Lime, and Magnesia," *Amer. Jour. Sci.*, 4th Ser., **28**, 293 (1909).

quenched, and examined. If this quenched charge contains only one crystalline phase, which in this case is called the primary phase for that part of the system, the process is repeated until a temperature is found at which the primary phase disappears and leaves only liquid (glass at room temperature). This temperature and composition locates a point on the melting curve of the system investigated.

The quenching method is the most accurate method of investigating the silicate systems and was the method used to determine most of the equilibrium diagrams assembled in this paper.

(4) Cone Deformation Method This method has been used to approximate the melting behavior in certain systems. The sources of error in the cone deformation method are as follows: (1) Cones of the same bulk chemical composition do not always deform at the same temperature because they may be compounded of different mineral species which are not ground and mixed until chemically homogeneous. (2) Cones of somewhat different chemical composition may begin to deform at the same temperature because of the presence of a eutectic common to both.

Day and Shepherd[6] state as follows:

> This method is peculiarly unsuited for such investigations (of silicates) for several reasons: Suppose the mixture to contain a eutectic with a greater or less excess of one of the components. The cone would begin to weaken as soon as the eutectic began to melt and its further progress would be governed entirely by the relative quantity of eutectic present and its viscosity after melting. No information whatever regarding inversions in the solid or of the component in excess could be obtained, and errors of more than 500°C would certainly occur in the interpretation of the softening in parts of the lime-silica curve.

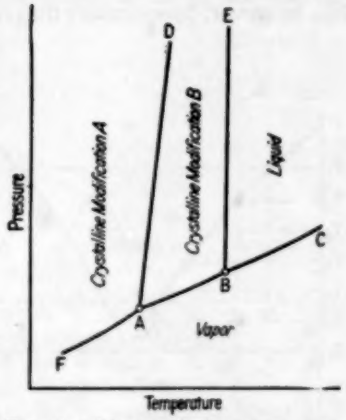

FIG. 1.—Phase relations in a one-component system.

(C) One-Component Systems

When a system consisting of a single component is considered, it follows from the Phase Rule that it is bivariant if one phase is present, univariant if two phases are present, and invariant if three phases are present. The independent variables are limited to the pressure and the temperature. The phase relations in a one-component system are usually illustrated by means of a pressure-temperature diagram since pressure and temperature are the independent variables. Such a system is shown in Fig. 1.

[6] A. L. Day and E. S. Shepherd, "The Lime-Silica Series of Minerals," *Amer. Jour. Sci.*, 4th Ser., **22**, 265–302 (1906).

FA (univariant) is the sublimation curve for modification *A*.

AB (univariant) is the sublimation curve for modification *B*.

BC (univariant) is the vapor pressure curve for the liquid.

Curve *AD* (univariant) is the transition curve for modifications *A* and *B* and represents the change of the transition point with pressure.

Curve *BE* (univariant) is the melting curve for modification *B* and represents the change of the melting point with pressure.

Point *A* (invariant) is the transition point for the two crystalline modifications. (It is called a triple point since it is the point at which the two solids and vapor are in equilibrium.)

Point *B* is the triple point for the equilibrium, crystalline modification *B*-liquid-vapor.

The system is bivariant in all parts not on these lines or their intersections.

In dealing with refractory substances it is at present impossible to measure directly the vapor pressures of the solid and liquid phases. It is possible, however, to construct diagrams for refractory substances showing qualitatively the vapor pressures for the different phases if the temperature-stability relations are known, since at any one temperature the unstable phase always has a higher vapor pressure than the stable phase. This has been done by Fenner for the silica system as shown in Fig. 22 (see p. 486).

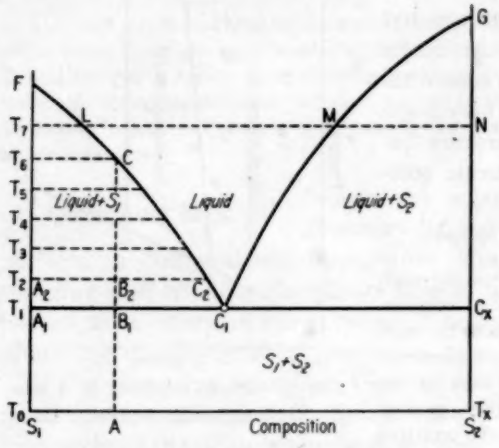

FIG. 2.—A two-component system without intermediate compounds or solid solutions.

(D) Two-Component Systems

Two-component systems have three independent variables, temperature, pressure, and composition. In systems of importance in ceramics where the pressure is maintained at one atmosphere, the diagrams may be reduced to two dimensions, the two variables being composition and temperature.

(1) Two-Component Systems without Solid Solutions

Figure 2 represents a typical two-component system of components S_1 and S_2 where no compounds or solid solutions are formed. Two methods of study of such systems are possible.

(a) Isoplethal Studies

This is a study of changes produced where the total composition of the system is held constant and the temperature is varied. An isopleth (line of constant composition) at composition C_1 will show sharp melting at temperature T_1 as this

is an invariant point. An isopleth at S_1 will show sharp melting at F for the same reason. Melts represented by isopleths at intermediate compositions between S_1 and C_1 do not show sharp melting but exhibit softening behavior which starts at T_1 and is completed at the intersection of the isopleth and the curve FC_1. Considering isopleth AC the melting begins at T_1 and the composition of the liquid phase varies along the line C_1C. The relative amounts of liquid and solid, S_1, at any one temperature, T_2, are found by the use of the so-called "lever reaction." The relative amounts of solid S_1 and of solution of composition C_2 are represented by the lengths C_2B_2 and B_2A_2, respectively.

The relative amounts of liquid and solid S_1 present at various temperatures from T_1 to T_6 plus dT for the isopleth A are shown in Fig. 3. This figure serves fairly well to illustrate the use of the "lever reaction." The compositions S_1, S_2, and the composition corresponding to C_1 are special cases to which curves of the type of Fig. 3 do not apply since melting of these compositions takes place at definite temperatures and not over temperature intervals.

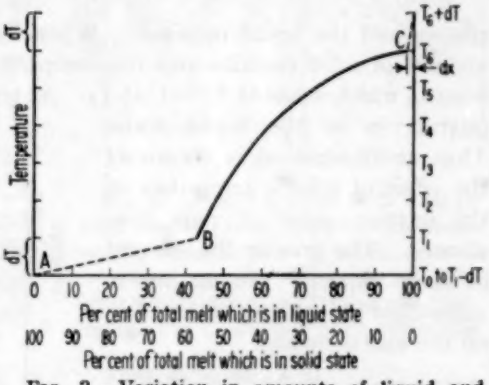

FIG. 3.—Variation in amounts of liquid and solid phase, S_1, upon heating composition A of Fig. 2 from the temperature T_6 to $T_6 + dT$ along the isopleth AC; dT and dx are infinitesimal increments in temperature and amount of solid phase, S, respectively.

A melt of composition A (Fig. 2) at a temperature T_7 consists entirely of a liquid phase and as it is cooled and the temperature T_6 is reached the solid S_1 begins to separate out and continues to separate as the temperature is lowered to T_1. Over the interval T_6 to T_1 the amount of solid S_1 increases as is shown in Fig. 3 and the composition of the liquid changes along the line of CC_1, Fig. 2. When C_1 is reached the temperature remains constant until the solid phases (S_1 and S_2) separate out together and until all of the liquid phase has disappeared. After complete crystallization of the two solid phases the temperature begins to drop until room temperature is reached, since no inversions in the solid phases are indicated by Fig. 2.

The above statements regarding the crystallization of melts are true only if the rate of cooling is sufficiently slow to allow equilibrium to be attained at every instant. A rapid rate of cooling will lead to quite different results.

If the two solids, S_1 and S_2 (Fig. 2) are selected in such proportion as

represented by point A and are heated, no reaction will take place until the temperature T_1 is reached. At this temperature a liquid of composition C_1 is formed. After heating until the complete disappearance of S_2 the ratio of solid to liquid at this point is represented by the ratio of the lengths B_1C_1 to A_1B_1. At temperature T_2 the ratio of solid to liquid is as B_2C_2 is to A_2B_2. As the temperature is raised the amount of solid decreases and the liquid increases. When T_6 is reached only a very small amount of solid remains and the composition of the liquid has changed from C_1 which it has at T_1 to C at T_6. At temperatures above T_6 the entire mixture is in the liquid state. Thus an illustration is shown of the effect of soluble impurities on the melting point of pure substances. The greater the amount of such impurity present up to saturation the greater is the effect on the melting point.

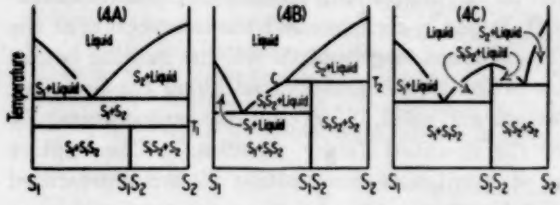

FIG. 4.—Two-component systems with compounds present: 4A, the compound S_1S_2 decomposes at a temperature below the eutectic temperature; 4B, the compound S_1S_2 decomposes at a temperature above the temperature of the eutectic; 4C, the compound S_1S_2 is stable at its melting point.

(b) Isothermal Studies If a charge of pure S_1 (referring to Fig. 2) is heated to temperature T_7 and held constant at this temperature and, at the same time, a small amount of S_2 is added to this charge a small amount of liquid of composition L will be formed. As the amount of S_2 is increased the amount of liquid, L, will increase until the point L is reached where, with further addition of S_2, the solid phase S_1 disappears and the charge is entirely liquid. As S_2 is added the composition of the liquid varies until point M is reached when the solid phase S_2 no longer completely dissolves. Further addition of S_2 to the charge increases the amount of S_2 present and decreases the amount of

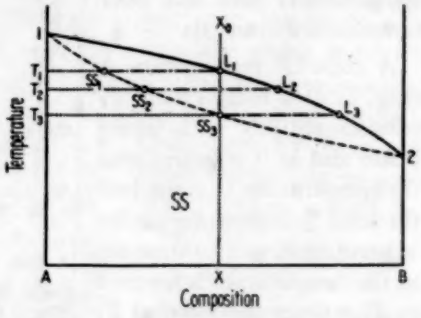

FIG. 5.—Complete solid solution without maximum or minimum in a binary system. The line $1L_1L_2L_32$ represents the composition of the liquid phase and is called the liquidus curve. The line $1SS_1SS_2SS_32$ represents the composition of the solid phase and is called the solidus curve. The tie lines, SS_1–L_1, SS_2–L_2, and SS_3–L_3, show the conjugate relation of liquid and solid phase for the three temperatures T_1, T_2, and T_3.

liquid present. Since the line FC_1 (Fig. 2) represents solutions saturated with S_1, and the line C_1G solutions saturated with S_2, the intersection C_1 (eutectic) must represent a solution saturated with both solids. The lines are thus solubility curves or freezing point curves.

(2) Two-Component Systems with Compounds Present

Three types of binary diagrams are shown in Fig. 4. Figure 4A shows a compound, S_1S_2, which decomposes at T_1 into the solids, S_1 and S_2. Figure 4B shows a compound, S_1S_2, with an incongruent melting point, that is, it decomposes at T_2 into a solid, S, and liquid, C, which has not the same composition as the compound, S_1S_2. Figure 4C shows a compound, S_1S_2, which melts congruently, that is, the liquid resulting from the melting of S_1S_2 is of the same composition as the solid, S_1S_2.

(3) Two-Component Systems with Solid Solutions Present

(a) Single Solid Solution

Figure 5 represents the case where the melting point of A is depressed by B and that of B is raised by A. Along the isopleth, X, the sample at the temperature of X_0 will consist entirely of liquid. If this melt is allowed to cool until the temperature reaches T_1 the solid of composition SS_1 appears. It is apparent that the solid is rich in A and the liquid rich in B. If the temperature is allowed to fall, the isopleth crosses the lines joining all compositions of solid from SS_1 to SS_3 and all compositions of liquid from L_1 to L_3. At temperature T_2 the liquid has a composition of L_2 and the solid solution a composition of SS_2. The solid is thus increasing in amount of B along SS_1–SS_3 and the liquid decreasing in amount of B along L_1–L_3 so that the last drop of liquid has the composition L_3 and the total solid the composition SS_3. Fractional crystallization can be obtained between T_1 and T_3 by removing the solid phase at any temperature between T_1 and T_3. It can be seen that in cooling such solid solution systems under equilibrium conditions there is a constant interchange of material between solid and liquid phases and a constant change in composition in all parts of the solid as cooling progresses. Figures 5, 6, and 8 show types of solid solution diagrams.

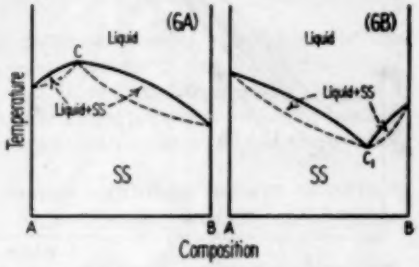

FIG. 6.—Binary systems with a single solid solution: 6A, system with maximum melting point at C which is not a compound since it is not an invariant point; 6B, system with minimum melting point at C_1 which is not a eutectic as it is not an invariant point.

The freezing point of a pure solid component is lowered by the presence of a second component in the liquid phase except in certain cases where the

solid phase is a solid solution. The freezing point of a solid solution may be either lower than that of the pure component, equal to it, or higher, as is shown in Fig. 7. It is shown that, as the amount of component B in the solid solution increases, the freezing point of the solid solution increases until it becomes equal to T_2 and as the amount of B increases in the solid solution the freezing point actually becomes higher than that of the pure component, A. If the concentration of the second component is greater in the liquid phase than in the solid phase, the freezing point is lowered and if it is greater in the solid phase than in the liquid phase, the freezing point is raised.

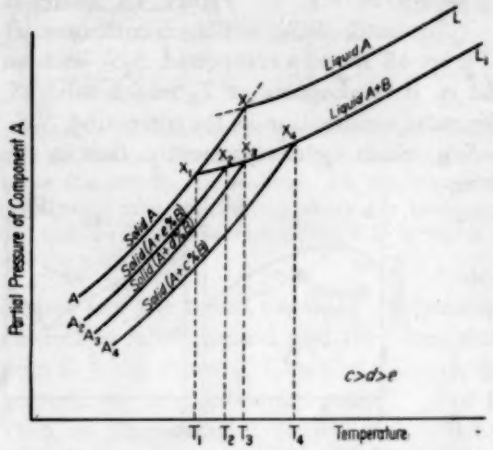

FIG. 7.—Vapor pressure of component A in solid and liquid phases (Hill in Taylor's Treatise on Physical Chemistry, p. 425, 1924).

AX = vapor pressure curve for pure A in pure solid phase.

LX = vapor pressure curve for pure A in pure liquid phase.

X = freezing point of pure A in solution of pure A.

X_1L_1 = vapor-pressure curve for pure A in solution with B.

X_1 = freezing point of pure A in equilibrium with solution containing both A and B.

X_2, X_3, and X_4 are the intersections of the vapor-pressure curves of pure component A in solid solutions of A and various amounts of B, and T_2, T_3, and T_4 are the corresponding freezing points of these solid solutions.

(b) Two Solid Solutions Figure 8 shows two cases where two solid solutions are present. In Fig. 8A at point c there are two solid solutions of compositions A and B, a liquid of composition c and a vapor phase. This number of phases (4) present in a two-component system makes the point c an invariant point which satisfies the definition of a eutectic. In Fig. 8B at point c there are two solid solutions of compositions A and B, a liquid solution of composition c, and a vapor phase making point c an invariant point. This latter point, c, is called a transition point as it marks the appearance of a new solid phase if one cools the system from a temperature above T_c to a temperature below T_c.

(4) Two-Component Systems with Two Liquid Phases The area abc in Fig. 9 represents the area in which the two liquid solutions are in equilibrium with a vapor phase.

The composition of these two solutions at any temperature, T_2, is represented by the points L and M or the extremities of the tie lines which are intersections of horizontal lines with the liquidus curves ab and bc. The point c at temperature T_1 is a quadruple point and in a two-component system an invariant point since there are two liquid phases, one solid (A) and a vapor phase present. The work of Greig[7] has shown that there are often similar conditions present in certain SiO_2-rich regions of silicate systems.

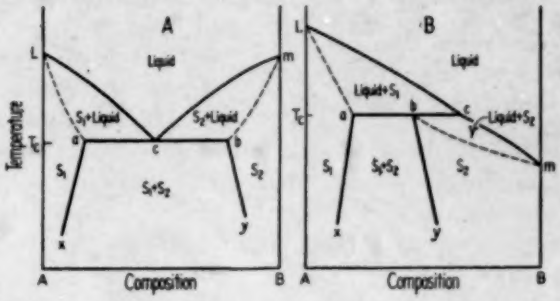

FIG. 8.—Solid solutions showing conjugate relationships. The two solid solutions, S_1 and S_2, have a conjugate relation to each other in the areas $abxy$. The solid solutions in areas Lac and mbc have a conjugate relation to the corresponding liquid phases present in these areas.

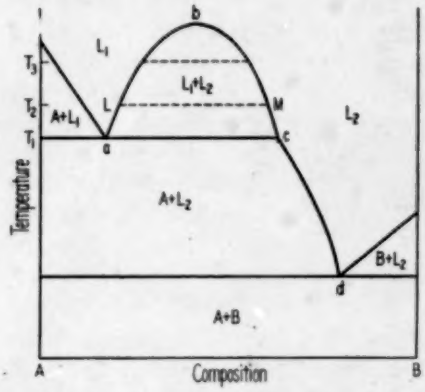

FIG. 9.—Conjugate liquid phases. The broken lines in the area abc show the conjugate relationship of the two liquid phases for the two temperatures, T_2 and T_3.

(E) Three-Component Systems

(1) Three-Component Systems without Solid Solution

The number of independent variables in a ternary system is four, namely, pressure, temperature, and two concentration variables, since a ternary solution requires a statement of its composition with respect to two components before its total composition is fixed. Five coexisting phases (a quintuple point) produce an invariant system, four give a univariant system, three bivariant, etc. A complete graphical representation of the ternary systems is a very difficult matter. If the pressure is held constant (one atmosphere), a simplified system results where the composition can be represented by triangular coördinates and the temperature by an ordinate at right angles to the triangular diagram giving a triangle prism as the space diagram. The

[7] "Immiscibility in Silicate Melts," *Amer. Jour. Sci.*, 5th Ser., **13**, 1–44 and 133–53 (1927).

temperatures are usually projected onto the equilateral triangle and are represented by isotherms on the composition triangle.

(a) Typical Cases of Three-Component Systems[8] without Solid Solutions

In Fig. 10 six typical cases of ternary systems are shown. Figure 10A shows a system without either binary or ternary compounds present. The field 1–4–2, *C* represents the field of stability of component *C* in equilibrium with solution. *C* is thus the primary phase for this area and is the last solid to disappear when any composition within this area is heated. It is also the first solid phase to appear when liquids represented by points in this area are allowed to cool. Points 1, 2, and 3 are binary eutectics while point 4 is a ternary eutectic. Lines 1–4, 2–4, 3–4 are known as boundary curves, each of which represents a condition of 3-phase equilibrium between two solid phases and liquid. The two solid phases at equilibrium along 1–4 are *A* and *C*, along 2–4 are *C* and *B*, and along 3–4 are *A* and *B*. Point 4 is a quadruple point (in a condensed system) at which solids *A*, *B*, and *C* are in equilibrium with solution.

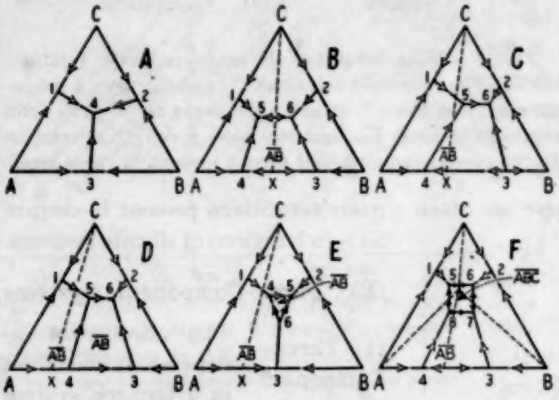

FIG. 10.—Six typical cases of three-component systems. (G. A. Rankin and F. E. Wright, *Amer. Jour. Sci.*, 4th Ser., 39, 1–79 (1915)). Isotherms are omitted, but the arrows indicate the direction of falling temperatures (p. 18).

Figure 10B shows a ternary system where a binary compound $\overline{AB}$ is present. This compound is stable at its melting point. According to the theorem of Alkemade,[9] if the line *C–X* crosses the line 5–6 the point of intersection will be a maximum on the boundary 5–6 and the points 5 and 6 will be eutectics. However, if *C–X* does not cross 5–6 but intersects 1–5 and 4–5 (as in Fig. 10C), then only 6 will be the eutectic. The line *C–X* is a conjugation line representing the binary system with components

[8] For a more complete treatment see G. A. Rankin and F. E. Wright, "Ternary System CaO–Al_2O_3–SiO_2," *Amer. Jour. Sci.*, 4th Ser., 39, 1 (1915).

[9] "A theorem by Van Rijn Van Alkemade serves as a very effective guide in regard to temperature changes in the interior of the triangle. If the two points in the triangle which correspond to the composition of two solid phases be connected by a line, the temperature at which these same two phases can be in equilibrium with solutions and vapor rises as the boundary curve approaches this line, becoming a maximum at the intersection though the boundary curve often ceases to be stable before this point is reached." (Bancroft, The Phase Rule, p. 149.)

C and $\overline{AB}$ and which divides the ternary system A–B–C into two ternary systems which may be treated individually.

In Fig. 10D the composition of $\overline{AB}$ lies outside the field 4–5–6–3 and the compound is unstable at its melting point. In the binary system A–B it dissociates at a temperature corresponding to point 4 into solid A and liquid. In the ternary system A–B–C the compound $\overline{AB}$ is the primary phase in the field 3–4–5–6 and is stable in this field.

In Fig. 10E, $\overline{AB}$ dissociates into solids A and B in the binary system A–B. In the ternary system compound $\overline{AB}$ has a stable field 4–5–6.

In Fig. 10F the system has a binary compound $\overline{AB}$ and a ternary compound $\overline{ABC}$, each of which has a congruent melting point as their respective compositions are within or on the boundaries of the fields in which they are the primary phases.

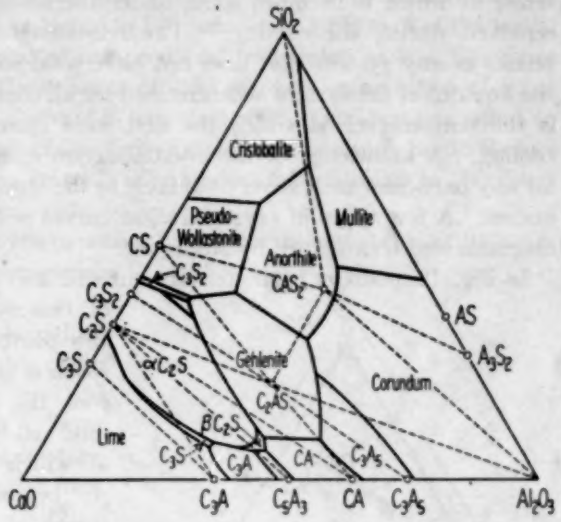

FIG. 11.—Three-component system, Al_2O_3–CaO–SiO_2, showing (1) boundary curves as solid lines, (2) composition lines as dotted lines. The final product of crystallization (on slow cooling) of ternary solutions of this system always consists of three solid phases whose fields of stability are adjacent. The same three solid phases will be the final product of crystallization from any solution whose composition lies within the triangle (composition triangle) formed by lines joining the compositions of these three phases. (G. A. Rankin and F. E. Wright, *Amer. Jour. Sci.*, 4th Ser., **39**, 1–52 (1915) (p. 52)). NOTE: C = CaO, A = Al_2O_3, S = SiO_2.

These simple cases are also applicable to complex systems as shown in Fig. 11.

(b) Crystallization in Ternary Systems[10] without Solid Solutions

Geer states that "the crystallization curve[11] denotes the locus of points which represent the compositions of the solutions formed on cooling any given solution from any given

[10] A more complete treatment of the subject can be found in any of the following references: (*a*) W. C. Geer, "Crystallization in Three-Component Systems," *Jour. Phys. Chem.*, **8**, 257 (1904); (*b*) G. A. Rankin and F. E. Wright, *Amer. Jour. Sci.*, 4th Ser., **39**, 1 (1915); and (*c*) O. Andersen, "The System Anorthite–Forsterite–Silica," *ibid.*, 4th Ser., **39**, 407 (1915).

[11] See footnote 10 (*a*)

temperature to the temperature (quintuple point in case of ternary systems) at which it becomes solid, under the assumption that no phase is removed during the cooling." The relations of solid phases to liquid phases of any system that does not have solid solutions are known when the liquidus of the system is determined for all compositions. The liquidus is the temperature at which the first solid (primary phase) appears on cooling. A knowledge of the crystallization curve or the melting curve for any particular melt is very valuable in the study of the firing of ceramic bodies. A few types of crystallization curves will be described using the diagrams and terms given by Andersen.[12]

In Fig. 12, point m is the ternary eutectic and all crystallization curves of this system are terminated at this point. If a liquid of composition a is chosen and allowed to cool the system remains liquid until the liquidus is intercepted, at which temperature the solid, A, begins to crystallize. The course of the crystallization curve from this point to the boundary m–k follows a straight line drawn through A and a. This is true for all crystallization curves where solid solutions are not present. As the liquid changes in composition from a to b solid A crystallizes. At b a second phase appears and the crystallization curve follows the boundary m–k with phases A and C crystallizing together. At point m the temperature remains constant until all liquid has disappeared, during which time the three solid phases A, B, and C are crystallizing together. The final product will be a mass of large crystals (on slow cooling) surrounded by smaller crystals of A, B, and C. The composition of the solid crystallizing at b is indicated by the intersection of the tangent to the curve m–b–k at the point b with the line A–C, which is point b''. The mean composition of the two solid phases that have crystallized between points b and m is represented by b'. In this case it is a mixture of A and C in the proportion $b'C:b'A$. The mean composition of the total solid which separates out between a and m (before B begins to crystallize) is represented by a'. During eutectic crystallization at m the composition of the total solid changes from a' to a, reaching the latter point as the last drop of liquid disappears. The amounts of solid separating between various temperatures

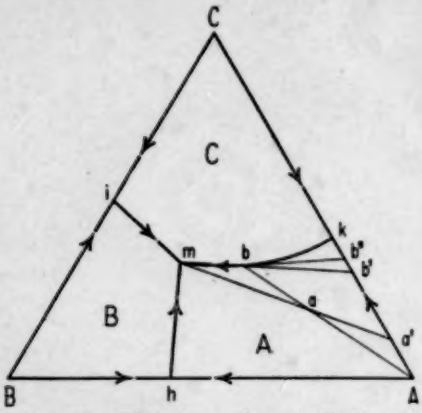

FIG. 12.—The course of crystallization in a ternary system (O. Andersen, *Amer. Jour. Sci.*, 4th Ser., **39**, 407–54 (1915) (p. 427)).

[12] See footnote 10 (*c*).

can be calculated by the use of the "lever reaction" as described in the case of the binary systems. Thus the amount of solid of composition A separated between a and b is equal to 100 times ab/Ab per cent of the initial composition a. The liquid of composition b remaining at b is 100 times aA/Ab per cent of a. The amount of solid of mean composition a' separated between a and m (before B has started to crystallize) is equal to 100 times $am/a'm$ per cent of a and the amount of remaining liquid (before ternary crystallization has started) of composition m is equal to 100 times $aa'/a'm$ per cent.

The case of a ternary system with a binary compound stable at its melting point is discussed in connection with Fig. 10B on page 474.

In Fig. 13 the quintuple points, o and m, lie on the same side of the conjugation line, C–$\overline{AB}$, and the quadruple points, h and j, lie on opposite sides. The field of A extends across the conjugation line, C–$\overline{AB}$, and the system C–$\overline{AB}$ is not a true binary system. The line o–m, according to the theorem of Alkemade, slopes toward m. In this case o is not a eutectic but an alteration point. Solid phase A crystallizes out along a–b when a melt of composition a is cooled. From b to o, A and $\overline{AB}$ crystallize together, but as the total composition of the solid separated between a and o is given at a', there must be liquid left when o is reached. As the point a is within the composition triangle A–$\overline{AB}$–C the final products of crystallization must be these three phases. It is evident from the diagram that the three phases which are in equilibrium at o are A–$\overline{AB}$–C. Therefore, in this case the final solidification must take place at o and not at m. During the final solidification at o, while the solid phases C and $\overline{AB}$ are crystallizing out, some of the phase A is redissolved. A melt, c, on the conjugation line C–$\overline{AB}$ crystallizes as follows: along c–b, A separates; along b–o, A and $\overline{AB}$ separate together; at o, C and $\overline{AB}$ separate and A completely dissolves. A melt, d, on the left of the conjugation line crystallizes as follows: along d–e, A separates out; along e–o, C and A crystallize together; at o, A dissolves and $\overline{AB}$ is formed (temperature remains constant until all of A disappears); along o–m, $\overline{AB}$ and C crystallize out together. At m the final products of crystallization are $\overline{AB}$, B, and C,

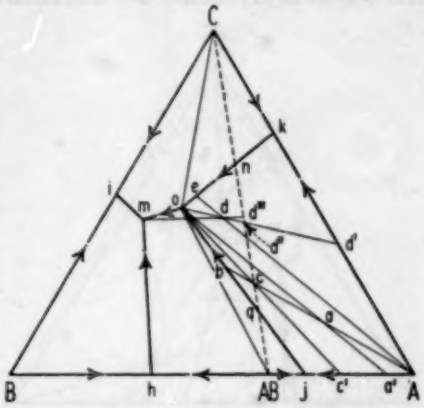

FIG. 13.—A ternary system with a binary compound which does not form a binary system with the third component (O. Andersen, *Amer. Jour. Sci.*, 4th Ser., **39**, 407–54 (1915) (p. 431)).

which is as one would expect since the point d lies in the composition triangle B–$\overline{AB}$–C. The mean composition of the solid separating out between d and o is represented by d'. After all of A has disappeared at o and crystallization begins to proceed along o–m the mean composition of the solid has changed to d''. Along o–m the mean composition of the solid changes from d'' to d''' and during the final crystallization at m from d''' to d.

In Fig. 14 the quadruple points, h and j, and the quintuple points, o and m, all lie on the same side of the conjugation line. A melt of composition e crystallizes as follows: along e–b, A separates out; at b the compound $\overline{AB}$ begins to crystallize out and A to redissolve and this process continues until o is reached. Final crystallization takes place when the composition of the liquid and the temperature of the system reaches o. In this case A does not completely dissolve and the final products are A, $\overline{AB}$, and C. If the tangent to the line j–o intersected the line A–$\overline{AB}$ and not its prolongation, the solid A would tend to increase in amount along j–o. A melt of composition a will crystallize as follows: from a to b, A separates out; between b and c, $\overline{AB}$ separates out and A dissolves (is resorbed), and at the point c all of A has disappeared, as the mean composition of total solid separated between a and c is represented by $\overline{AB}$. From c the crystallization curve leaves the boundary j–o and continues to d while $\overline{AB}$ is separating. From d to m, B and $\overline{AB}$ separate together and at m, $\overline{AB}$, B, and C crystallize together. All melts in the field j–o–AB pass through the field h–m–o–j. The line j–o in this case is called an alteration curve and is indicated by double arrows.

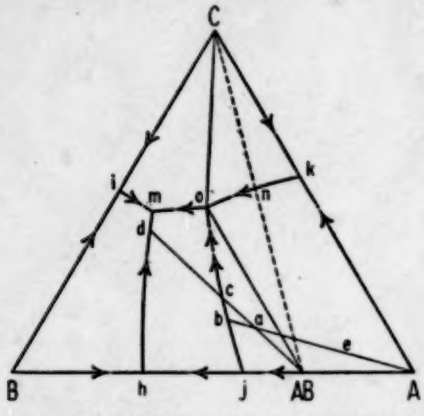

FIG. 14.—A ternary system containing a binary compound unstable at its melting point (O. Andersen, *Amer. Jour. Sci.*, 4th Ser., 39, 407–54 (1915) (p. 433)).

Figure 15 illustrates a case of recurrent crystallization. Thus at the point c (in the crystallization of a melt of composition a) the phase A disappears and the crystallization curve follows the straight line to point d, at which point A begins to separate and continues to do so along with $\overline{AB}$ until point o is reached. At the point o the temperature remains constant and A dissolves with separation of C and $\overline{AB}$. Along o–m, C and $\overline{AB}$ separate together and the final product of crystallization at m is B, $\overline{AB}$, and C, as the original point lies within the composition triangle

B–$\overline{AB}$–C. A melt e crystallizes as follows: along e–b, A separates; between b and p separation of $\overline{AB}$ and partial solution of A; from p to o, A and $\overline{AB}$ separate together. At o, A partly dissolves while C and $\overline{AB}$ separate out and the final products of crystallization are $\overline{AB}$, A, and C.

(c) Summary Relating to Crystallization within Ternary Systems Not Containing Solid Solutions[13]

(*a*) On cooling a liquid the first phase to appear is the primary phase for that part of the system in which the composition of the melt is represented.

(*b*) The crystallization curve follows to the nearest boundary the extension of the straight line connecting the composition of the original liquid with that of the primary phase of that field. The composition of the liquid within the primary fields is represented by points on the crystallization curve. This curve is the intersection of a plane (passed perpendicular to the base triangle and passing through the compositions of the original melt and the primary phase) with the liquidus surface.

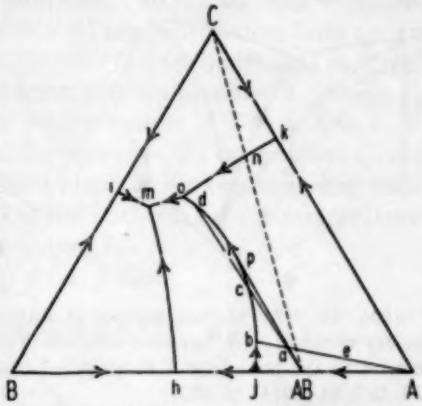

FIG. 15.—Recurrent crystallization in a ternary system (O. Andersen, *Amer. Jour. Sci.*, 4th Ser., 39, 407–54 (1915) (p. 435)).

(*c*) At the boundary line a new phase appears which is the primary phase of the adjacent field. The two phases separate together along this boundary as the temperature is lowered.

(*d*) Two conditions might be present that would alter the crystallization along the boundary: (*i*) The first phase will increase as is the case where the tangent to the boundary curve intersects the line connecting the compositions of the two phases separating or it will decrease (be resorbed) if this tangent intersects the prolongation of this line. (*ii*) The crystallization curve will leave the boundary curve when the first phase has become completely resorbed leaving only the second solid phase. This may be inferred from a study of the mean composition of the solid separating between successive points on the crystallization curve.

(*e*) The crystallization curve always ends at that quintuple point which represents the equilibrium between liquid, vapor, and the three solid phases of the three components within whose composition triangle the composition of the original liquid was found.

---

[13] G. A. Rankin and F. E. Wright and O. Andersen, *loc. cit.*

(*f*) The composition of the solid which is crystallizing at any point on a boundary line is shown by the intersection of the tangent at that point with the line joining the composition of the two solid phases which are crystallizing at the given point.

(*g*) The mean composition of the total solid which has crystallized to any point on the crystallization curve is found by extending the line connecting the given point with the original liquid composition to that line connecting the compositions of the phases that have been separating.

(*h*) The mean composition of the solid that has separated between two points on a boundary is found at the intersection of a line, passing through

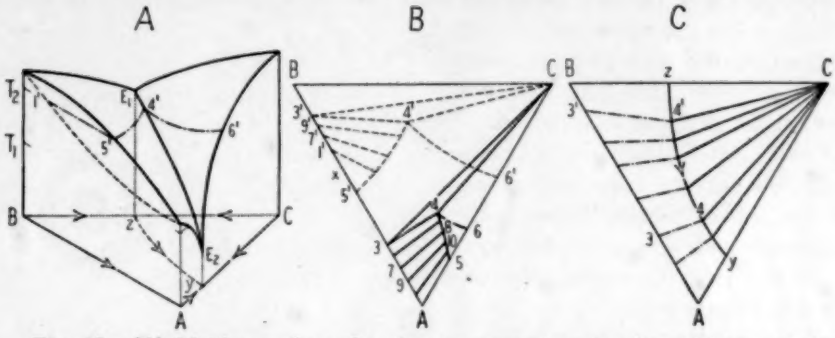

FIG. 16.—(A) Melting surface of a three-component system in which one of the binary systems, A–B, has solid solutions present. In the ternary system these solutions extend to the boundary E_1E_2 (modified from N. L. Bowen, *Amer. Jour. Sci.*, 4th Ser., **38**, 207–64 (1914) (p. 221)).

(B) Position of solid-phase indicating lines at temperatures T_1 and T_2. At T_1 the lines are full and at T_2 they are broken.

(C) Three-phase boundaries of system shown in (A).

these two points, with the line connecting the compositions of the two solid phases separating along this boundary.

(2) Three-Component Systems with Solid Solutions[14]

In systems where there are no solid solutions it is necessary only to locate the boundary curves and isotherms to determine the crystallization of any mixture within the system

[14] (*a*) N. L. Bowen, "The Crystallization of Haplobasaltic, Haplodioritic, and Related Magmas," *Amer. Jour. Sci.*, 4th Ser., **40**, 161–85 (1915).

(*b*) J. B. Ferguson and H. E. Merwin, "Wollastonite and Related Solid Solutions in the Ternary System CaO–MgO–SiO_2," *ibid.*, 4th Ser., **48**, 165–89 (1919).

(*c*) N. L. Bowen, "Diopside–Forsterite–Silica," *ibid.*, 4th Ser., **38**, 207–64 (1914).

(*d*) F. A. H. Schreinemakers, "Mischkristalle in Systemen dreier Stoffe, Part I," *Z. phys. Chem.*, **50**, 169 (1904–1905); Part II, **51**, 547; Part III, **52**, 513.

(*e*) H. E. Boeke and W. Eitel, Grundlagen der Physikalisch-Chemischen Petrographie. Zweite Auflage; Gebruder Borntraeger, Berlin.

(*f*) G. W. Morey, "The Interpretation of Phase Equilibrium Diagrams," *Glass Ind.*, **12**, 69–80 (1931).

(*g*) G. W. Morey, "Analytical Methods in Phase-Rule Problems," *Jour. Phys. Chem.*, **34**, 1745–50 (1930).

as the crystallization curve follows a straight line, radiating from the composition of the separating solid to the intersection of the line with a boundary curve and along the boundary curve to the ternary eutectic. Crystallization curves in solid solution areas of ternary systems are not straight lines and the liquid follows a curved course in reaching the boundary curve. The composition of the solid changes as the temperature is lowered as was shown for binary systems (Fig. 5). In the discussion of crystallization in a ternary system containing solid solution it is necessary to know the position of the isotherms, boundary curves, and conjugation lines.[15] These conjugation lines have been referred to by some writers as solid-phase-indicating lines as they indicate the composition of the solid phase in equilibrium with a definite liquid base. In special cases where the extremities of these conjugation lines or solid-phase-indicating lines are on the boundary lines of the three-phase system, they are designated as three-phase boundaries. A simple case of solid solution in ternary systems is shown in Fig. 16, A and B. In the binary system A–B, the line $1'$–$5'$ (Fig. 16A) and similar lines parallel to the base give the composition of the solid phase in equilibrium with the liquid phase at the corresponding temperature. The line 5–4–6 (Fig. 16B) is the isotherm for the temperature T_1 and line $5'$–$4'$–$6'$ that for the temperature T_2.

The phases present at T_1 (Fig. 16B) are as follows:

Area 5–4–6, all liquid.
Area A–5–4–3, liquid 5 to 4 and solid solution A to 3.
Area 6–4–C, liquid 6 to 4 and solid C.
Area 3–4–C, liquid 4, solid solution 3, and solid C.
Area 3–C–B, solid C and solid solution 3 to B.

The phases present at T_2 (Fig. 16B) are as follows:

Area A–$5'$–$4'$–$6'$, all liquid.
Area $5'$–$4'$–$3'$, liquid $4'$ to $5'$ and solid solution $1'$ to $3'$.
Area $6'$–$4'$–C, liquid $6'$ to $4'$ and solid C.
Area $3'$–$4'$–C, liquid $4'$, solid solution $3'$, and solid C.
Area $3'$–C–B, solid C and solid solution $3'$ to B.

The points 4 and $4'$ represent the composition of liquids in equilibrium with two solid phases, namely, a solid solution at either 3 or $3'$ and a solid of composition C, and they lie on the boundary E_1–E_2 of Fig. 16A. As the extremities of the lines 3–4 and $3'$–$4'$ lie on boundaries of the ternary system these lines are two of the many possible three-phase boundaries which are shown in Fig. 16C. Any melts represented by a composition in the area Z–Y–C (Fig. 16C) on crystallizing follow a radial line from C with phase C separating out until the boundary Z–Y is reached at which point of intersection a solid solution begins to separate out. The composition of the solid solution at any given temperature is represented by the other extremity of three-phase boundary at that temperature. Thus a

[15] See footnote 14 (*c*).

liquid solution of composition 4′ is in equilibrium with solid solution of composition 3′ and solid *C*. As the temperature drops the liquid solution changes in composition along *Y–Z* toward *Y* while at the same time the solid solution is changing along *B–A* toward *A* and the solid *C* remains unchanged in composition. All solutions do not reach *Y* before complete solidification takes place as the original composition of the melt determines the final solidification temperature and the temperature at which incipient fusion takes place.

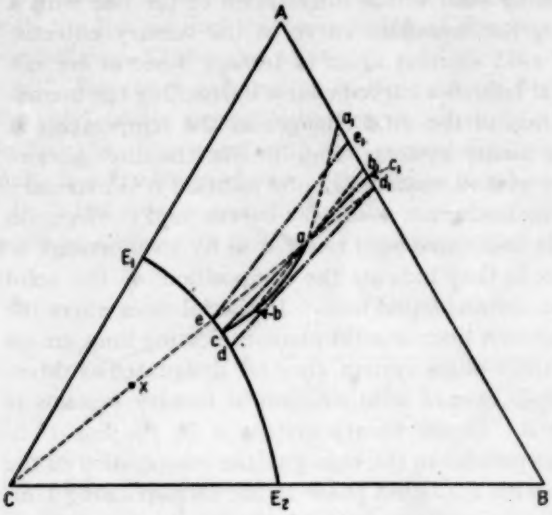

FIG. 17.—Course of crystallization in a ternary system where one of the binary systems is a complete solid solution series (modified from N. L. Bowen, *Amer. Jour. Sci.*, 4th Ser., 40, 161–89 (1916) (p. 179)).

For purposes of discussion consider a system shown in Fig. 17, which is somewhat similar to that shown in Fig. 16A. The line *a–c* is the crystallization curve for melt *a* to the boundary E_1E_2. The first solid to separate is represented by a_1. As the temperature drops the composition of the liquid changes along *a–b–c*. When the composition of the liquid has reached *b*, the composition of the solid solution has changed to b_1. The crystallization curve reaches the boundary E_1E_2 at *c*, which is on the three-phase boundary $c–a–c_1$ through the point *a*. The composition of

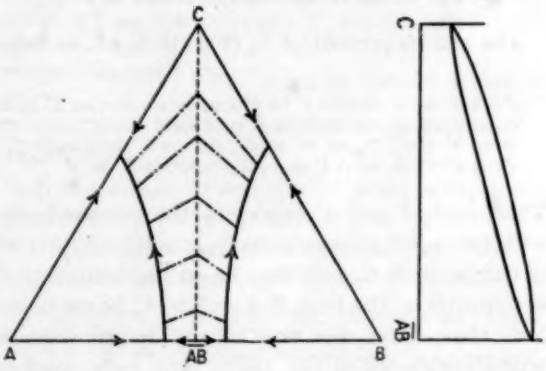

FIG. 18.—A ternary system containing a binary compound stable at its melting point which forms a complete series of solid solutions with the third component (N. L. Bowen, *Amer. Jour. Sci.*, 4th Ser., 38, 207–64 (1914) (p. 223)).

the solid solution in equilibrium with the liquid solution c is c_1. The simultaneous crystallization of C and solid solution continues along E_1E_2 toward E_2. At point d, which is on a three-phase boundary with d_1 (d_1 being the intersection of line Cd with the base AB), all of the liquid is used up and complete solidification takes place. The solid mixture consists of solid C and solid solution of composition d_1. All of this occurs on the assumption that the crystallization is taking place at a sufficiently slow rate so as to permit the solid solution to attain equilibrium at every instant with the liquid solution. A melt of composition x (Fig. 17) will crystallize as follows: Solid C will begin to crystallize when the temperature has reached the isotherm passing through the intersection of the vertical projection of x with the melting surface C–E_1–E_2. Solid C continues to crystallize along x–e until point e is reached, when a solid solution of composition e_1 (the intersection of the three-phase boundary through e with the base A–B) begins to separate with solid C, and the crystallization continues along E_1–E_2 toward E_2 with change in composition of the liquid phase as represented by points on E–E_2 and change in composition of solid solution as represented by the other extremities of the three-phase boundaries on the base line A–B. At point d the liquid phase is completely used up and solidification takes place. The final composition of the solid solution in equilibrium with liquid solution d is again d_1 and this solid solution is the one found in the solidified product of the melt x along with solid C.

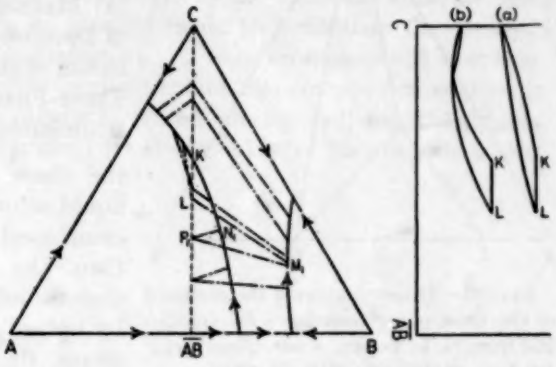

FIG. 19.—A ternary system containing a binary compound unstable at its melting point which forms a series of solid solutions with the third component (see N. L. Bowen, *Amer. Jour. Sci.*, 4th Ser., **38**, 207–64 (1914) (p. 225)). See also N. L. Bowen, The Evolution of Igneous Rocks, Princeton University Press.

Figure 18 illustrates a case where the compound $\overline{AB}$ forms a complete series of solid solutions with the component C. This case can be considered as two ternary systems of the type represented in Fig. 16A, namely, systems C–$\overline{AB}$–A and C–$\overline{AB}$–B.

Figure 19 illustrates a case where the compound $\overline{AB}$ is unstable at its melting point and this system can not be treated as the last case was

treated. Mixtures in the region C–K behave as true binary mixtures. There are two possibilities in this region of the ternary system as are shown in Fig. 19 at (*a*) and (*b*). Mixtures in the region K to L behave on melting as true binary mixtures until the temperature of the isotherm passing through K is reached, at which point solid A begins to separate out. Mixtures between L and $\overline{AB}$ melt at temperatures above that of the point K with the separation of pure A. The broken lines in Fig. 19 are the three-phase boundaries for this type of system.

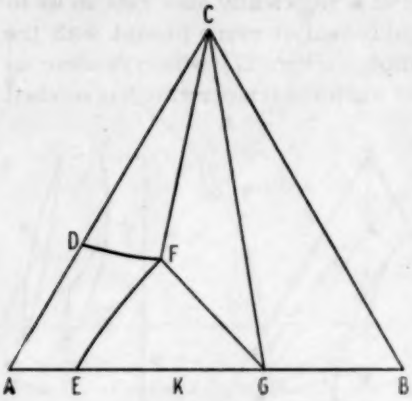

FIG. 20.—Determination of the position of the three-phase boundary, *FG* (modified from N. L. Bowen, *Amer. Jour. Sci.*, 4th Ser., **40**, 161–89 (1916) (p. 222)).

(a) Methods of Determination of the Three-Phase Boundaries[16]

(1) If a mixture in a system containing solid solutions is quenched from a definite temperature and found to contain the three phases, solid solution, liquid solution as glass, and a solid component of an adjacent field, then the determination of the composition of the solid solution by optical methods is sufficient to locate the three-phase boundary for the temperature from which the melt was quenched. This can be explained by the use of Fig. 20. Suppose that the lines D–F and F–E are the isotherms for the system A–B–C at the temperature T. The phases present in the areas are as follows:

Area *D*–*F*–*E*–*A*, all liquid.
Area *E*–*F*–*G*, liquid *E* to *F* and solid solution *K* to *G* (the solid solution *G* being in equilibrium with the liquid *C* at this temperature).
Area *C*–*D*–*F*, liquid *D* to *F* and solid *C*.
Area *C*–*F*–*G*, liquid *F*, solid solution *G*, and solid *C*.
Area *B*–*G*–*C*, solid solution, *GB* and solid *C*.

In order to be able to predict the phases present at T, it is necessary to know the position of the line FG or in other words the composition of the solid solution at the temperature T, which is the point G as F is already known. This composition may be determined by optical methods provided the optical properties, especially the refractive indices, of the complete series of solid solutions in the binary system are known. Lines CF and CG also bound the three-phase field CFG but are merely straight lines radiating from C.

(2) A three-phase boundary may also be determined by starting with a

[16] See footnote 14, p. 480; also N. L. Bowen, "System Diopside–Forsterite–Silica," *Amer. Jour. Sci.*, 4th Ser., **40**, 161–85 (1915).

mixture of known composition and (1) determining the temperature at which the three-phase area is entered by cooling the melt from a higher temperature to a lower temperature or (2) determining the temperature of beginning of melting by starting with a mixture of solid *C* (Fig. 20) and a solid solution of known composition lying between *A* and *B*.

III. Comments on the Diagrams

The diagrams of systems which form the major part of this publication are, for the most part, as nearly accurate copies as possible of the original diagrams. Where systems have been studied by more than one worker that version was taken which was thought by the compilers to be the most accurate. There has been no attempt made to recalculate the drawings and make them uniform in statement. It is to be understood that temperatures are given in degrees Centigrade and that composition is given in weight percentage unless otherwise stated on the individual diagrams. The arrangement is stated under Part II of the List of Illustrations, p. 459.

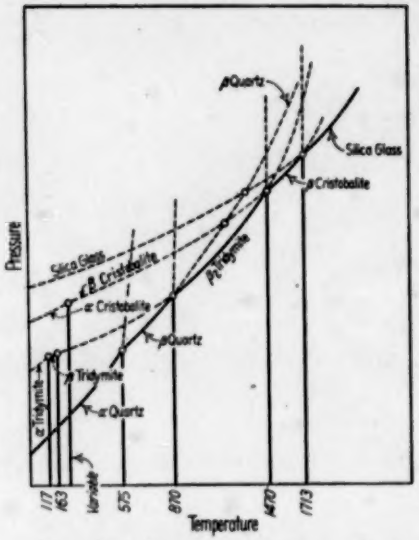

FIG. 22.—Stability relations of the silica minerals (Fenner, *Amer. Jour. Sci.*, 4th Ser., **36**, 331–84 (1913) (p. 338)); silica glass, β-cristobalite inversion point (taken from J. W. Greig, *ibid.*, 5th Ser., **13**, 1–44 (1927)).

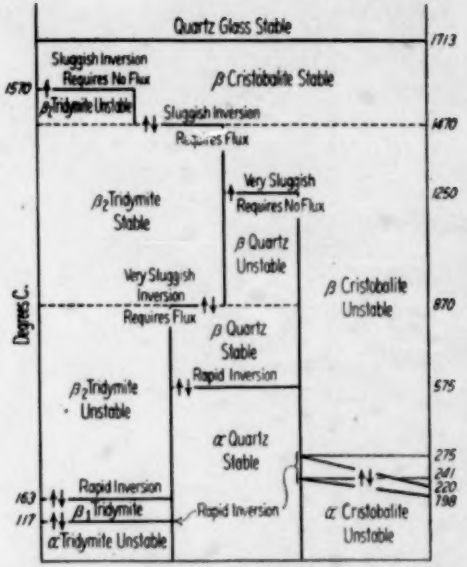

FIG. 21.—Stability relations of the silica minerals modified from J. S. McDowell (*Trans. Amer. Inst. Mining Met. Eng.*, **57**, 3–61 (1917) (p. 7)); melting point of cristobalite from J. W. Greig (*Amer. Jour. Sci.*, 5th Ser., **13**, 1–44 (1927)). See also Hewitt Wilson, Ceramics—Clay Technology, p. 206.

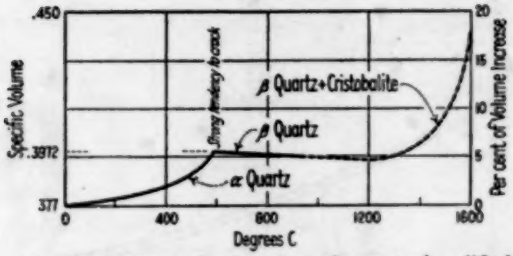

FIG. 23.—Thermal expansion of quartz (modified from A. L. Day, R. B. Sosman, and J. C. Hostetter, *Amer. Jour. Sci.*, 4th Ser., **37**, 1–39 (1914)). See also Hewitt Wilson, Ceramics—Clay Technology, p. 207.

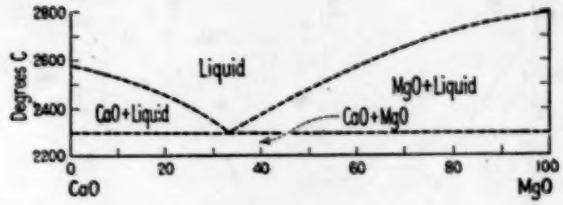

FIG. 24.—System CaO–MgO (G. A. Rankin and H. E. Merwin, *Jour. Amer. Chem. Soc.*, **38**, 568–88 (1916) (p. 571)). See also Hewitt Wilson, Ceramics—Clay Technology, p. 238.

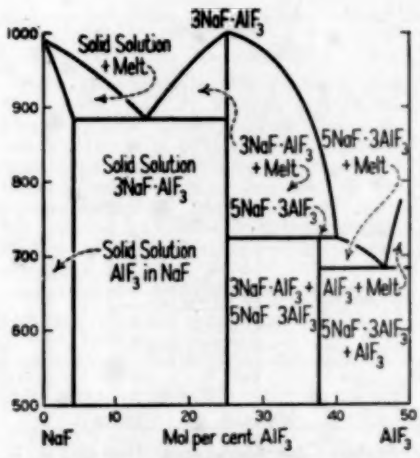

FIG. 25.—System NaF–AlF (Fedotieff and Iljinsky, *Z. anorg. Chem.*, **80**, 113–54 (1913) (adapted from diagram on p. 121)).

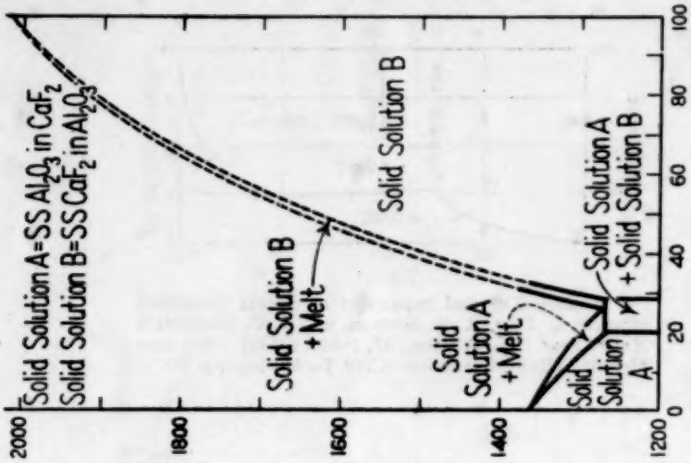

FIG. 26.—System CaF_2–Al_2O_3 (Pascal, Z. *Elektrochem.*, **19**, 610–13 (1913) (p. 611)).

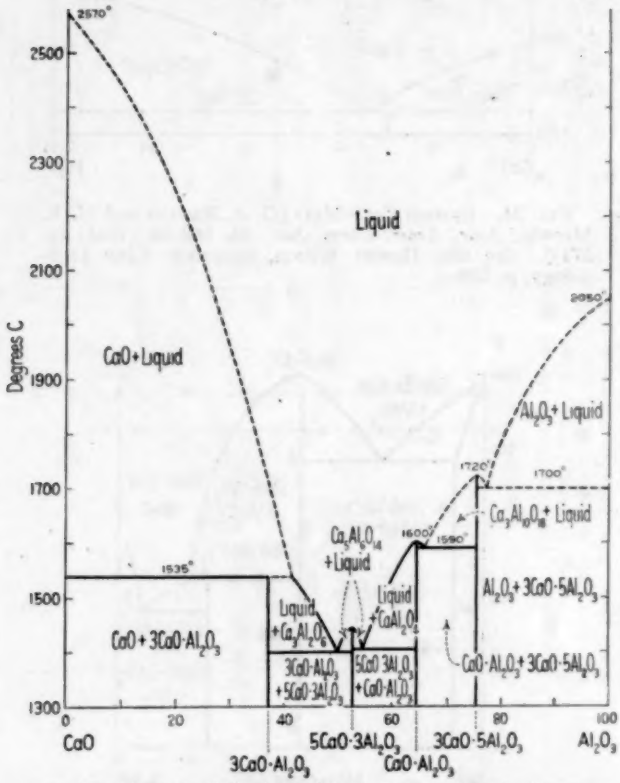

FIG. 27.—System CaO–Al_2O_3 (A. L. Day and R. B. Sosman, *Amer. Jour. Sci.*, 4th Ser., **31**, 341–49 (1911); G. A. Rankin and F. E. Wright, *ibid.*, 4th Ser., **39**, 1–79 (1915) (p. 11)); E. S. Shepherd, G. A. Rankin, and F. E. Wright, *ibid.*, 4th Ser., **28**, 293–333 (1909) (p. 306)). See also Hewitt Wilson, Ceramics—Clay Technology, p. 235.

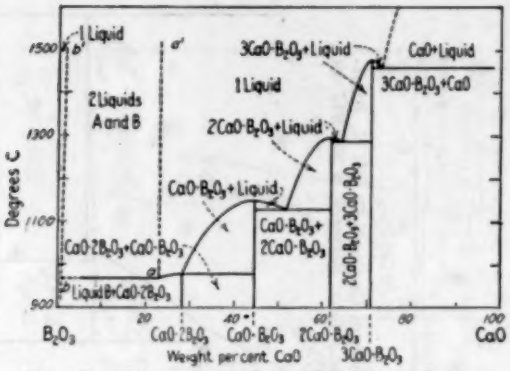

FIG. 28.—The system $CaO–B_2O_3$ (E. T. Carlson, Bur. Stand., *Jour. Research*, **9**, 825–32 (1932) (p. 830)).

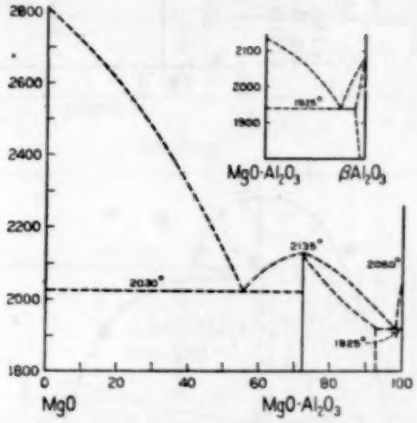

FIG. 29.—Systems $MgO–\alpha Al_2O_3$ and $MgO–\beta Al_2O_3$ (G. A. Rankin and H. E. Merwin, *Jour. Amer. Chem. Soc.*, **38**, 568–88 (1916) (p. 571)). *Errata:* Lower right-hand corner of lower figure should show lettering αAl_2O_3. See also G. A. Rankin and H. E. Merwin, *Amer. Jour. Sci.*, 4th Ser., **45**, 301–25 (1918) (p. 304); Hewitt Wilson, Ceramics—Clay Technology, p. 236.

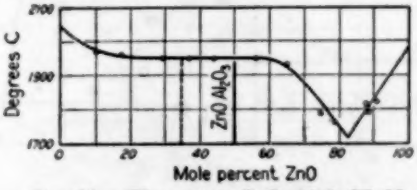

FIG. 30.—The system $ZnO–Al_2O_3$ (E. N. Bunting, Bur. Stand., *Jour. Research*, **8**, 279–87 (1932) (p. 280)).

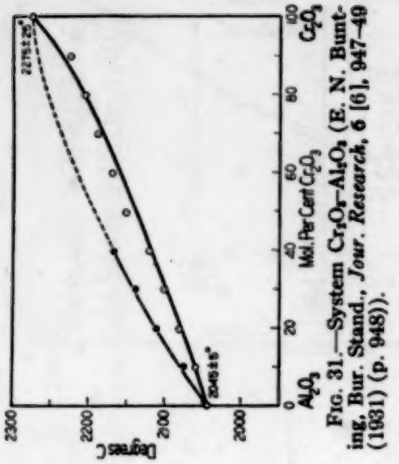

FIG. 31.—System Cr_2O_3–Al_2O_3 (E. N. Bunting, Bur. Stand., *Jour. Research*, **6** [6], 947–49 (1931) (p. 948)).

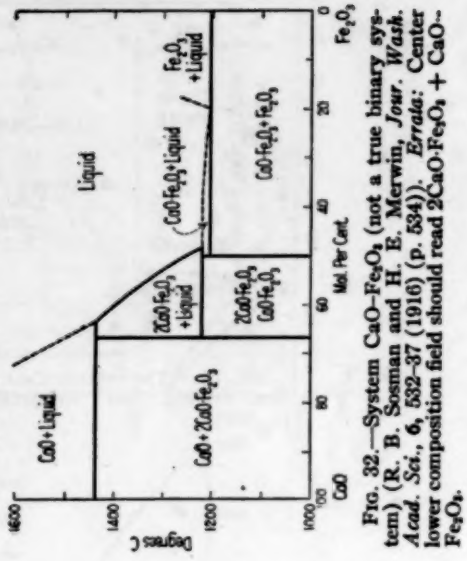

FIG. 32.—System CaO–Fe_2O_3 (not a true binary system) (R. B. Sosman and H. E. Merwin, *Jour. Wash. Acad. Sci.*, **6**, 532–37 (1916) (p. 534)). *Errata:* Center lower composition field should read 2CaO·Fe_2O_3 + CaO–Fe_2O_3.

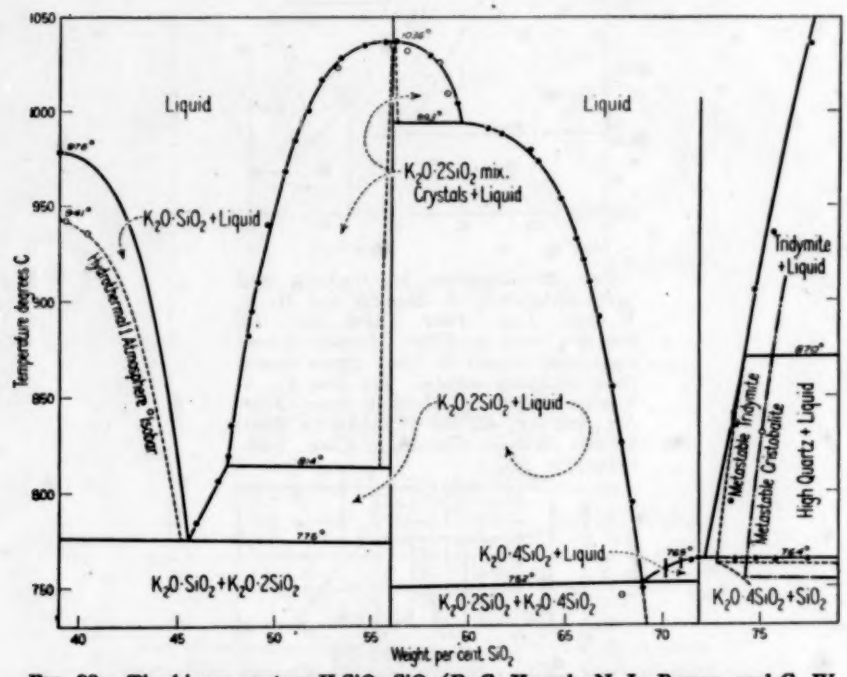

FIG. 33.—The binary system K_2SiO_3–SiO_2 (F. C. Kracek, N. L. Bowen, and G. W. Morey, *Jour. Phys. Chem.*, **33**, 1857–79 (1929) (p. 1872)). See also Glastechnische Tabellen, p. 22.

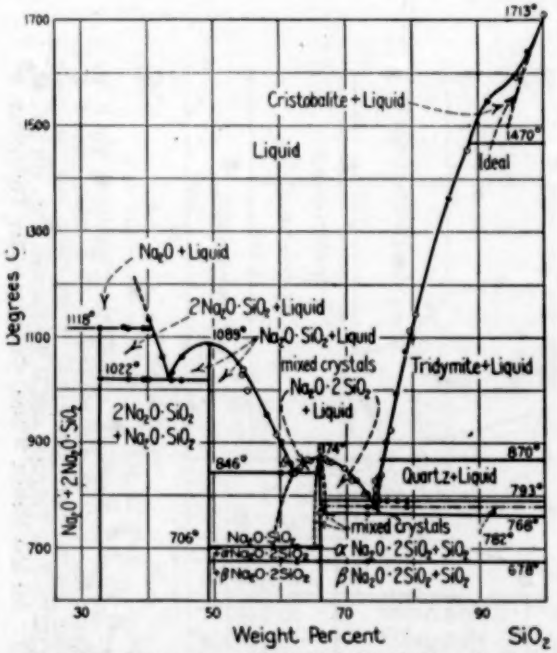

FIG. 35.—The system Na_2O–SiO_2 (F. C. Kracek, *Jour. Phys. Chem.*, **34**, 1583–98 (1930) (p. 1588)). See also *Jour. Soc. Glass Tech*, **9**, 240 (1925). See also Hewitt Wilson, Ceramics—Clay Technology, p. 243; Glastechnische Tabellen, p. 20.

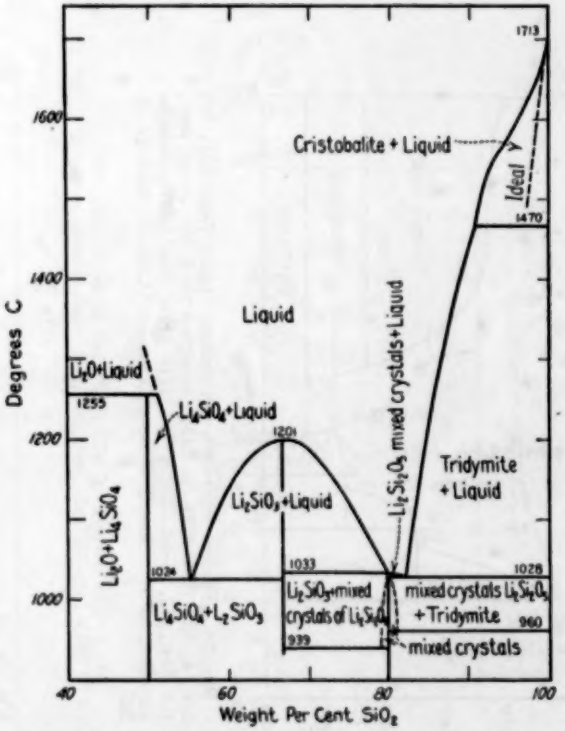

FIG. 34.—The system Li_2O–SiO_2 (F. C. Kracek, *Jour. Phys. Chem.*, **34**, 2641–50 (1930) (p. 2645)). See also Glastechnische Tabellen, p. 18.

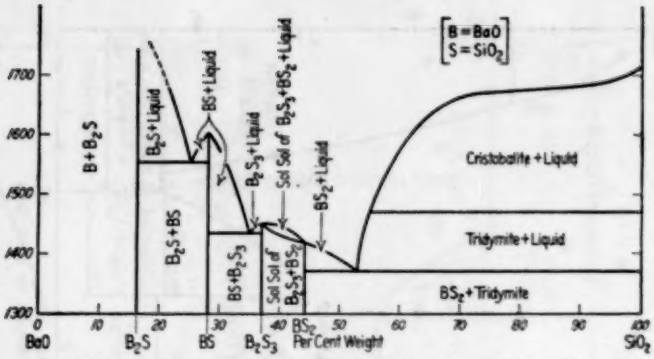

FIG. 36.—System BaO–SiO_2 (P. Eskola, *Amer. Jour. Sci.*, 5th Ser., **4**, 331–75 (1922) (p. 345); modified by J. W. Greig, *ibid.*, 4th Ser., **13**, 1–44 (1927) (p. 27)). See also Glastechnische Tabellen, p. 31; Hewitt Wilson, Ceramics—Clay Technology, p. 247.

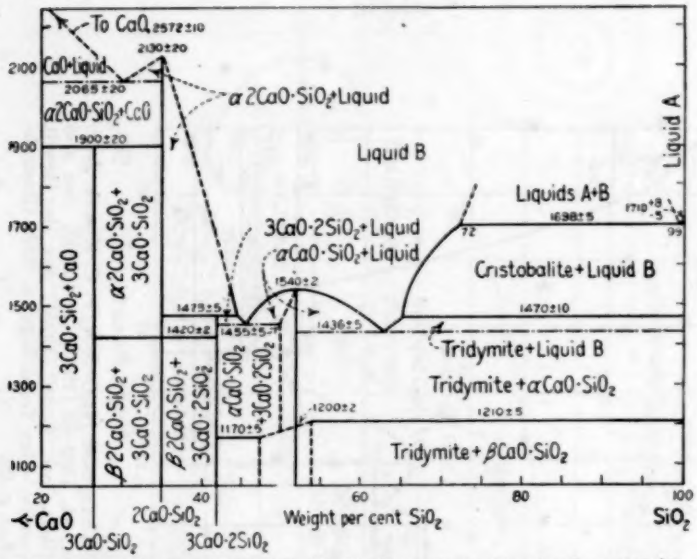

FIG. 37.—System CaO–SiO_2 (A. L. Day, E. S. Shepherd, and F. E. Wright, *Amer. Jour. Sci.*, **22**, 265–302 (1906); G. A. Rankin and F. E. Wright, *ibid.*, 4th Ser., **39**, 1–79 (1915); J. W. Greig, *ibid.*, 5th Ser., **13**, 1–44 (1927); J. B. Ferguson and H. E. Merwin, *ibid.*, 4th Ser., **48**, 81 (1919)). See also Hewitt Wilson, Ceramics—Clay Technology, p 233.

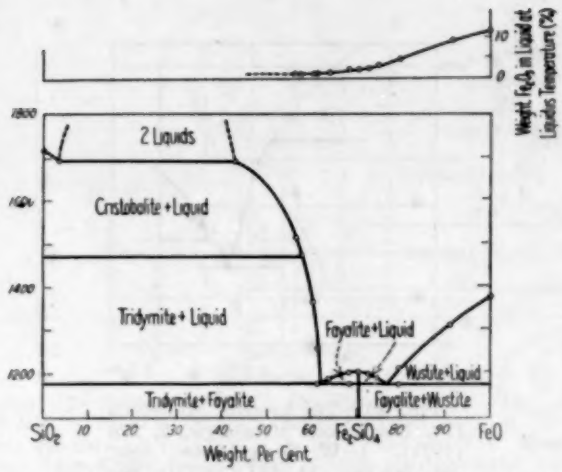

FIG. 38.—System FeO–SiO_2 (N. L. Bowen and J. F. Schairer, *Amer. Jour. Sci.*, 5th Ser., **24**, 177–213 (1932) (p. 200)).

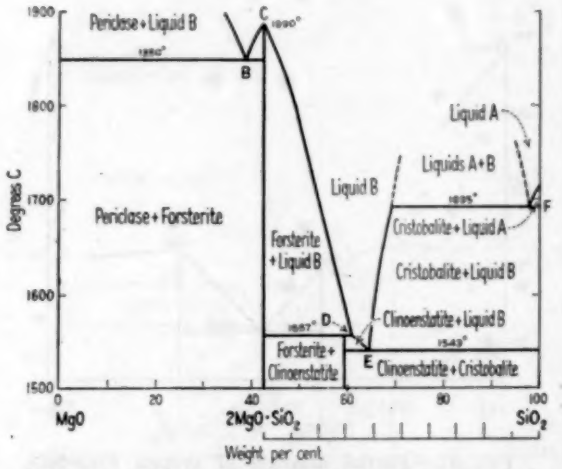

FIG. 39.—System MgO–SiO_2 (N. L. Bowen and O. Andersen, *Amer. Jour. Sci.*, 4th Ser., **37**, 487–500 (1914) (p. 488) and N. L. Bowen, *ibid.*, 4th Ser., **38**, 207–64 (1914); later modified by J. W. Greig, *ibid.*, 5th Ser., **13**, 1–44, 133–54 (1927) (p. 40)). See also Glastechnische Tabellen, p. 24; Hewitt Wilson, Ceramics—Clay Technology, p. 236.

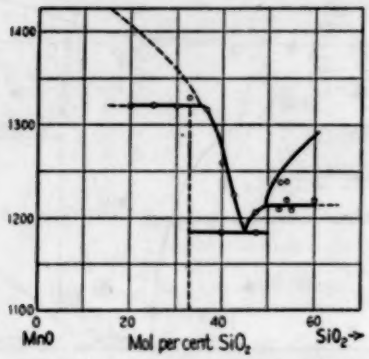

FIG. 40.—The system MnO–SiO_2 (Fr. Doerinckel, *Metallurgie*, **8**, 208 (1911). J. W. Greig, *Amer. Jour. Sci.*, 5th Ser., **13**, 137 (1927)). See also Glastechnische Tabellen, p. 33; J. R. Cain, *Met. Chem. Eng.*, **23**, 879 (1920).

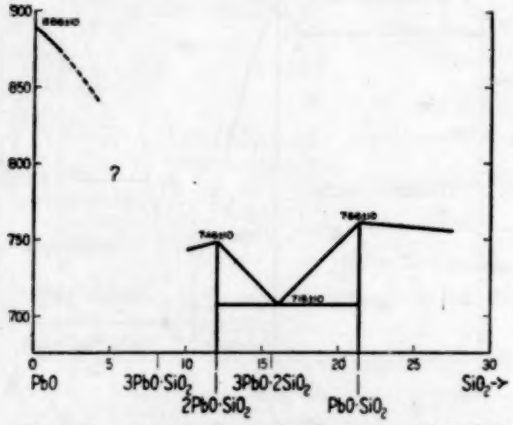

FIG. 41.—Partial diagram of system PbO–SiO_2 (H. C. Cooper, L. I. Shaw, and N. E. Loomis, *Amer. Jour. Sci.*, 4th Ser., **42**, 461 (1909); J. B. Ferguson, International Critical Tables, Vol. 4, 83–97 (1928) (p. 86)). See also K. A. Krakau and N. A. Vakhrameev, *Trans. Opt. Inst.* [Leningrad], **7** [70], 1–32 (1931); Glastechnische Tabellen, p. 36.

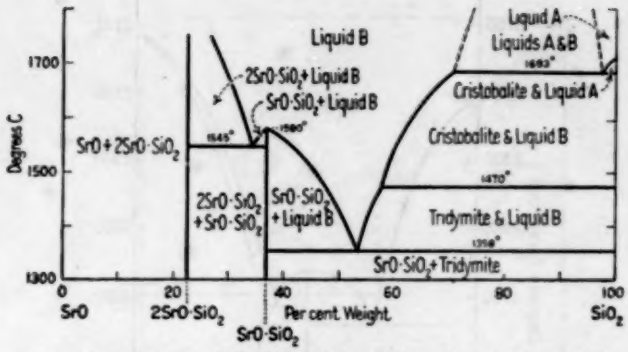

FIG. 42.—System SrO–SiO_2 (P. Eskola, *Amer. Jour. Sci.*, 5th Ser., **4**, 331–75 (1922) (p. 336); modified by J. W. Greig, *ibid.*, 5th Ser., **13**, 1–44 (1927) (p. 19)). See also F. C. Kracek, *Jour. Amer. Chem. Soc.*, **52**, 1440 (1930); Glastechnische Tabellen, p. 30; Hewitt Wilson, Ceramics—Clay Technology, p. 248.

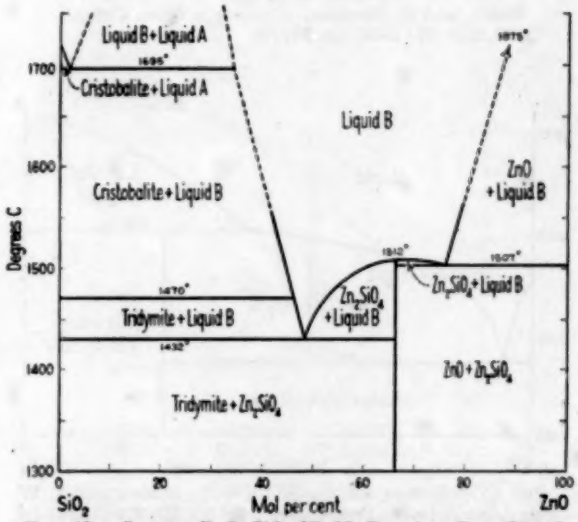

FIG. 43.—System ZnO–SiO_2 (E. N. Bunting, Bur. Stand., *Jour. Research*, **4**, 131–36 (1930) (p. 134)). See also E. N. Bunting, *Jour. Amer. Ceram. Soc.*, **13** [1], 5–10 (1930) (p. 8); Glastechnische Tabellen, p. 35.

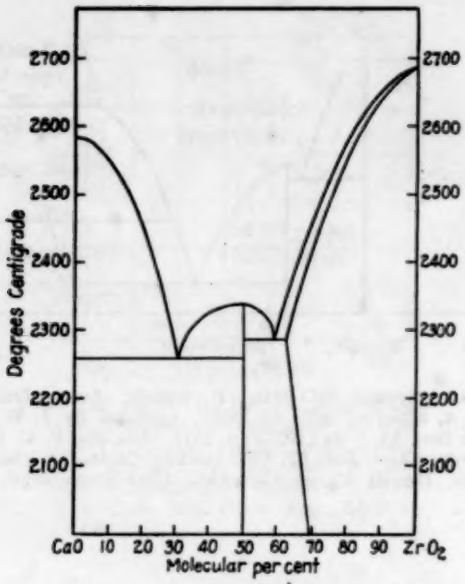

FIG. 44.—System ZrO_2–CaO (O. Ruff, F. Ebert, and E. Stephan, *Z. anorg. allgem. Chem.*, **180**, 215–24 (1929) (p. 219)).

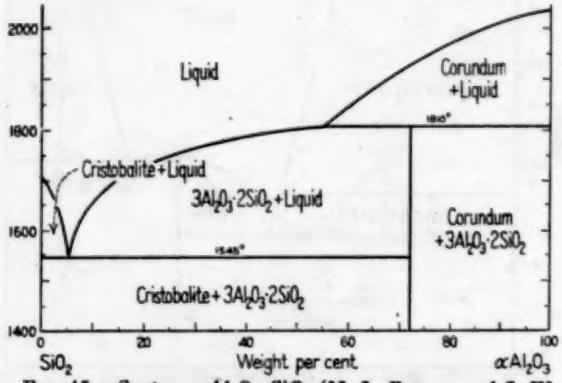

FIG. 45.—System αAl_2O_3–SiO_2 (N. L. Bowen and J. W. Greig, *Jour. Amer. Ceram. Soc.*, **7** [4], 238–54 (1924) (p. 242); N. L. Bowen and J. W. Greig, *Jour. Wash. Acad. Sci.*, **14**, 183–91 (1924); J. W. Greig, *Jour. Amer. Ceram. Soc.*, **8** [8], 465–84 (1925); *Amer. Jour. Sci.*, 5th Ser., **11**, 1 (1926); *ibid.*, **13**, 1–44 (1927)). See also Glastechnische Tabellen, p. 37; Hewitt Wilson, Ceramics—Clay Technology, p. 232.

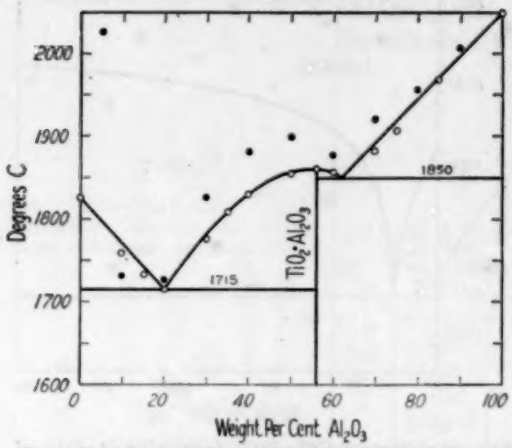

FIG. 46.—System Al_2O_3–TiO_2 (unpublished data of E. N. Bunting). Solid dots represent determinations of H. v. Wartenberg and H. J. Reusch, *Z. anorg. allgem. chem.*, **207**, 1–20 (1932) (p. 10).

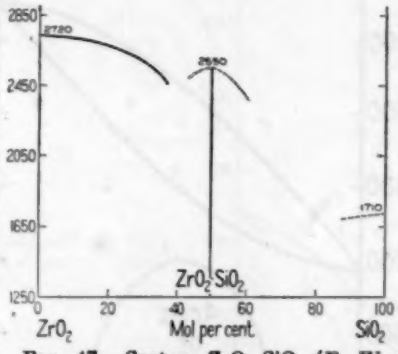

FIG. 47.—System ZrO_2–SiO_2 (E. W. Washburn and E. E. Libman, *Jour. Amer. Ceram. Soc.*, **3**, 634–40 (1920) (p. 638); H. v. Wartenberg and W. Gurr, *Z. anorg. allgem. Chem.*, **196**, 379–80 (1931) give as melting point ZrO_2–SiO_2; Glastechnische Tabellen, p. 39; Hewitt Wilson, Ceramics—Clay Technology, p. 249). See also Figs. 53 and 84.

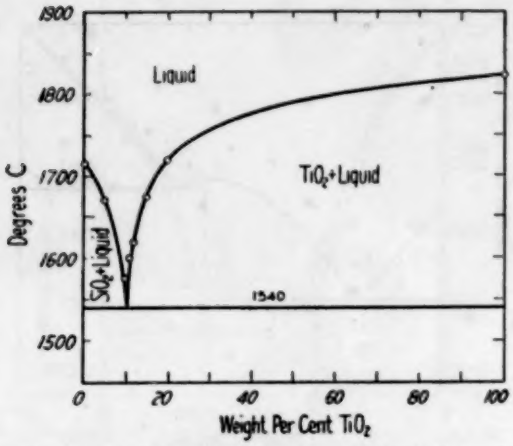

FIG. 48.—System SiO_2–TiO_2 (unpublished data of E. N. Bunting).

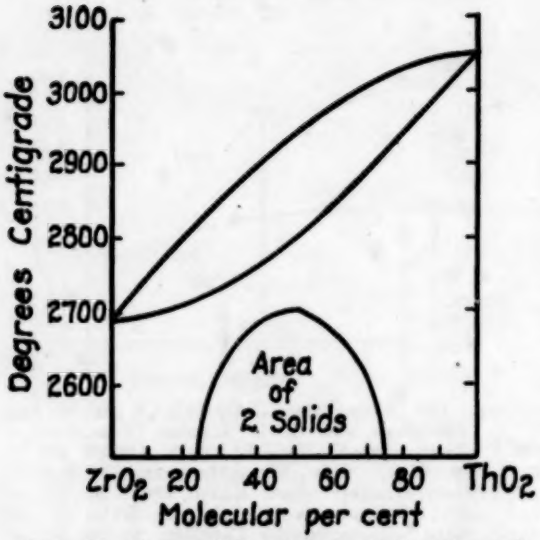

FIG. 49.—System ZrO_2–ThO_2 (probable diagram). (O. Ruff, F. Ebert, and H. Woitinek, *Z. anorg. allgem. Chem.*, **180**, 255 (1929) (p. 255)).

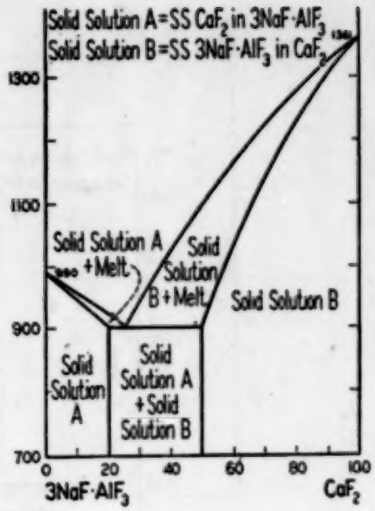

FIG. 50.—System CaF_2–$3NaF \cdot AlF_3$ (P. Pascal, *Z. Elektrochem.*, **19**, 610–13 (1913) (adapted from diagram on p. 611)).

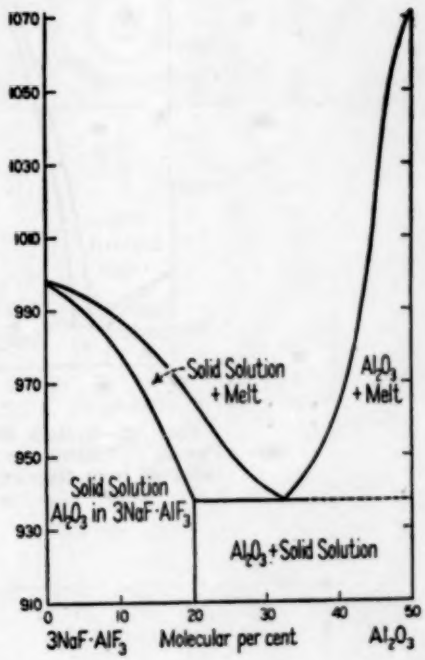

FIG. 51.—System Al_2O_3–$3NaF \cdot AlF_3$ (Lorenz, Jabs, and Eitel, *Z. anorg. Chem.*, **83**, 39–50 (1913) (p. 42)).

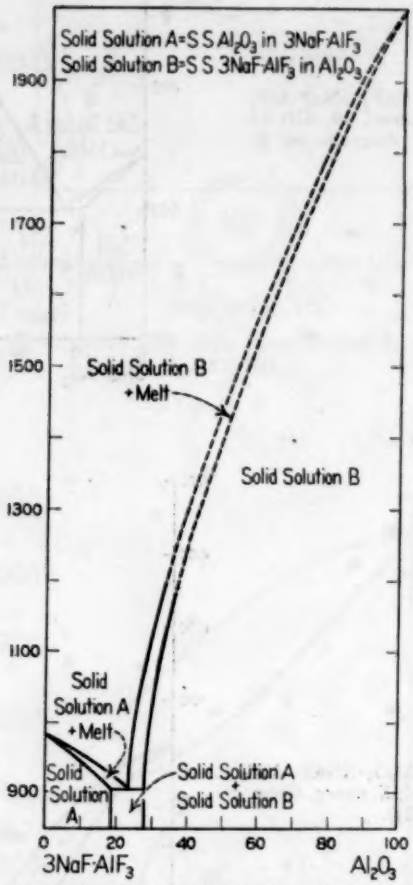

FIG. 52.—System 3NaF·AlF_3–Al_2O_3 (P. Pascal, *Z. Elektrochem.*, **19**, 610–13 (1913) (adapted from diagram on p. 611)).

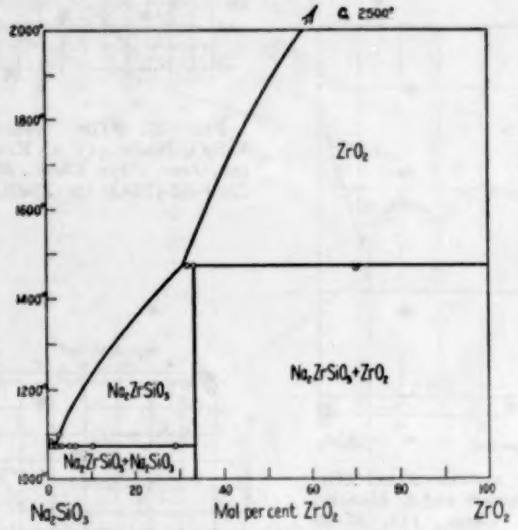

FIG. 53.—The system Na_2SiO_3–ZrO_2 (J. D'Ans and J. Löffler, *Z. anorg. allgem. Chem.*, **191**, 1–35 (1930) (p. 19)). See also Figs. 47 and 84.

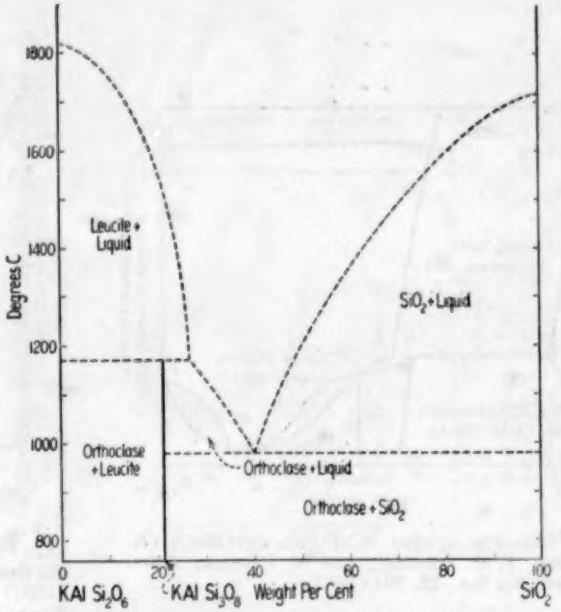

FIG. 54.—System $KAlSi_2O_6$–SiO_2 (G. W. Morey and N. L. Bowen, *Amer. Jour. Sci.*, 5th Ser., **4**, 1–21 (1922) (p. 10)). See also Hewitt Wilson, Ceramics—Clay Technology, p. 46.

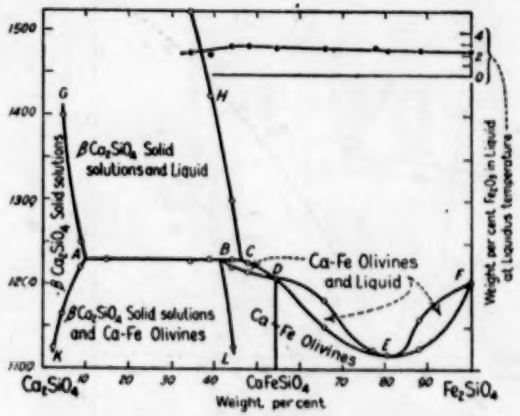

FIG. 58.—The system $2CaO \cdot SiO_2$–$2FeO \cdot SiO_2$ (N. L. Bowen, J. F. Schairer, and E. Posnjak, *Amer. Jour. Sci.*, 5th Ser., **25**, 281 (1933)).

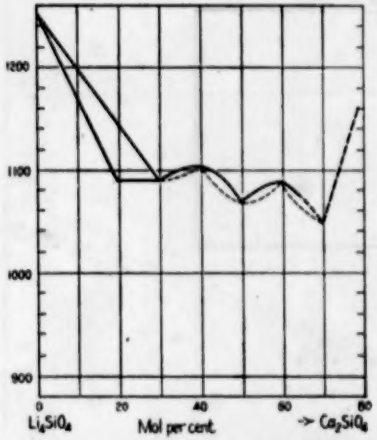

FIG. 57.—The system $2Li_2O \cdot SiO_2$–$2CaO \cdot SiO_2$ (R. Schwarz and A. Haacke, *Z. anorg. allgem. Chem.*, **115**, 87–99 (1921) (p. 95)). See also Glastechnische Tabellen, p. 40.

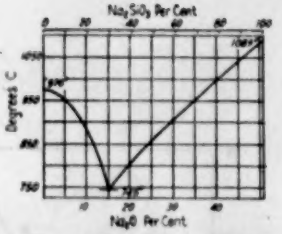

FIG. 55.—The system K_2SiO_3–Na_2SiO_3 (F. C. Kracek, *Jour. Phys. Chem.*, **36**, 2529–52 (1932) (p. 2540)).

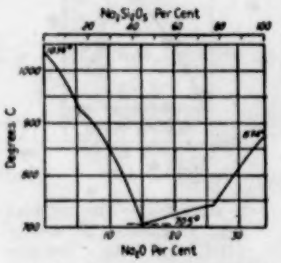

FIG. 56.—The system $K_2Si_2O_5$–$Na_2Si_2O_5$ (F. C. Kracek, *Jour. Phys. Chem.*, **36**, 2529–52 (1932) (p. 2540)).

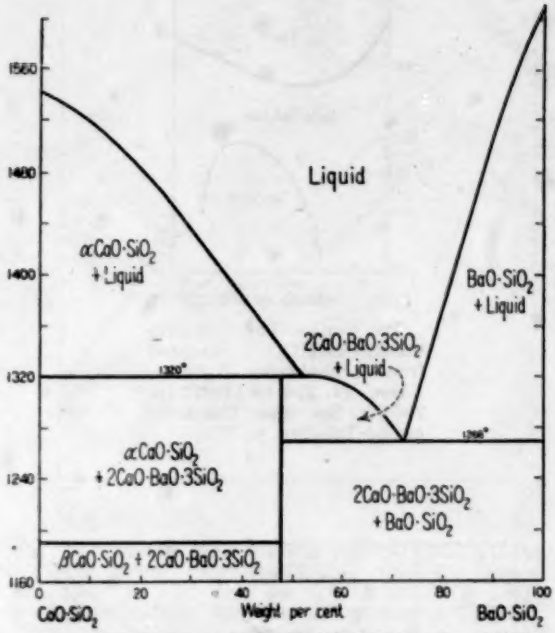

FIG. 59.—System $BaO{\cdot}SiO_2$–$CaO{\cdot}SiO_2$ (P. Eskola, *Amer. Jour. Sci.*, 5th Ser., **4**, 331–75 (1922) (p. 358)). See also Glastechnische Tabellen, p. 71.

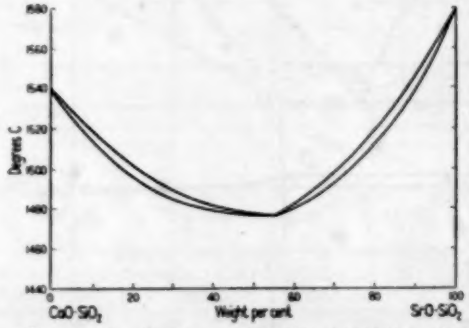

FIG. 60.—System $CaO{\cdot}SiO_2$–$SrO{\cdot}SiO_2$ (P. Eskola, *Amer. Jour. Sci.*, 5th Ser., **4**, 331–75 (1922) (p. 353)). Liquid above and solid solutions below the curves. See also Glastechnische Tabellen, p. 70.

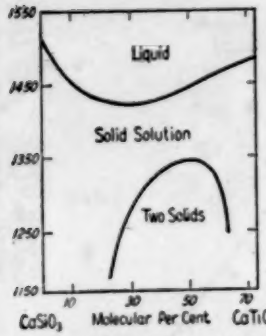

FIG. 61.—The system $CaSiO_3$–$CaTiO_3$ (adapted from S. Smolensky, *Z. anorg. Chem.*, **73**, 294–98 (1912) (p. 295)). See also Glastechnische Tabellen, p. 77.

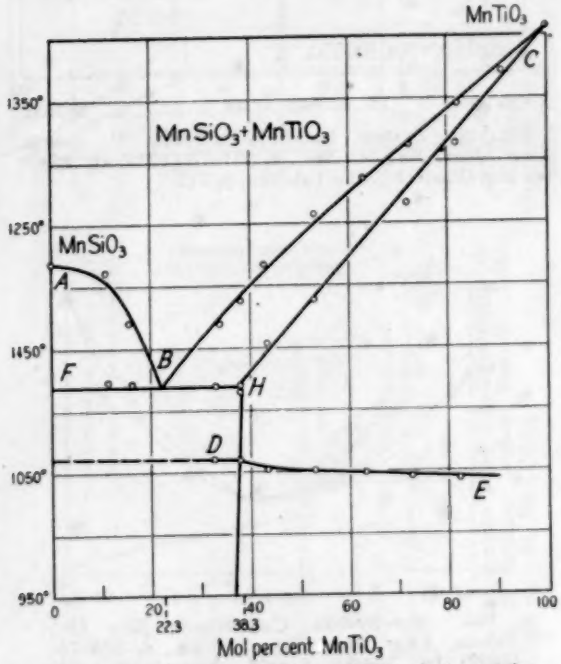

FIG. 62.—The system $MnSiO_3$–$MnTiO_3$ (adapted from S. Smolensky, *Z. anorg. Chem.*, **73**, 299 (1912)). See also Glastechnische Tabellen, p. 78.

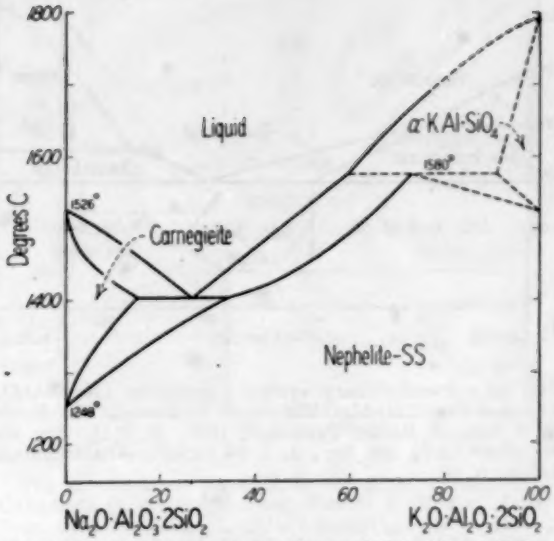

FIG. 63.—System nephelite (carnegieite) ($Na_2O \cdot Al_2O_3$–$2SiO_2$)–kaliophilite ($K_2O \cdot Al_2O_3 \cdot 2SiO_2$) (N. L. Bowen, *Amer. Jour. Sci.*, 4th Ser., **43,** 115–32 (1917) (p. 126)). *SS* = mixed crystals. See also Glastechnische Tabellen, p. 79.

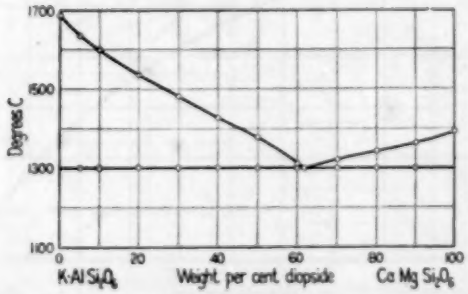

FIG. 64.—The binary system: leucite (K_2O–$Al_2O_3 \cdot 4SiO_2$)–diopside ($CaO \cdot MgO \cdot 2SiO_2$) (N. L. Bowen and J. F. Schairer, *Amer. Jour. Sci.*, 5th Ser., **18,** 301–12 (1929) (p. 304)). See also Glastechnische Tabellen, p. 88. Note: Above the liquidus the word "liquid" should be inserted; at the left below the liquidus, the words "leucite + liquid"; at the right below the liquidus, "diopside + liquid."

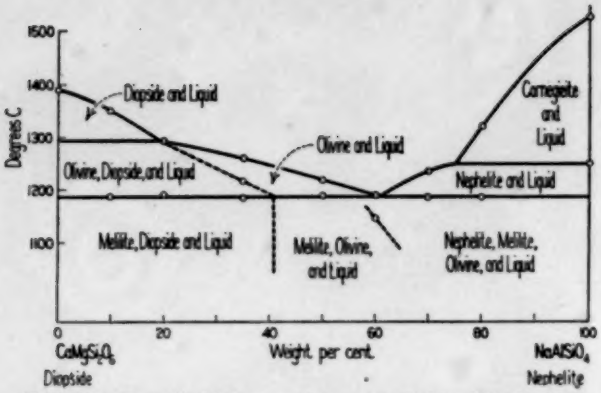

FIG. 65.—Pseudo-binary system: nephelite ($Na_2O \cdot Al_2O_3 \cdot 2SiO_2$)–diopside ($CaO \cdot MgO \cdot 2SiO_2$) (N. L. Bowen, The Evolution of Igneous Rocks, Princeton, 1928, p. 261). See also *Amer. Jour. Sci.*, 5th Ser., **3**, 1–34 (1922); Glastechnische Tabellen, p. 86.

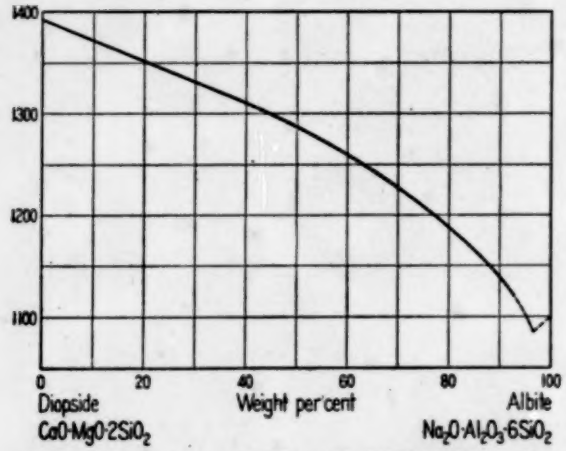

FIG. 66.—System diopside ($CaO \cdot MgO \cdot 2SiO_2$)–albite ($Na_2O \cdot Al_2O_3 \cdot 6SiO_2$) (N. L. Bowen, *Amer. Jour. Sci.*, 4th Ser., **40**, 161–85 (1915) (p. 165)). See also Glastechnische Tabellen, p. 87.

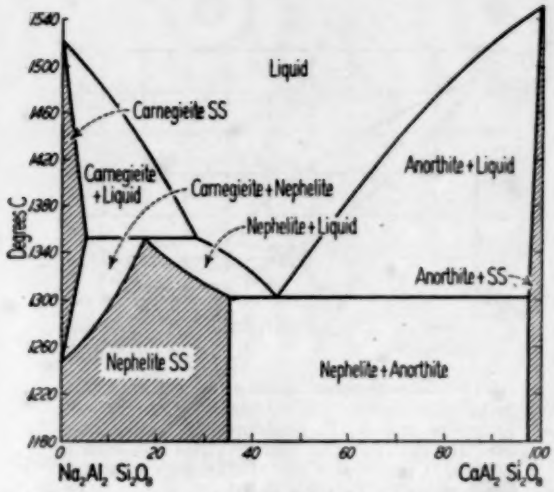

FIG. 67.—System $Na_2Al_2Si_2O_8$ (nephelite, carnegieite)–$CaAl_2Si_2O_8$ (anorthite) (according to N. L. Bowen, *Amer. Jour. Sci.*, 4th Ser., **33**, 551–73 (1912) (p. 559)); thesis, Massachusetts Institute of Technology, 1912; Glastechnische Tabellen, p. 81.

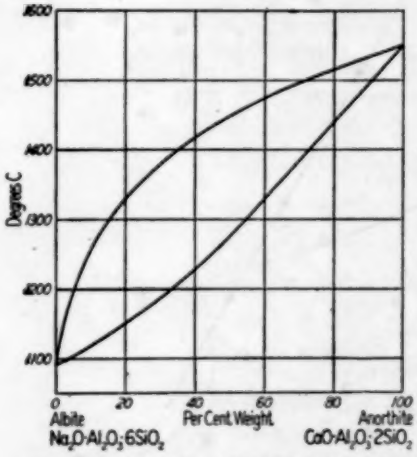

FIG. 68.—System albite ($Na_2O \cdot Al_2O_3 \cdot 6SiO_2$)–anorthite ($CaO \cdot Al_2O_3 \cdot 2SiO_2$) (N. L. Bowen, *Amer. Jour. Sci.*, 4th Ser., **40**, 161–85 (1915) (p. 164)). See also Hewitt Wilson, Ceramics—Clay Technology, p. 222; Glastechnische Tabellen, p. 81.

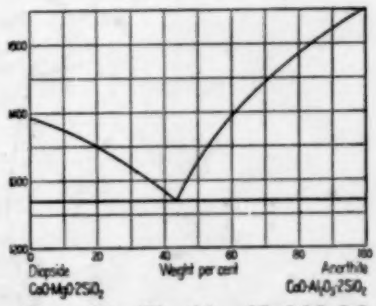

FIG. 69.—Diopside ($CaO \cdot MgO \cdot 2SiO_2$)–anorthite ($CaO \cdot Al_2O_3 \cdot 2SiO_2$) (N. L. Bowen, *Amer. Jour. Sci.*, 4th Ser., **40**, 161–85 (1915) (p. 164)). See also Hewitt Wilson, Ceramics—Clay Technology, p. 224; Glastechnische Tabellen, p. 84.

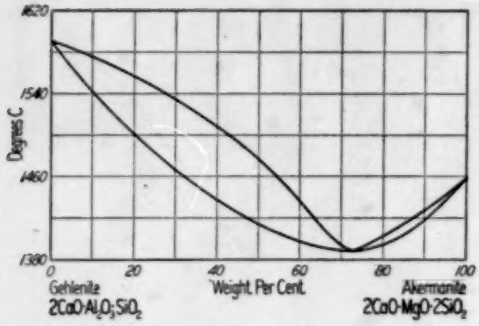

FIG. 70.—System gehlenite ($2CaO \cdot Al_2O_3 \cdot SiO_2$)–akermanite ($2CaO \cdot MgO \cdot 2SiO_2$) (J. B. Ferguson and A. F. Buddington, *Amer. Jour. Sci.*, 4th Ser., **50**, 131 (1920)). See also Hewitt Wilson, Ceramics—Clay Technology, p. 223; Glastechnische Tabellen, p. 84.

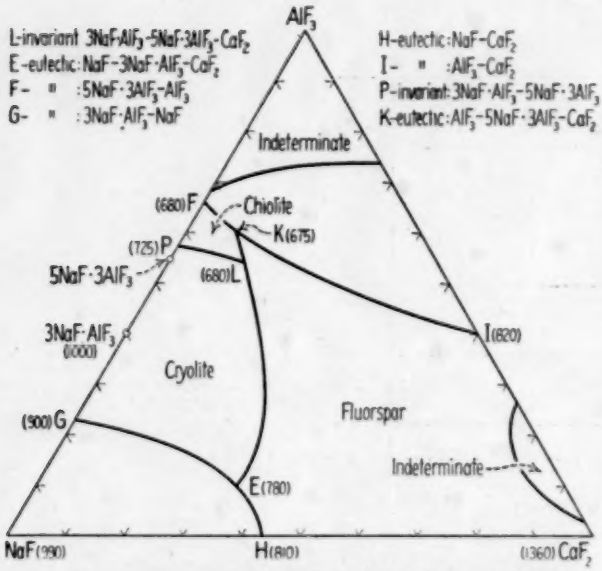

FIG. 71.—System AlF_3–NaF–CaF_2 (Fedotieff and Iljinsky, *Z. anorg. allgem. Chem.*, **129**, 93–107 (1923)).

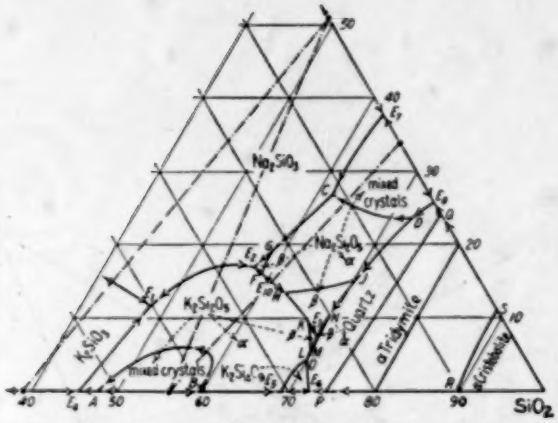

FIG. 72.—The system K_2SiO_3–Na_2SiO_3–SiO_2 (F. C. Kracek, *Jour. Phys. Chem.*, **36**, 2529–52 (1932) (p. 2538)).

A	= 814°	E	= 775°	HJ	= 678°
B	= 995°	E_6	= 752°	KL	= 590°
C	= 740°	E_8	= 764°	MN	= 573°
D	= 765°	E_7	= 846°	O	= 640°
E_1	= 645°	E_9	= 793°	PQ	= 870°
E_2	= 665°	E_{10}	= 705°	RS	= 1470°
E_3	= 540°	FG	= 678°		

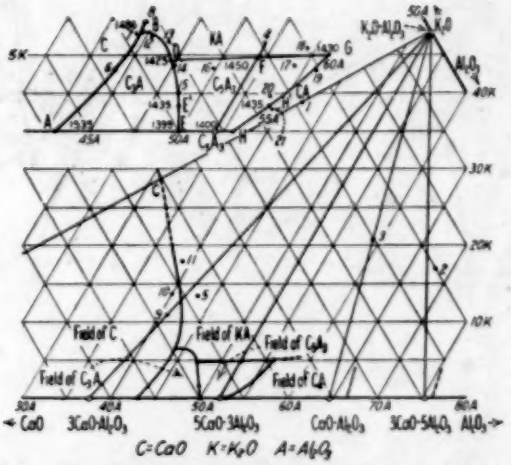

FIG. 73.—System K_2O–CaO–Al_2O_3 (unpublished work by L. T. Brownmiller).

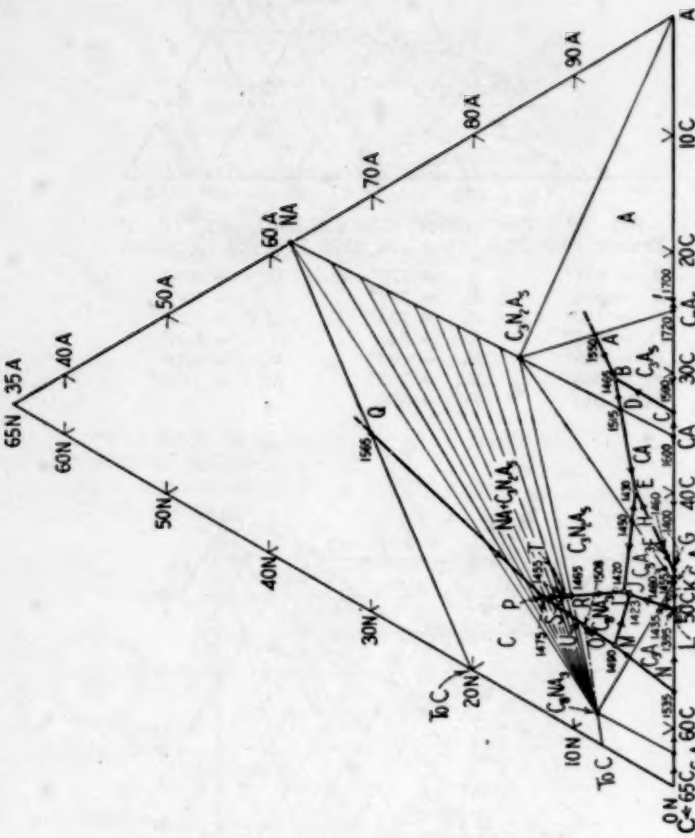

FIG. 74.—System CaO–Na_2O–Al_2O_3 (L. T. Brownmiller and R. H. Bogue, Bur. Stand., *Jour. Research*, **8**, 289–308 (1932) (p. 293)).

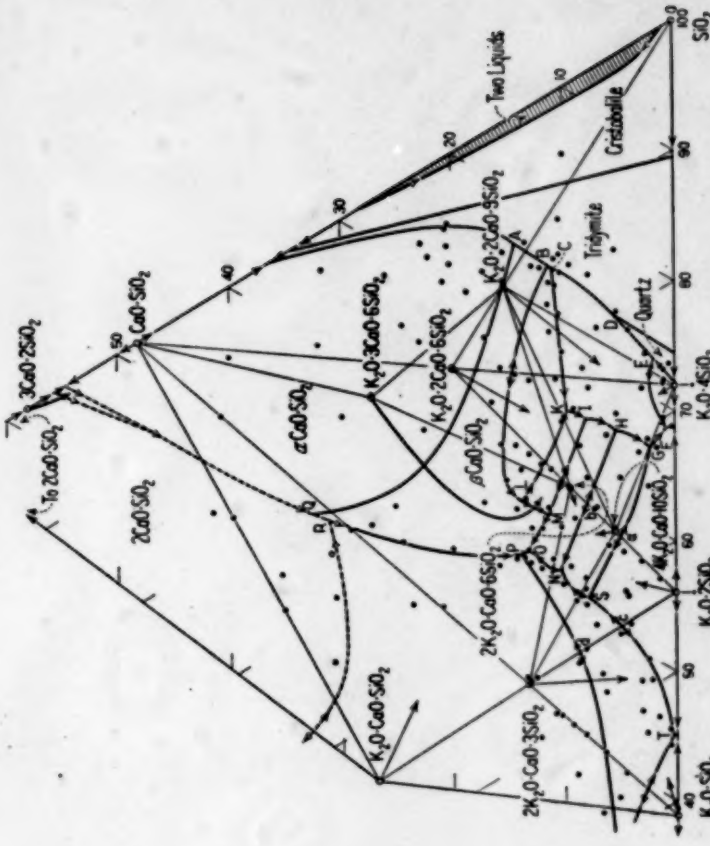

FIG. 75.—System K_2O–CaO–SiO_2 (G. W. Morey, F. C. Kracek, and N. L. Bowen, *Jour. Soc. Glass Tech.*, **14** [54], 149–87 (1930) (p. 158)). See also Glastechnische Tabellen, p. 56.

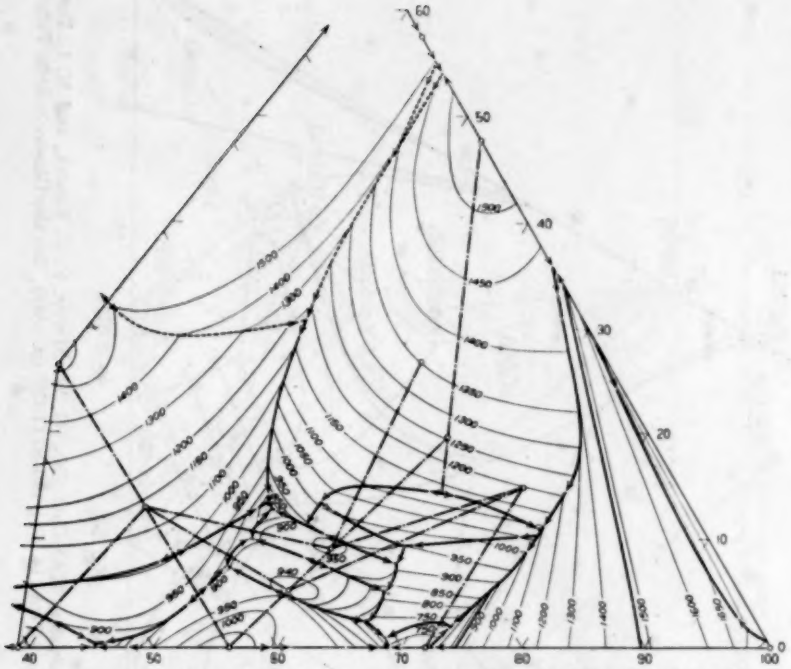

FIG. 76.—A portion of the ternary system K_2O–CaO–SiO_2; (G. W. Morey, F. C. Kracek, and N. L. Bowen, *Jour. Soc. Glass Tech.*, **14** [54], 149–87 (1930) (p. 158)). Isotherms are shown within the fields of the various compounds given on Fig. 75.

Compounds	CaO	Na_2O	SiO_2	Temp.	
SiO_2			100.0	1710	M
α $CaO \cdot SiO_2$	48.3		51.7	1540	M
β $CaO \cdot SiO_2$	48.3		51.7	1180	I
$Na_2O \cdot SiO_2$		50.8	49.2	1088	M
$Na_2O \cdot 2SiO_2$		34.1	65.9	874	M
$2Na_2O \cdot CaO \cdot 3SiO_2$	15.6	34.4	50.0	1141	D
$Na_2O \cdot 3CaO \cdot 6SiO_2$	28.5	10.5	61.0	1047	D
$Na_2O \cdot 2CaO \cdot 3SiO_2$	31.6	17.5	50.9	1284	M

M = Melting Point.
D = Decomposition Point.
I = Inversion Point.

Point		Crystal Phases	CaO	Na_2O	SiO_2	Temp.
▲	A	$NS-N_2CS_3$	3.0			1060
•	B	$N_2CS_3-NC_2S_3$	11.5			1141
▲	C	$NC_2S_3-\alpha CS$	33.0			1280
▲	D	$\alpha CS-S$	37.0		63.0	1436
•	E	T-Quartz		24.3	75.7	870
▲	F	Quartz-NS_2		26.4	73.6	790
•	K	$NS_2-NS-N_2CS_3$	1.8	31.5	60.7	821
○	L	$N_2CS_3-NC_2S_3-NS_2$	2.0	36.6	61.4	827
○	N	$NS_2-NC_2S_3-NC_3S_6$	5.2	24.1	70.7	740
•	O	$NC_2S_3-Q-NS_2$	5.2	21.3	73.5	725
•	P	$Q-NC_3S_6-T$	7.0	18.7	74.3	870
○	Q	$T-\beta CS-NC_3S_6$	12.9	13.7	73.4	1035
○	R	$NC_3S_6-NC_2S_3-\beta CS$	14.5	19.0	66.5	1030
•	S	$\beta CS-NC_2S_3-\alpha CS$	19.5	17.7	62.8	1110
•	T	$\alpha CS-S-\beta CS$	15.6	11.4	73.0	1110
▲	I	$NS-NS_2$		38.0		840

▲ Binary Eutectic
• Ternary Eutectic
• Decomposition Point
○ Reaction Point
○ Inversion Point
C = CaO N = Na_2O
S = SiO_2 Q = Quartz
T = Tridymite

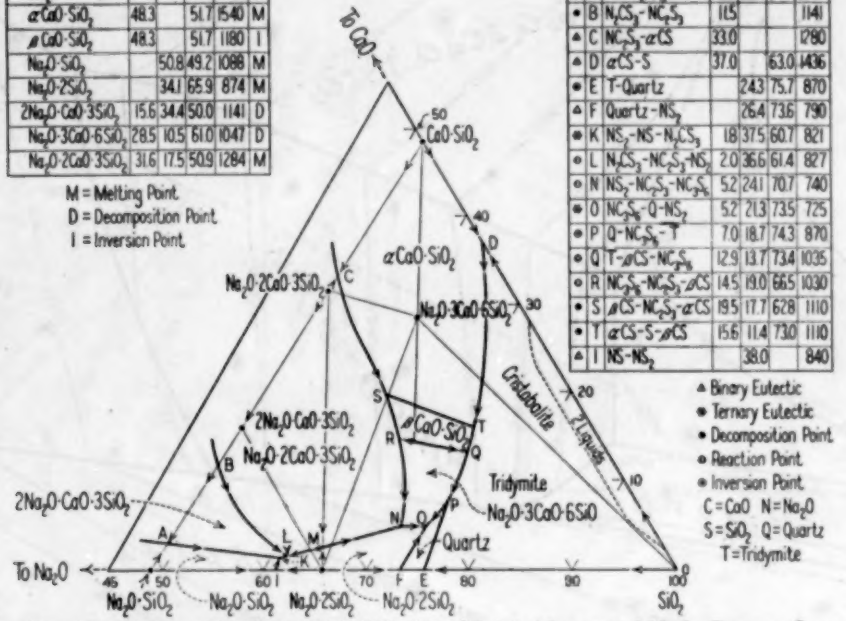

FIG. 77.—System $CaO \cdot SiO_2$–$Na_2O \cdot SiO_2$–SiO_2 (G. W. Morey and N. L. Bowen, *Jour. Soc. Glass Tech.*, **9**, 226–64 (1925) (p. 233)). See also Hewitt Wilson, p. 245; Glastechnische Tabellen, p. 43.

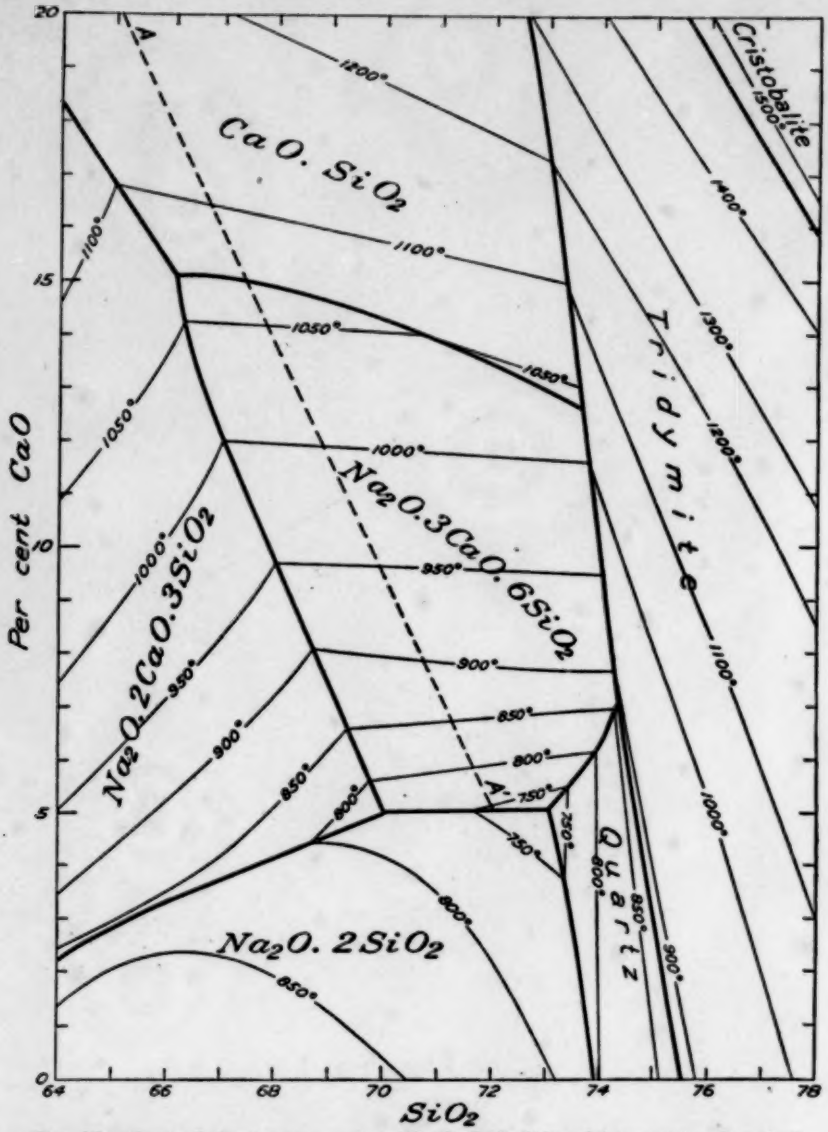

FIG. 78.—Part of the ternary system Na_2O–CaO–SiO_2, of interest to glass technology (G. W. Morey, *Jour. Amer. Ceram. Soc.*, 13 [10], 683 (1930)). Weight per cent SiO_2 is indicated along the horizontal axis; weight per cent CaO along the vertical axis; weight per cent Na_2O is obtained by subtracting the sum of CaO and SiO_2 from 100%.

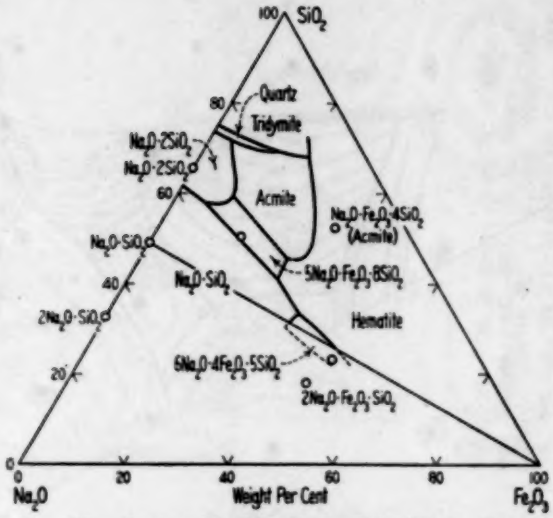

FIG. 79.—System Na_2SiO_3–Fe_2O_3–SiO_2 (N. L. Bowen, J. F. Schairer, and H. W. V. Willems, *Amer. Jour. Sci.*, 5th Ser., **20**, 405–55 (1930) (p. 435)). For details see Figs. 80, 81, 82, and 83. See also Glastechnische Tabellen, p. 48.

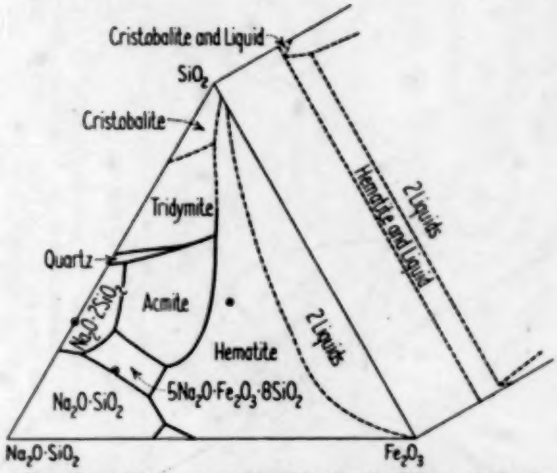

FIG. 80.—The system Na_2SiO_3–Fe_2O_3–SiO_2 and the indicated equilibrium diagram of the binary system SiO_2–Fe_2O_3 in broken lines (N. L. Bowen, J. F. Schairer, and H. W. V. Willems, *Amer. Jour. Sci.*, 5th Ser., **20**, 405–55 (1930) (p. 425)). See also Figs. 79, 81, 82, and 83.

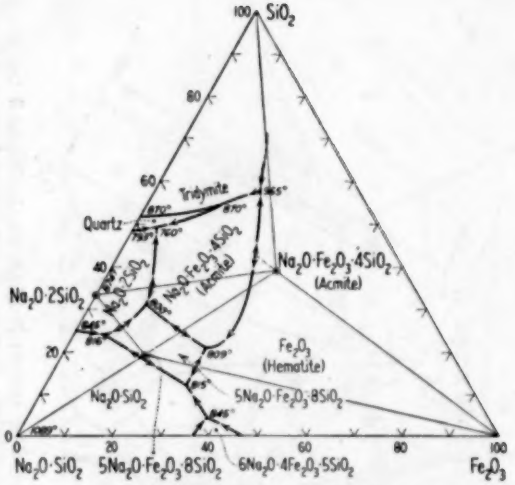

FIG. 82.—System Na_2SiO_3–Fe_2O_3–SiO_2 (N. L. Bowen, J. F. Schairer, and H. W. V. Willems, *Amer. Jour. Sci.*, 5th Ser., **20**, 405–55 (1930) (p. 419)). See also Figs. 79, 80, 81, and 83.

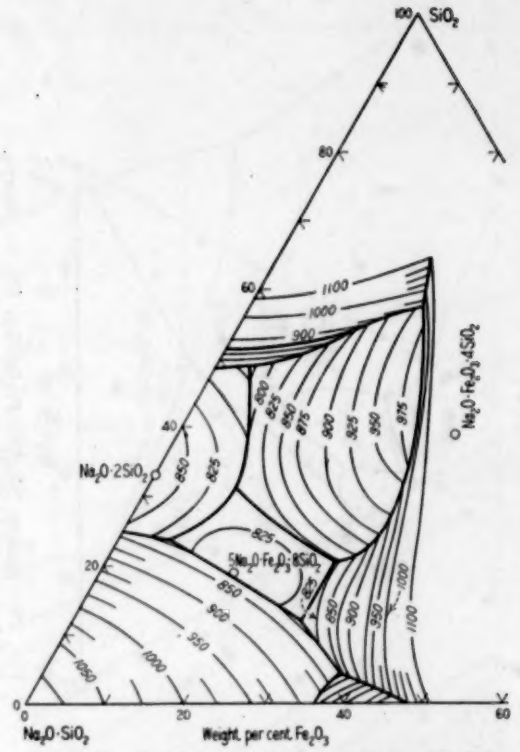

FIG. 81.—Isotherms of the system Na_2SiO_3–Fe_2O_3–SiO_2 (N. L. Bowen, J. F. Schairer, and H. W. V. Willems, *Amer. Jour. Sci.*, 5th Ser., **20**, 405–55 (1930) (p. 420)). See also Figs. 79, 80, 82, and 83.

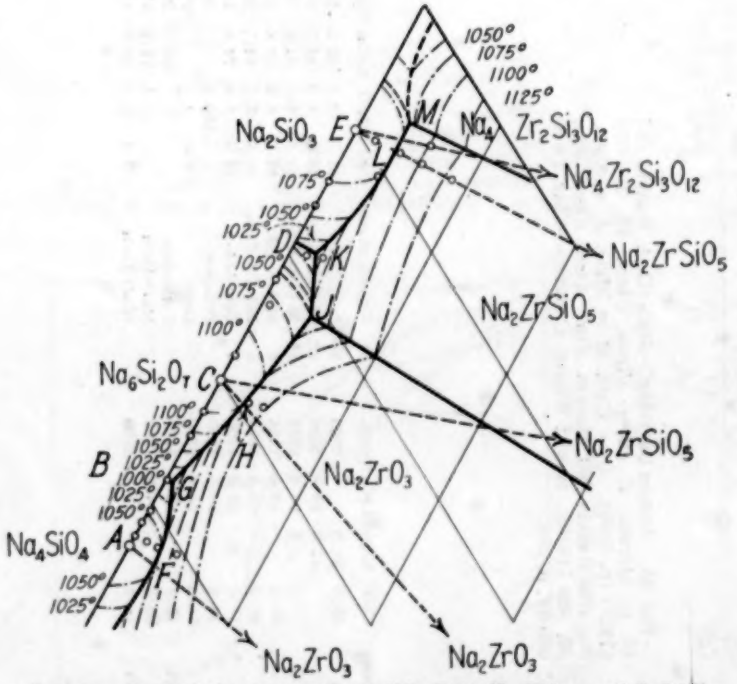

FIG. 84.—Part of the system Na_2O–SiO_2–ZrO_2 (J. D'Ans and J. Löffler, *Z. anorg. allgem. Chem.*, **191**, 1–35 (1930) (p. 22); Glastechnische Tabellen, p. 50). Doctor's dissertation of J. Löffler, Univ. of Berlin, 1930. See also Figs. 47 and 53.

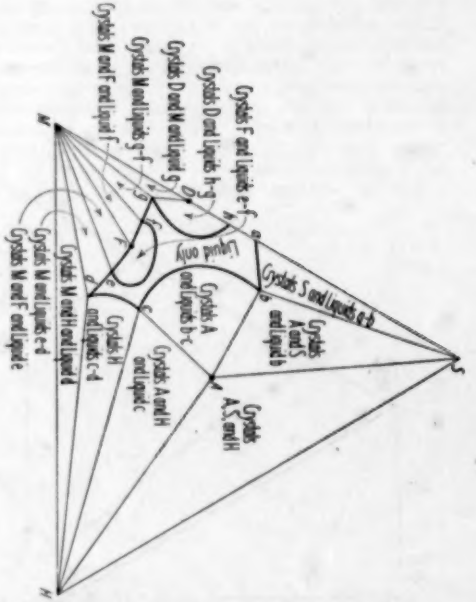

FIG. 83.—The isotherm of 825°C of the system Na_2SiO_3–Fe_2O_3–SiO_2 (N. L. Bowen, J. F. Schairer, and H. W. V. Willems, *Amer. Jour. Sci.*, 5th Ser., **20**, 405–55 (1930) (p. 421)). See also Figs. 79, 80, 81, and 82.

A	= $Na_2O{\cdot}Fe_2O_3{\cdot}4SiO_2$.	*H*	= Fe_2O_3.
D	= $Na_2O{\cdot}2SiO_2$.	*M*	= $Na_2O{\cdot}SiO_2$.
F	= $5Na_2O{\cdot}Fe_2O_3{\cdot}8SiO_2$.	*S*	= SiO_2.

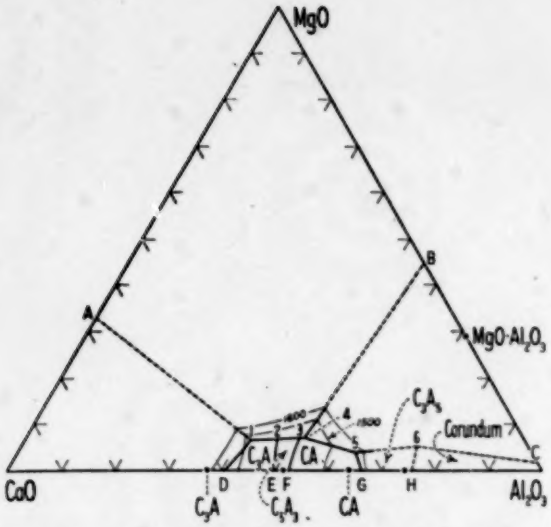

FIG. 85.—System CaO–MgO–Al_2O_3 (G. A. Rankin and H. E. Merwin, *Z. anorg. allgem. Chem.*, **96**, 291–316 (1916) (p. 309)). *C* = CaO, *M* = MgO, *A* = Al_2O_3. See also Rankin and Merwin, *Jour. Amer. Chem. Soc.*, **38**, 568 (1916); Hewitt Wilson, Ceramics—Clay Technology, p. 240.

Pt	Crystal phases	CaO	MgO	Al_2O_3	Temp.
A	C-M	67.0	33.0		2300
B	M-MA		45.0	55.0	2030
C	MA-A		2.0	98.0	1925
D	C-C_3A	59.0		41.0	1535
E	C_3A-C_3A_5	50.0		50.0	1395
F	C_3A_5-CA	47.0		53.0	1400
G	CA-CA_2	33.5		66.5	1590
H	CA_2-A	24.0		76.0	1700
	$5CaO·3Al_2O_3$	47.8		52.2	1455
	$CaO·Al_2O_3$	35.4		64.6	1600
	$3CaO·5Al_2O_3$	24.8		75.2	1720

Pt	Crystal phases	CaO	MgO	Al_2O_3	Temp.
1	M-C-C_3A	51.5	6.2	42.3	1450
2*	M-C_3A-C_3A_5	46.0	6.3	47.7	1345
3*	M-C_3A_5-CA	41.5	6.7	51.8	1345
4	M-MA-CA	45.7	6.9	52.4	1370
5	MA-CA-C_3A_5	33.3	3.5	63.2	1550
6	C_3A_5-MA-A	21.0	5.0	74.0	1680
	Periclase		100.0		2800
	Lime	100.0			2370
	Corundum			100.0	2050
	$MgO·Al_2O_3$		28.4	71.6	2135
	$3CaO·Al_2O_3$	62.2		37.8	1535

* Eutectic.

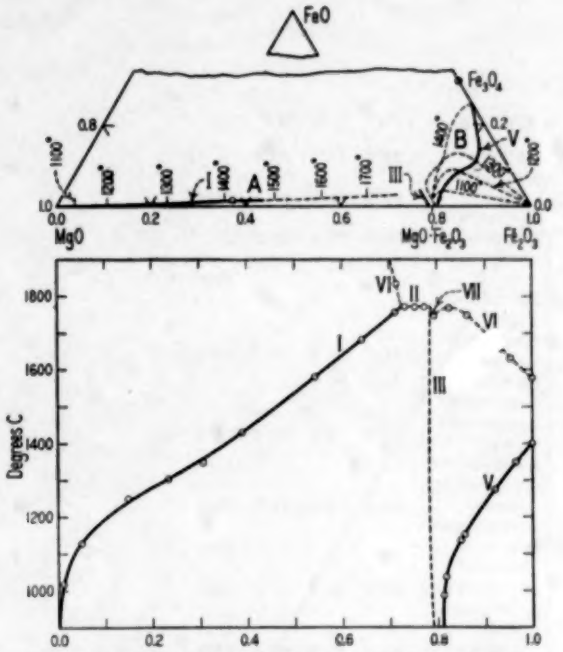

FIG. 86.—System MgO–FeO–Fe_2O_3 in air at one atmosphere (adapted from H. S. Roberts and H. E. Merwin, *Amer. Jour. Sci.*, 5th Ser., **21**, 145–57 (1931) (p. 150)). In the upper diagram compositions are expressed in weight per cent. In the lower diagram abscissae represent the compositions that would be obtained after oxidizing all of the iron to the ferric condition. The system has two solid solution fields, *A* and *B*. *Errata:* The Roman numeral VI above liquidus on the left should be Roman numeral IV. For 0.2, 0.4, 0.6, 0.8, and 1.0 on the sides of the triangular diagram read 20, 40, 60, 80, and 100, respectively.

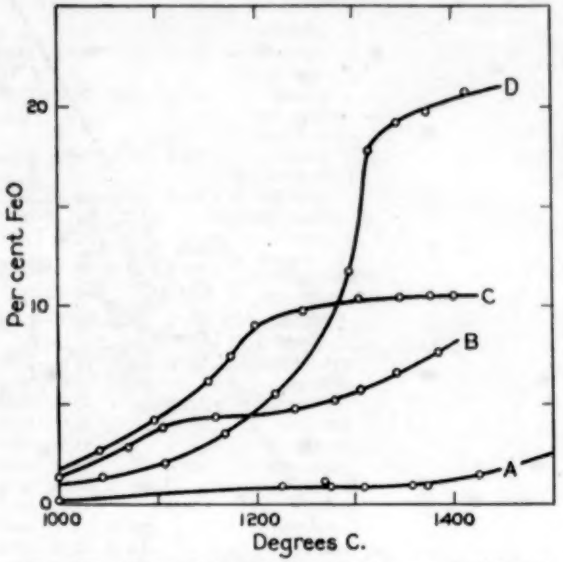

FIG. 87.—FeO and temperature for four compositions in solid solution field *B* (Fig. 86). System MgO–FeO–Fe_2O_3 (H. S. Roberts and H. E. Merwin, *Amer. Jour. Sci.*, 5th Ser., **21**, 145–57 (1931) (p. 151)).

Curve	Initial composition
A	80.0 Fe_2O_3, 20.0 MgO
B	82.9 " 17.1 "
C	86.8 " 13.2 "
D	94.1 " 5.9 "

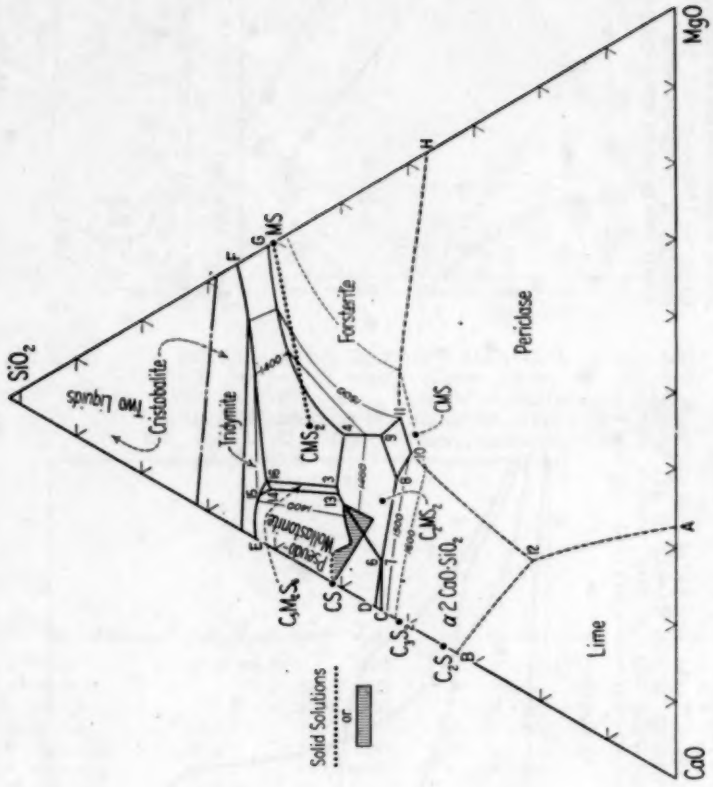

FIG. 88.—System CaO–MgO–SiO_2 (J. B. Ferguson and H. E. Merwin, *Amer. Jour. Sci.*, 4th Ser., **48**, 81–123 (1919) and modified by J. W. Greig, *ibid.*, 5th Ser., **13**, 1–44 (1927) (p. 34)). C = CaO. M = MgO. S = SiO_2. See also Hewitt Wilson, Ceramics—Clay Technology, p. 239; Glastechnische Tabellen, p. 62. See also Fig. 89.

(See Figure 88)

Pt	Crystal phases	CaO	MgO	SiO_2	Temp.
A	C-M	67.0	33.0		2300
B	C-C_3S	67.5		32.5	2065
C	C_3S-C_2S_3	55.5		44.5	1475
D	C_2S_3-CS	54.5		45.5	1455
E	CS-S	37.0		63.0	1436
F	S-Clinoenstatite		35.0	65.0	1543
G	Clinoenstatite-M_3S		37.5	62.5	1557
H	M_3S-M		63.0	37.0	1850
	Periclase		100.0		2800
	Lime	100.0			2575
	Cristobalite			100.0	1713
	$2CaO \cdot SiO_2$	65.0		35.0	2130
	$3CaO \cdot 2SiO_2$	58.2		41.8	1475
	$CaO \cdot SiO_2$	48.2		51.8	1540
	$2MgO \cdot SiO_2$		57.1	42.9	1890
	$MgO \cdot SiO_2$		40.0	60.0	1557
	$CaO \cdot MgO \cdot 2SiO_2$	26.0	18.5	55.5	1391
1*	Diopside-S-$C_4M_2S_6$	30.6	8.0	61.4	1320
3*	$C_4M_2S_6$ C_2MS_2 S solution diopside	36.0	12.6	51.4	1350
4*	C_2MS_2 forsterite diopside	29.8	20.2	50.0	1357
6*	Pseudowollastonite C_3S_2-C_2MS_2	49.2	6.3	44.5	1377
7	BC_3S-C_3S_2-C_2MS_2	49.5	6.2	44.3	1387
8*	C_2MS_2-αC_2S Monticellite S solution	39.0	18.3	42.7	1436
9	C_2MS_2-forsterite Monticellite S solution	33.3	22.3	44.4	1436
10	M-monticellite S solution αC_2S	37.3	22.3	40.3	1498
11	M-forsterite Monticellite S solution	32.1	26.4	41.5	1502
12*	M-C-αC_2S				1900
13	Pseudowollastonite $C_4M_2S_6$-C_2MS_2	36.7	12.3	51.0	1365
14	Pseudowollastonite Wollastonite SS-$C_4M_2S_6$	31.6	7.6	61.0	1340
15	Pseudowollastonite Wollastonite SS-S	31.3	7.2	61.5	1335
16	S-wollastonite SS $C_4M_2S_6$				1330
	$CaO \cdot MgO \cdot SiO_2$	34.6	25.6	39.8	
	$2CaO \cdot MgO \cdot 2SiO_2$	41.2	14.7	44.1	1458
	$5CaO \cdot 2MgO \cdot 6SiO_2$	38.9	11.1	50.0	

* Eutectic.

C = CaO. M = MgO. S = SiO_2.

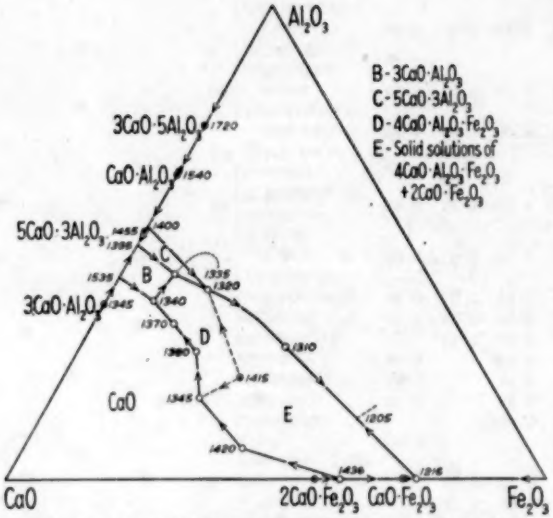

FIG. 90.—Partial diagram of the system CaO–Al_2O_3–Fe_2O_3 (W. C. Hansen, L. T. Brownmiller, and R. H. Bogue, *Jour. Amer. Chem. Soc.*, **50**, 396–406 (1928) (p. 402)). See also Fig. 91.

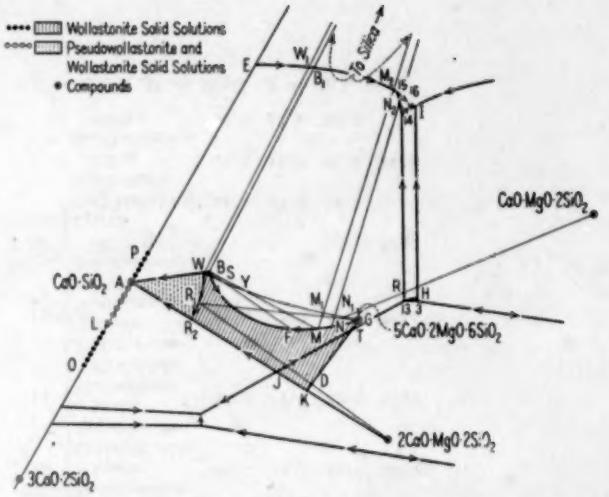

FIG. 89.—Part of CaO–MgO–SiO_2 system which deals with calcium metasilicate and related solid solutions (J. B. Ferguson and H. E. Merwin, *Amer. Jour. Sci.*, 4th Ser., **48**, 165–89 (1919) (p. 176)). See also Hewitt Wilson, Ceramics—Clay Technology, p. 239. See also Fig. 88.

Solid solutions

AP = wollastonite and silica
AO = " " $3CaO \cdot 2SiO_2$
AL = pseudowollastonite and $3CaO \cdot 2SiO_2$
AW = " " diopside
AB = wollastonite and diopside
AD = " " akermanite
AR_2 = pseudowollastonite and akermanite

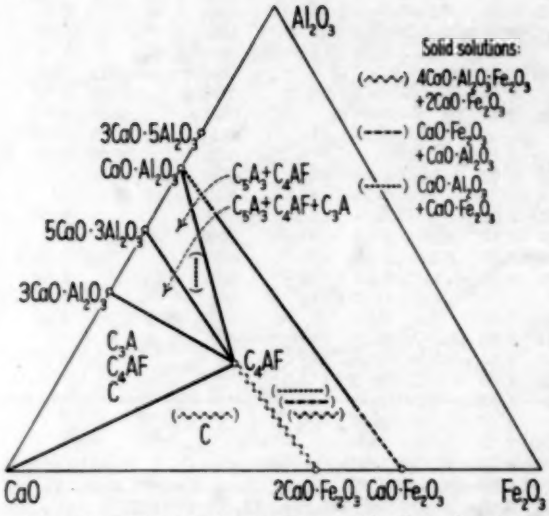

FIG. 91.—Final products of crystallization of melts in a portion of the system CaO–Al_2O_3–Fe_2O_3 (W. C. Hansen, L. T. Brownmiller, and R. H. Bogue, *Jour. Amer. Chem. Soc.*, **50**, 396–406 (1928) (p. 401)). See also Fig. 90.

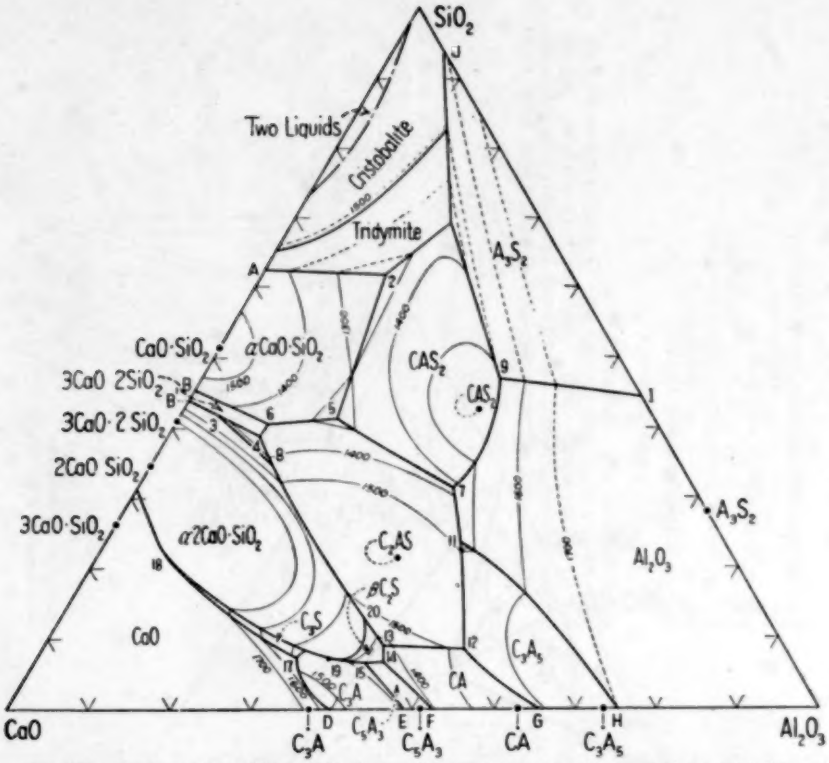

FIG. 92.—System CaO–Al_2O_3–SiO_2 (according to G. A. Rankin and F. E. Wright and modified by N. L. Bowen and J. W. Greig, *Jour. Amer. Ceram. Soc.*, **7** [4], 238 (1924) and J. W. Greig, *Amer. Jour. Sci.*, 5th Ser., **13**, 35–41 (1927)). See also Glastechnische Tabellen, p. 73. C = CaO. A = Al_2O_3. S = SiO_2.

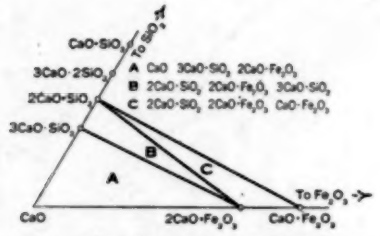

FIG. 93.—Composition triangles in system CaO–SiO_2–Fe_2O_3 (W. C. Hansen and R. H. Bogue, *Jour. Amer. Chem. Soc.*, **48**, 1261–67 (1926) (p. 1262)).

(See Figure 92)

Pt	Crystal Phases	CaO	Al_2O_3	SiO_2	Temp.
A*	S-CS	37.0		63.0	1436
B*	CS-C_3S_2	54.5		45.4	1455
B'	C_3S_2-C_2S	55.5		44.5	1475
C*	C_2S-C	67.5		32.5	2065
D	C-C_3A	59.0	41.0		1535
E*	C_3A-C_3A_2	50.0	50.0		1395
F*	C_3A_2-CA	47.0	53.0		1400
G*	CA-CA_2	33.5	66.5		1590
H*	CA_2-A	24.0	76.0		1700
I	A-AS_2		55.0	45.0	1800
J*	AS_2-S		5.5	94.5	1545
	CaO	100.0			2570
	SiO_2			100	1713
	Al_2O_3		100		2050
	$CaSiO_3$	48.2		51.8	1540
	α-$2CaO{\cdot}SiO_2$	65.0		35.0	2130
	$3CaO{\cdot}2SiO_2$	58.2		41.8	1475

* Binary eutectic.

Pt	Crystal Phases	CaO	Al_2O_3	SiO_2	Temp.
1†	CaS_2-AS_2-S	9.8	19.8	70.4	1345
2†	CaS_2-S-αCS	23.3	14.7	62.2	1170
3	CaS_2-αC_2S-βC_2S	53.0	4.2	42.8	1415
4	βC_2S-C_2S_3-C_3AS	48.2	11.9	39.2	1335
5†	CAS_2-C_3AS-αCS	38.0	20.0	42.0	1265
6†	C_3AS-C_2S_3-αCS	47.2	11.8	41.0	1310
7†	CAS_2-C_3AS-A	29.2	39.0	31.8	1380
8	αC_2S-βC_2S-C_3AS	49.0	14.4	36.6	1415
9	CAS_2-A-AS_2	15.6	36.5	47.9	1512
11	C_3A_2-C_3AS-A	31.2	44.5	24.3	1475
12†	C_3AS-CA-C_3A_2	37.5	53.2	9.3	1505
13	C_3AS-βC_2S-CA	48.3	42.0	9.7	1512
14†	βC_2S-CA-C_3A_2	49.5	43.7	6.8	1335
15†	βC_2S-C_3A-C_3A_2	52.0	41.2	6.8	1335
17	C-C_2S-C_3A	59.7	32.8	7.5	1470
18	C-αC_2S-C_2S	68.4	9.2	22.4	1900
	$3CaO{\cdot}SiO_2$	73.6		26.4	1900
	$3CaO{\cdot}Al_2O_3$	62.2	37.8		1535
	$5CaO{\cdot}3Al_2O_3$	47.8	52.2		1455
	$CaO{\cdot}Al_2O_3$	35.4	64.6		1600
	$3CaO{\cdot}5Al_2O_3$	24.8	75.2		1720
	$Al_2O_3{\cdot}SiO_2$		62.8	37.2	1545‡
	$CaO{\cdot}Al_2O_3{\cdot}2SiO_2$	20.1	38.6	43.3	1550
	$2CaO{\cdot}Al_2O_3{\cdot}SiO_2$	40.8	37.2	22.0	1590
	$3Al_2O_3{\cdot}2SiO_2$		71.8	28.2	1810

† Eutectic.

‡ Decomposes at 1545° into mullite and liquid.

C = CaO. A = Al_2O_3. S = SiO_2.

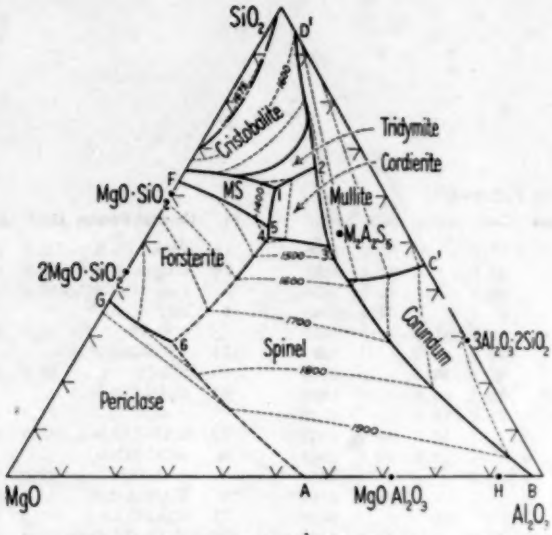

FIG. 94.—System MgO–Al_2O_3–SiO_2 (G. A. Rankin and H. E. Merwin, *Amer. Jour. Sci.*, 4th Ser., **45**, 301–25 (1918) (p. 322); modified according to J. W. Greig, *ibid.*, 5th Ser., **13**, 1–44 (1927)). See also Hewitt Wilson, Ceramics—Clay Technology, p. 238; Glastechnische Tabellen, p. 68.

Pt	Crystalline phases	MgO	Al_2O_3	SiO_2	Temp.
1*	MS-S-$M_2A_2S_5$	20.3	18.3	61.4	1345
2	S-A_2S_3-$M_2A_2S_5$	10.0	23.5	66.5	1425
3	A_2S_3-MA-$M_2A_2S_5$	16.1	34.8	49.1	1460
4	MA-M_2S-$M_2A_2S_5$	25.7	22.8	51.5	1370
5	M_2S-MS-$M_2A_2S_5$	25.0	21.0	54.0	1360
6*	M_2S-M-MA	56.0	16.0	28.0	1700
7	A-MA-A-S_2	15.2	42.0	42.8	1575
	$MgO·Al_2O_3$	28.4	71.6		2135
	$2MgO·SiO_2$	57.1		42.9	1890
	$Al_2O_3·SiO_2$		62.8	37.2	
	$2MgO2·Al_2O_3·5SiO_2$	13.7	34.9	51.4	
	$3Al_2O_3·2SiO_2$		71.8	28.2	1810†
	$MgO·SiO_2$	40.0		60.0	1557†

Pt	Crystalline phases	MgO	Al_2O_3	SiO_2	Temp.
A	M-MA	45.0	55.0		2030
B	MA-A	2.0	98.0		1925
C'	A-AS		55.0	45.0	1810
D'	AS-S		5.5	94.5	1545
E	S-MS	35.0		65.0	1543
F	MS-M_2S	37.5		62.5	1557
G	M_2S-M	63.0		37.0	1850
H	MA-BA	8.0	92.0		1925
	Periclase	100.0			2800
	Corundum		100.0		2050
	Cristobalite			100.0	1713

M = MgO. A = Al_2O_3. S = SiO_2.

* Eutectic.

† Incongruent melting point.

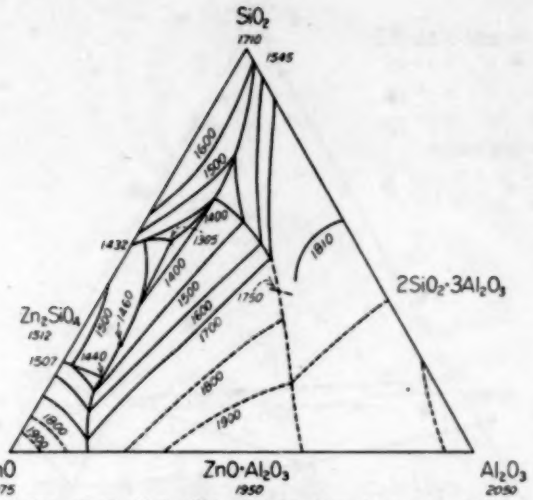

FIG. 95.—ZnO–Al_2O_3–SiO_2 (E. N. Bunting, Bur. Stand., *Jour. Research*, **8**, 279–87 (1932) (p. 281)).

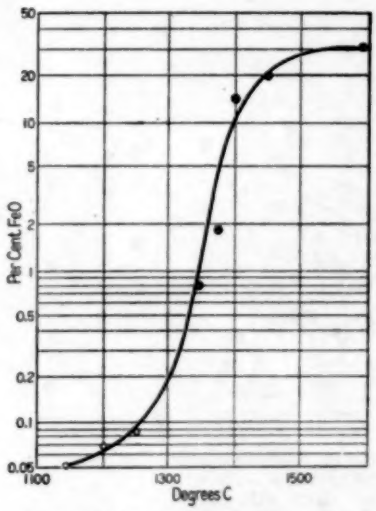

FIG. 96.—Isobar for the system Fe_2O_3–Fe_3O_4–O_2 at 152 mm. oxygen pressure (J. C. Hostetter and H. S. Roberts, *Jour. Amer. Ceram. Soc.*, **4**, 927–38 (1921) (p. 932)).

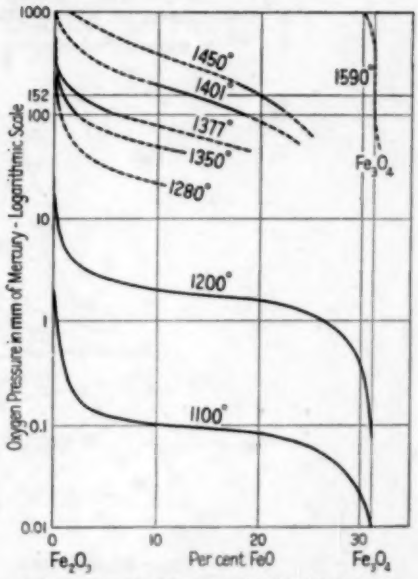

FIG. 97.—System Fe_2O_3–Fe_3O_4–O_2 (R. B. Sosman and J. C. Hostetter, *Jour. Wash. Acad. Sci.*, **5**, 293–303 (1915); J. C. Hostetter and H. S. Roberts, *Jour. Amer. Ceram. Soc.*, **4** [11], 927–38 (1921) (p. 931)). See also Hewitt Wilson, Ceramics—Clay Technology, p. 162.

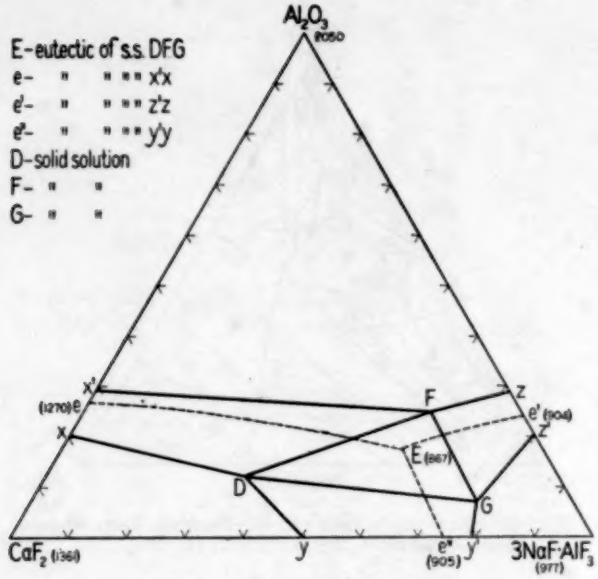

FIG. 98.—System CaF_2–Al_2O_3–$3NaF \cdot AlF_3$ (P. Pascal, *Z. Elektrochem.*, **19**, 610–13 (1913) (adapted from diagram on p. 613)).

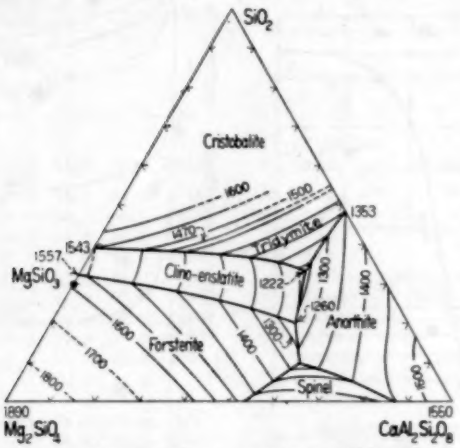

FIG. 99.—System anorthite ($CaO \cdot Al_2O_3$–$2SiO_2$)–forsterite ($2MgO \cdot SiO_2$)–silica (SiO_2) (O. Andersen, *Amer. Jour. Sci.*, 4th Ser., **39**, 407–54 (1915) (p. 437)). See also J. W. Greig, *ibid.*, 5th Ser., **13**, 1–44 and 133–54 (1927); Glastechnische Tabellen, p. 84.

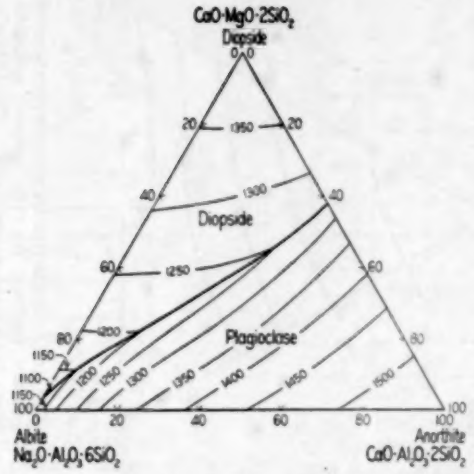

FIG. 100.—System diopside ($CaO \cdot MgO \cdot 2SiO_2$)–albite ($Na_2O \cdot Al_2O_3 \cdot 6SiO_2$)–anorthite ($CaO \cdot Al_2O_3 \cdot 2SiO_2$) (N. L. Bowen, *Amer. Jour. Sci.*, 4th Ser., **40**, 161–85 (1915)). Eutectics: binary { 97% albite, 3% diopside 1085°C; 42% anorthite, 58% diopside 1270°C. See also Hewitt Wilson, Ceramics—Clay Technology, pp. 225–27; Glastechnische Tabellen, p. 87.

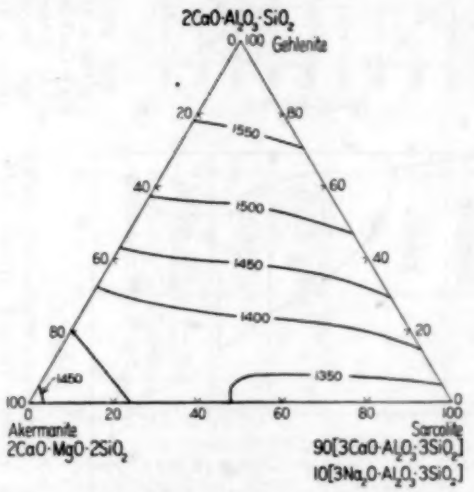

FIG. 101.—Isotherms for temperatures of complete melting in system gehlenite–akermanite–sarcolite (A. F. Buddington, *Amer. Jour. Sci.*, 5th Ser., **3**, 35–87 (1922) (p. 57)). See also Glastechnische Tabellen, p. 85.

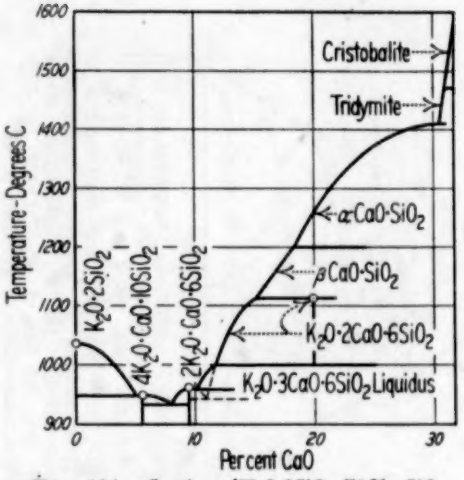

FIG. 104.—Section ($K_2O \cdot 2SiO_2$–70% SiO_2–30% CaO) through ternary system K_2O–CaO–SiO_2 (G. W. Morey, F. C. Kracek, and N. L. Bowen, *Jour. Soc. Glass Tech.*, **14**, 149–87 (1930) (p. 162)).

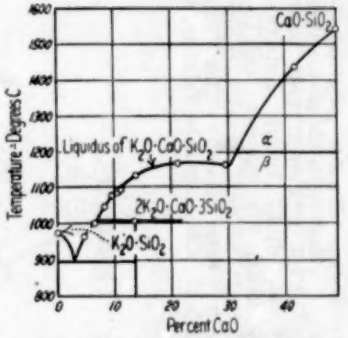

FIG. 103.—Section $K_2O \cdot SiO_2$ to $CaO \cdot SiO_2$ through ternary system K_2O–CaO–SiO_2 (G. W. Morey, F. C. Kracek, and N. L. Bowen, *Jour. Soc. Glass Tech.*, **14**, 149–87 (1930) (p. 160)).

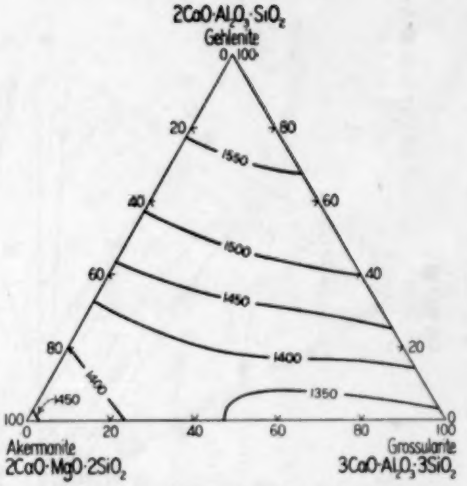

FIG. 102.—Isotherms for the temperatures of complete melting for the system gehlenite ($2CaO \cdot Al_2O_3 \cdot SiO_2$)–akermanite ($2CaO \cdot MgO \cdot 2SiO_2$)–grossularite ($3CaO \cdot Al_2O_3 \cdot 3SiO_2$) (A. F. Buddington, *Amer. Jour. Sci.*, 5th Ser., **3**, 35–87 (1922) (p. 48)).

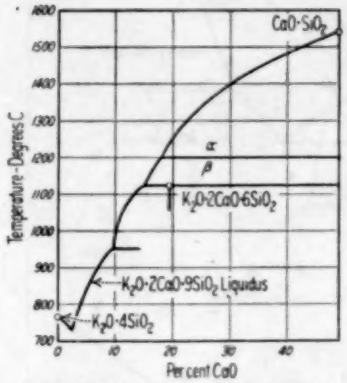

FIG. 105.—Section $K_2O \cdot 4SiO_2$ to $CaO \cdot SiO_2$ through ternary system K_2O–CaO–SiO_2 (G. W. Morey, F. C. Kracek, and N. L. Bowen, *Jour. Soc. Glass Tech.*, **14**, 149–87 (1930) (p. 163)).

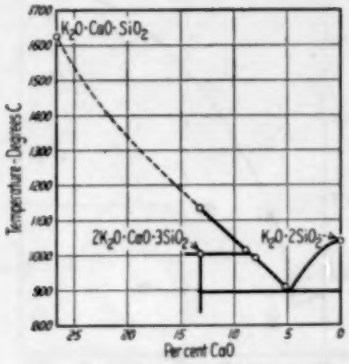

FIG. 106.—Section $K_2O \cdot CaO \cdot SiO_2$ to $K_2O \cdot 2SiO_2$ through ternary system K_2O–CaO–SiO_2 (G. W. Morey, F. C. Kracek, and N. L. Bowen, *Jour. Soc. Glass Tech.*, **14**, 149–87 (1930) (p. 161)).

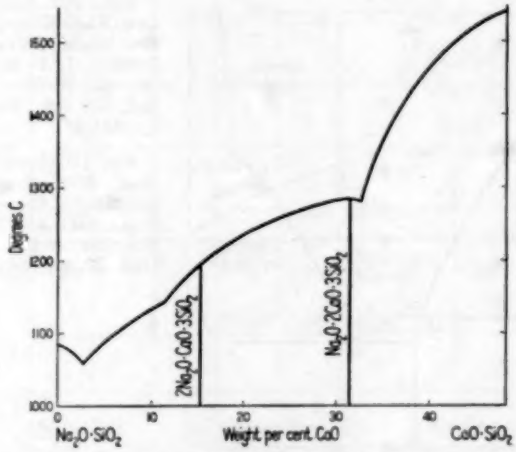

FIG. 107.—System $Na_2O \cdot SiO_2$–$CaO \cdot SiO_2$ (according to G. W. Morey and N. L. Bowen, *Jour. Soc. Glass Tech.*, **9**, 249–64 (1925) (p. 226)).

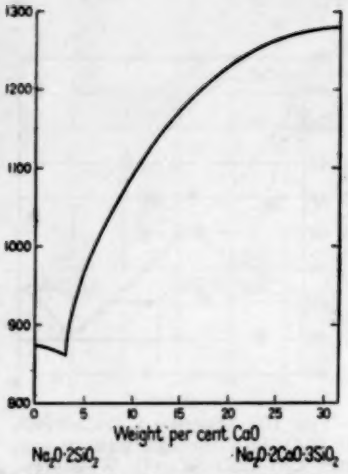

FIG. 108.—System $Na_2O \cdot 2SiO_2$–$Na_2O \cdot 2CaO \cdot 3SiO_2$ (according to G. W. Morey and N. L. Bowen, *Jour. Phys. Chem.*, **28**, 1167–79 (1924) (adapted from diagram on p. 1174)). See also Glastechnische Tabellen, p. 44.

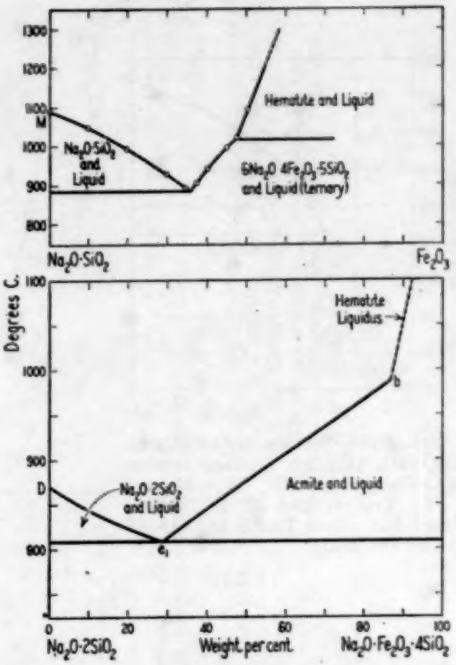

FIG. 109 (upper).—The section $Na_2O \cdot SiO_2$–Fe_2O_3 of the system Na_2SiO_3–Fe_2O_3–SiO_2 (N. L. Bowen, J. F. Schairer, and H. W. V. Willems, *Amer. Jour. Sci.*, 5th Ser., **20**, 405–55 (1930) (p. 424)).

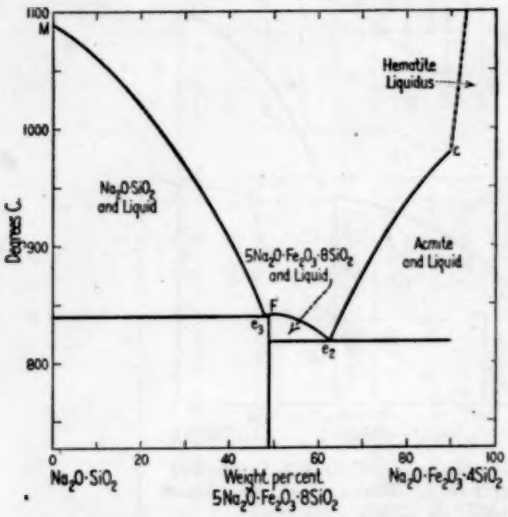

FIG. 111.—The section $Na_2O \cdot SiO_2$–$Na_2O \cdot Fe_2O_3$–$4SiO_2$ of the system Na_2SiO_3–Fe_2O_3–SiO_2 (N. L. Bowen, J. F. Schairer, and H. W. V. Willems, *Amer. Jour. Sci.*, 5th Ser., **20**, 405–55 (1930) (p. 429)).

FIG. 110 (lower).—The section $Na_2O \cdot 2SiO_2$–$Na_2O \cdot Fe_2O_3 \cdot 4SiO_2$ (acmite) of the system Na_2SiO_3–Fe_2O_3–SiO_2 (N. L. Bowen, J. F. Schairer, and H. W. V. Willems, *ibid.*, **20**, 405–55 (1930) (p. 430)).

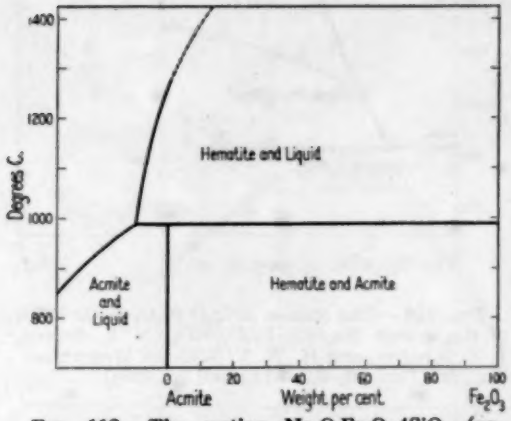

FIG. 112.—The section $Na_2O \cdot Fe_2O_3 \cdot 4SiO_2$ (acmite)–Fe_2O_3 (hematite) (N. L. Bowen and J. F. Schairer, *Amer. Jour. Sci.*, 5th Ser., **18**, 365–78 (1929) (p. 368)).

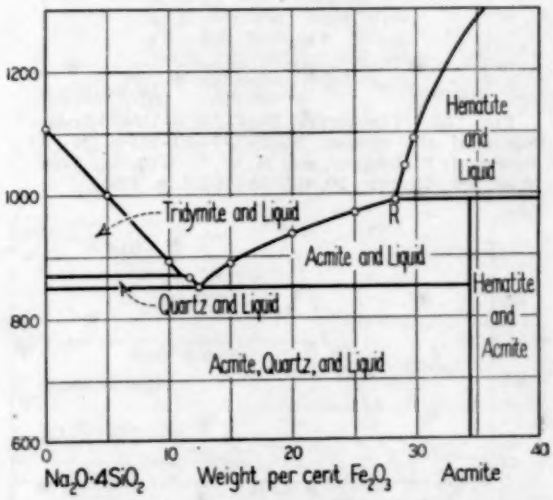

FIG. 113.—The section $Na_2O \cdot 4SiO_2$–$Na_2O \cdot Fe_2O_3 \cdot 4SiO_2$ (acmite) of the system Na_2O–SiO_2–Fe_2O_3 (N. L. Bowen and J. F. Schairer, *Amer. Jour. Sci.*, 5th Ser., **18**, 365–74 (1929) (p. 368)).

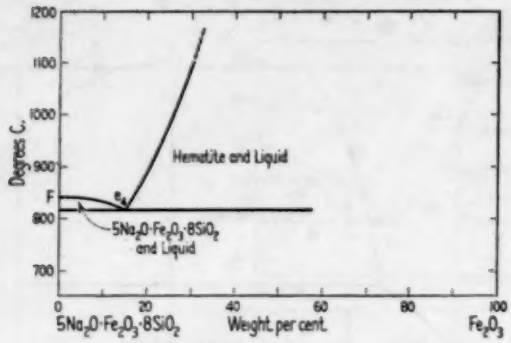

FIG. 114.—The section $5Na_2O \cdot Fe_2O_3 \cdot 8SiO_2$–$Fe_2O_3$ of the system Na_2SiO_3–Fe_2O_3–SiO_2 (N. L. Bowen, J. F. Schairer, and H. W. V. Willems, *Amer. Jour. Sci.*, 5th Ser., **20**, 405–55 (1930) (p. 428)).

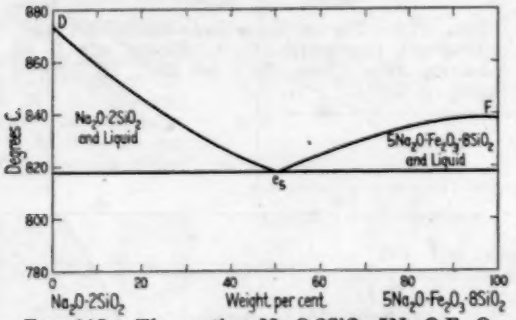

FIG. 115.—The section $Na_2O \cdot 2SiO_2$–$5Na_2O \cdot Fe_2O_3$–$8SiO_2$ of the system Na_2SiO_3–Fe_2O_3–SiO_2 (N. L. Bowen, J. F. Schairer, and H. W. V. Willems, *Amer. Jour. Sci.*, 5th Ser., **20**, 405–55 (1930) (p. 428)).

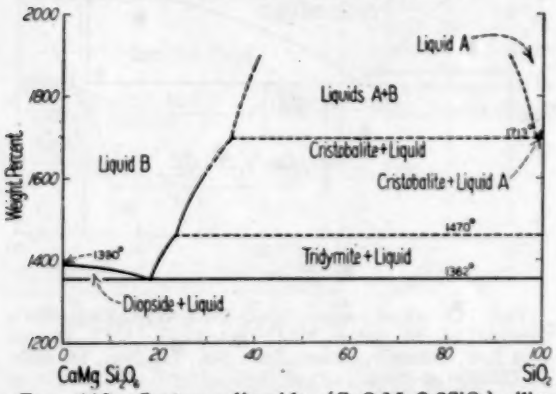

FIG. 116.—System diopside ($CaO \cdot MgO \cdot 2SiO_2$)–silica (N. L. Bowen, *Amer. Jour. Sci.*, 4th Ser., **38**, 207–64 (1914) (p. 211)). See also Glastechnische Tabellen, p. 63.

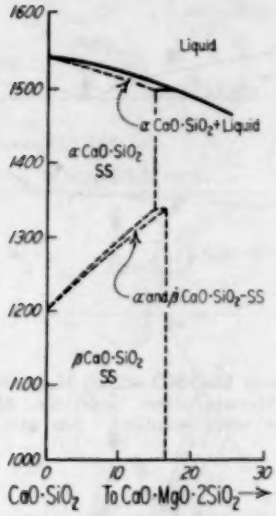

FIG. 117.—Phase relations along that portion of the $CaO\cdot SiO_2$ – $CaO\cdot MgO\cdot 2SiO_2$ line which includes the wollastonite–diopside solid solutions (J. B. Ferguson and H. E. Merwin, *Amer. Jour. Sci.*, 4th Ser., **48**, 165–89 (1919) (p. 184)). See also Glastechnische Tabellen, p. 63.

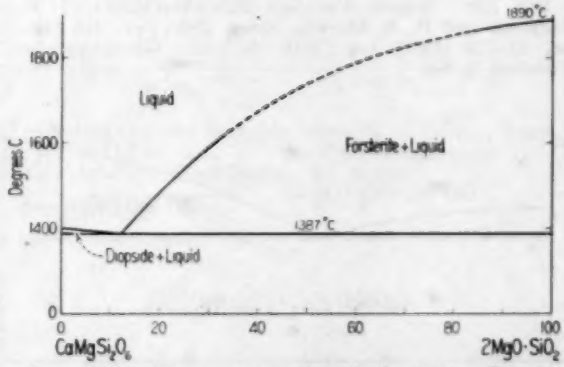

FIG. 118.—The system diopside–forsterite (N. L. Bowen, *Amer. Jour. Sci.*, 4th Ser., **38**, 207–64 (1914) (p. 212)). See also Glastechnische Tabellen, p. 64.

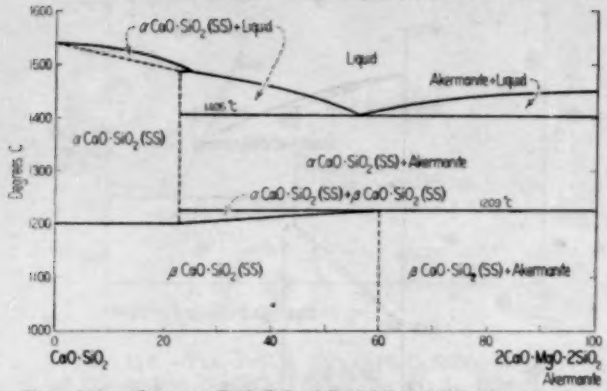

FIG. 119.—System $CaO \cdot SiO_2$–$2CaO \cdot MgO \cdot 2SiO_2$ (J. B. Ferguson and H. E. Merwin, *Amer. Jour. Sci.*, **48**, 81–123 (1919) (p. 120)). *SS* = solid solution. See also Glastechnische Tabellen, p. 64.

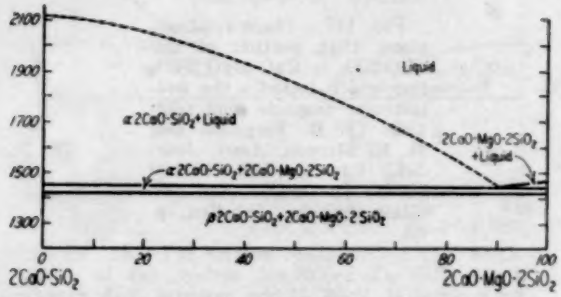

FIG. 120.—System $2CaO \cdot SiO_2$–$2CaO \cdot MgO \cdot 2SiO_2$ (J. B. Ferguson and H. E. Merwin, *Amer. Jour. Sci.*, 4th Ser., **48**, 81–123 (1919) (p. 119)). See also Glastechnische Tabellen, p. 64.

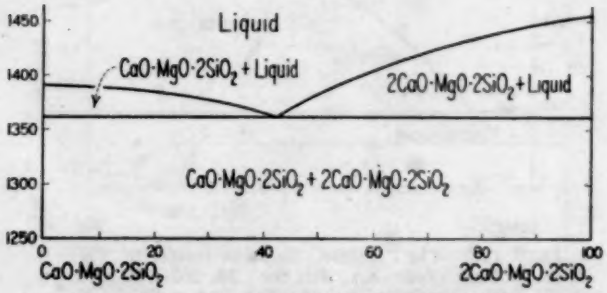

FIG. 121.—System $CaO \cdot MgO \cdot 2SiO_2$–$2CaO \cdot MgO \cdot 2SiO_2$ (J. B. Ferguson and H. E. Merwin, *Amer. Jour. Sci.*, 4th Ser., **48**, 81–123 (1919) (p. 118)). See also Glastechnische Tabellen, p. 64.

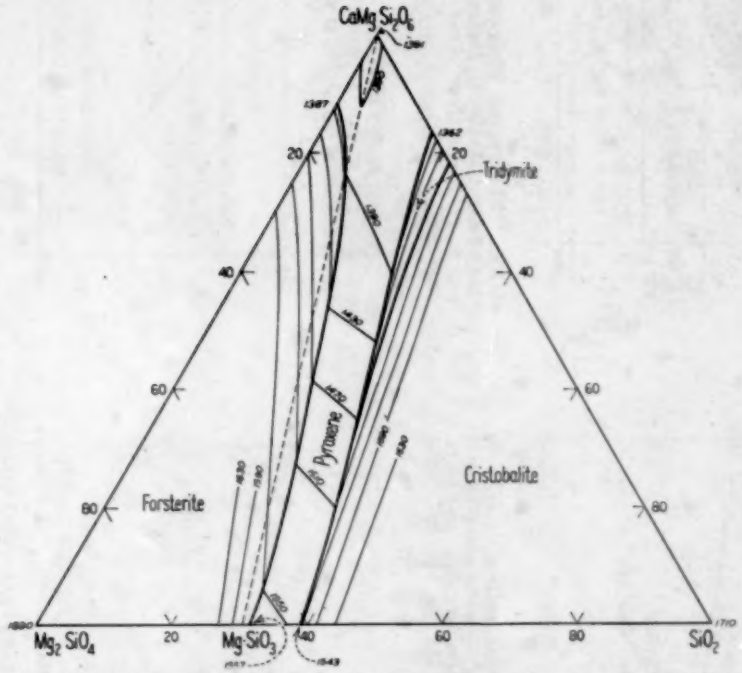

FIG. 122.—System diopside–forsterite–silica (N. L. Bowen, *Amer. Jour. Sci.*, 4th Ser., **38**, 207–64 (1914) (p. 217)). See also Glastechnische Tabellen, p. 63; Hewitt Wilson, Ceramics—Clay Technology, p. 243.

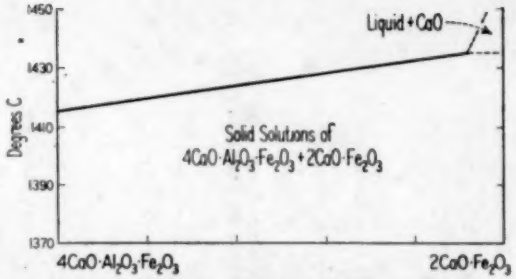

FIG. 125.—Diagram showing melting relations in the solid solutions of $4CaO \cdot Al_2O_3 \cdot Fe_2O_3$ and $2CaO \cdot Fe_2O_3$ (W. C. Hansen, L. T. Brownmiller, and R. H. Bogue, *Jour. Amer. Chem. Soc.*, **50**, 396–406 (1928) (p. 400)).

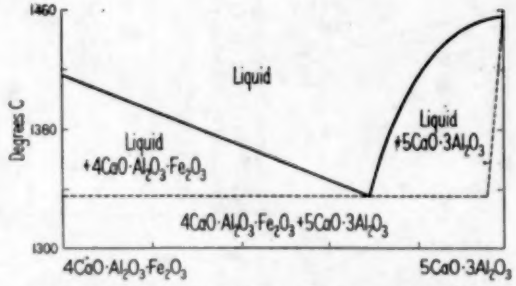

FIG. 126.—System $4CaO \cdot Al_2O_3 \cdot Fe_2O_3$–$5CaO \cdot 3Al_2O_3$ (W. C. Hansen, L. T. Brownmiller, and R. H. Bogue, *Jour. Amer. Chem. Soc.*, **50**, 396–406 (1928) (p. 403)).

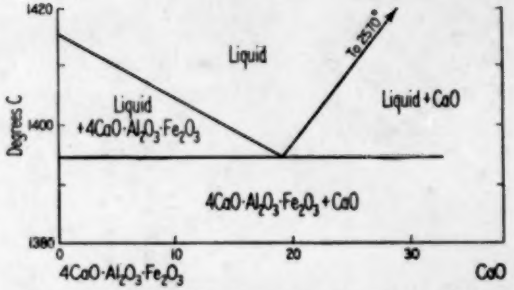

FIG. 123.—Partial diagram of system $4CaO$–$Al_2O_3 \cdot Fe_2O_3$–CaO (W. C. Hansen, L. T. Brownmiller, and R. H. Bogue, *Jour. Amer. Chem. Soc.*, **50**, 396–406 (1928) (p. 399)).

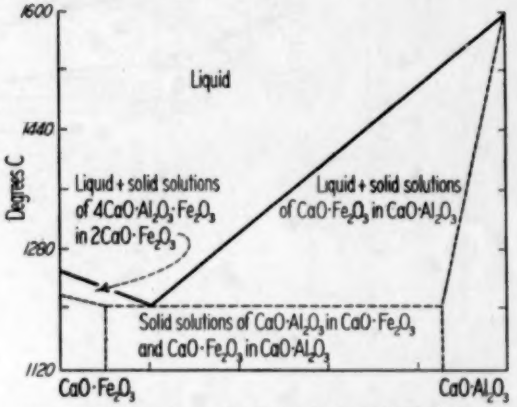

FIG. 124.—System $CaO \cdot Fe_2O_3$–$CaO \cdot Al_2O_3$ (W. C. Hansen, L. T. Brownmiller, and R. H. Bogue, *Jour. Amer. Chem. Soc.*, **50**, 396–406 (1928) (p. 404)).

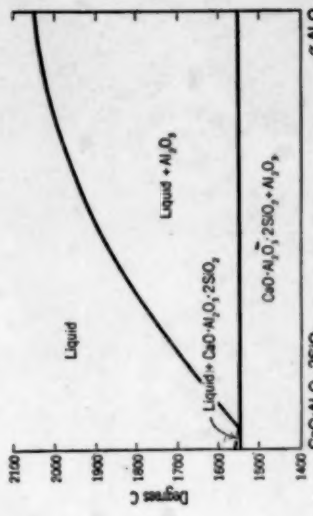

FIG. 127.—System $CaO·Al_2O_3·2SiO_2$–αAl_2O_3 (G. A. Rankin and F. E. Wright, *Amer. Jour. Sci.*, 4th Ser., **39**, 1–79 (1915) (p. 40)). See also Glastechnische Tabellen, p. 75.

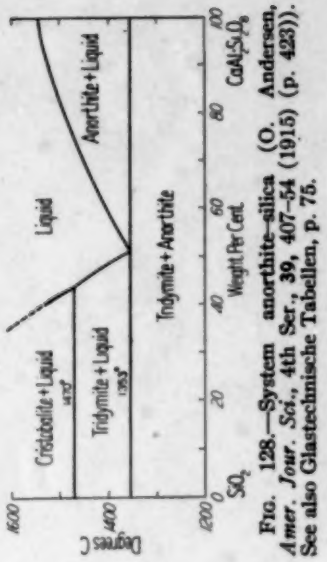

FIG. 128.—System anorthite–silica (O. Andersen, *Amer. Jour. Sci.*, 4th Ser., **39**, 407–54 (1915) (p. 423)). See also Glastechnische Tabellen, p. 75.

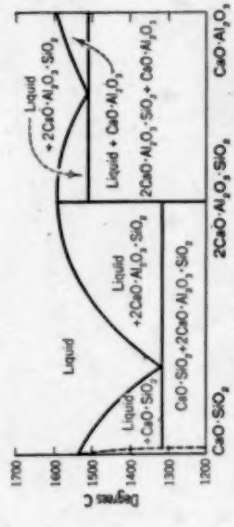

FIG. 129.—System $CaO·SiO_2$–$CaO·Al_2O_3$ (G. A. Rankin and F. E. Wright, *Amer. Jour. Sci.*, 4th Ser., **39**, 1–79 (1915) (p. 50)). See also Glastechnische Tabellen, p. 75.

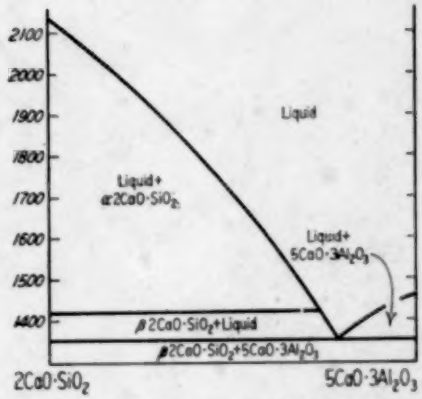

FIG. 130.—System $2CaO·SiO_2$–$5CaO·3Al_2O_3$ (G. A. Rankin and F. E. Wright, *Amer. Jour. Sci.*, 4th Ser., **39**, 1–79 (1915) (p. 49)). See also Glastechnische Tabellen, p. 76.

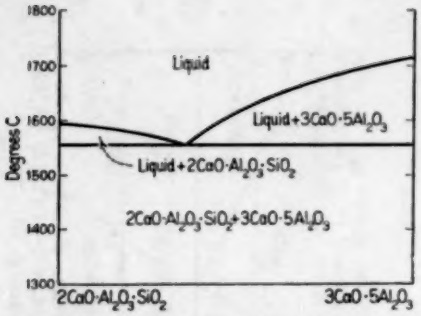

FIG. 131.—System $2CaO \cdot Al_2O_3 \cdot SiO_2$–$3CaO \cdot 5Al_2O_3$ (G. A. Rankin and F. E. Wright, *Amer. Jour. Sci.*, 4th Ser., **39**, 1–79 (1915) (p. 49)). See also Glastechnische Tabellen, p. 76.

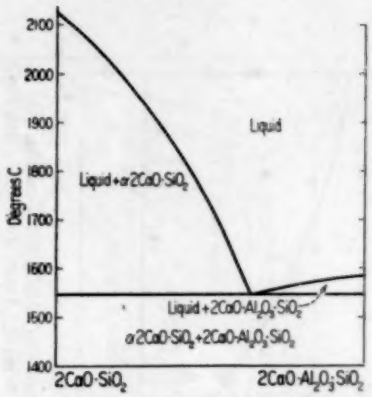

FIG. 132.—System $2CaO \cdot SiO_2$–$2CaO \cdot Al_2O_3 \cdot SiO_2$ (G. A. Rankin and F. E. Wright, *Amer. Jour. Sci.*, 4th Ser., **39**, 1–79 (1915) (p. 47)). See also Glastechnische Tabellen, p. 76.

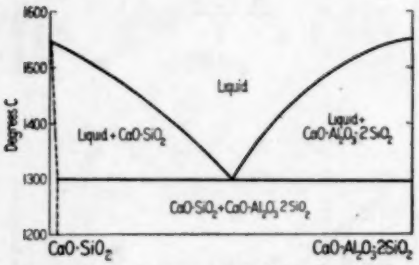

FIG. 133.—System $CaO \cdot SiO_2$–$CaO \cdot AlO_3$–$2SiO_2$ (G. A. Rankin and F. E. Wright, *Amer. Jour. Sci.*, 4th Ser., **39**, 1–79 (1915) (p. 46)). See also Glastechnische Tabellen, p. 75.

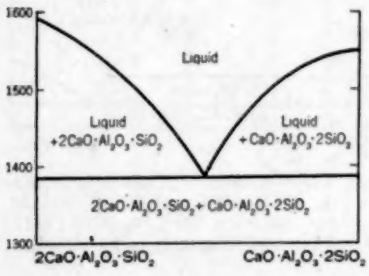

FIG. 134.—System $2CaO \cdot Al_2O_3 \cdot SiO_2$–$CaO \cdot Al_2O_3 \cdot 2SiO_2$ (G. A. Rankin and F. E. Wright, *Amer. Jour. Sci.*, 4th Ser., **39**, 1–79 (1915) (p. 49)). See also Glastechnische Tabellen, p. 76.

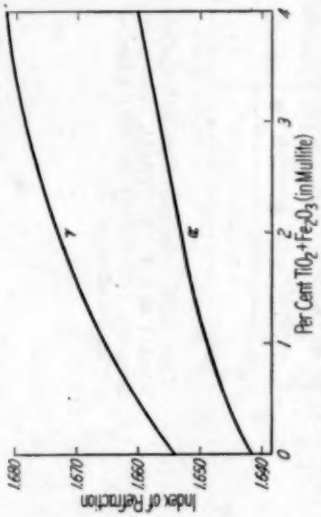

FIG. 135.—Effect of TiO_2 and Fe_2O_3 on refractive indices of mullite (N. L. Bowen, J. W. Greig, and E. G. Zies, *Jour. Wash. Acad. Sci.*, **14**, 183–91 (1924) (p. 188)).

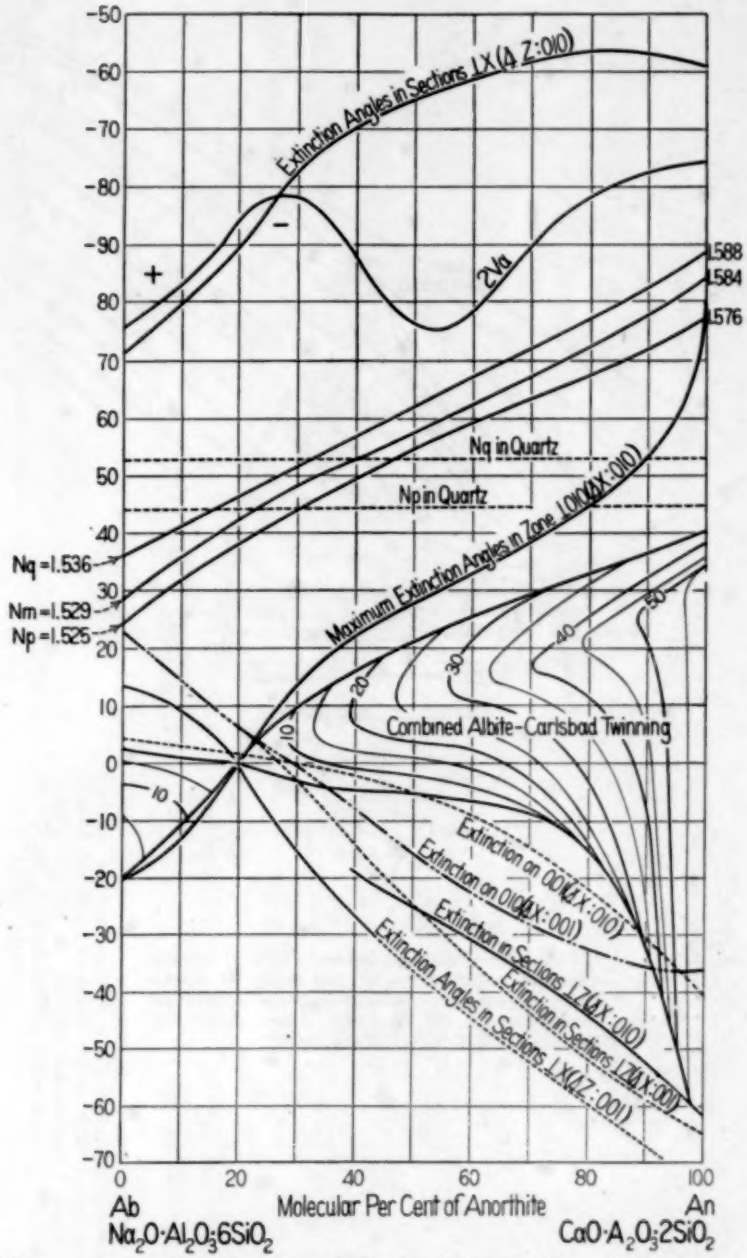

FIG. 136.—Optical properties of the plagioclase feldspars ($Na_2O \cdot Al_2O_3 \cdot 6SiO_2$–$CaO \cdot Al_2O_3 \cdot 2SiO_2$) (modified from F. E. Wright, *Amer. Jour. Sci.*, 4th Ser., **36**, 540–42 (1913)).

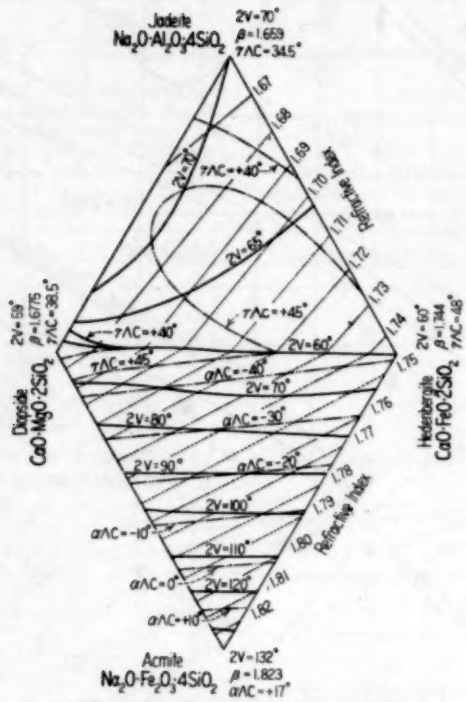

FIG. 137.—Relations between optical properties and composition in the series of monoclinic pyroxenes, jadeite–diopside–acmite–hedenbergite (A. N. Winchell, *Amer. Jour. Sci.*, 5th Ser., **6**, 504–20 (1923) (p. 519)).

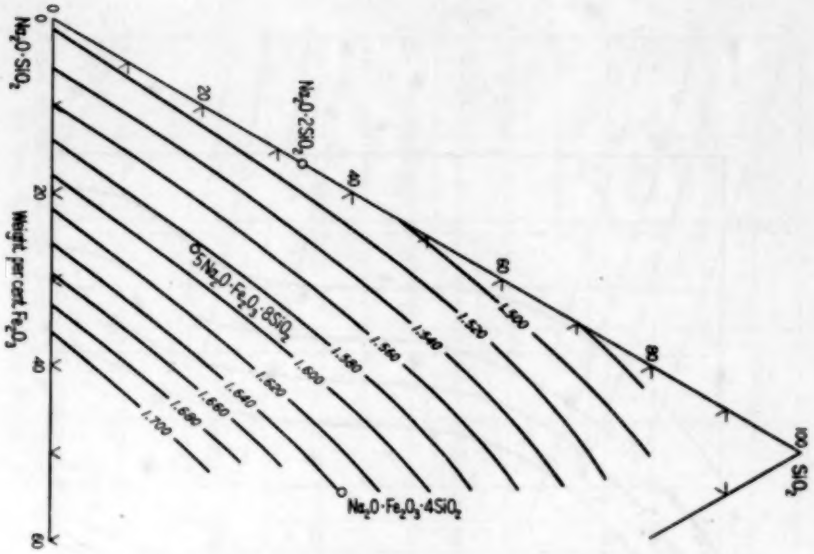

FIG. 138.—Refractive indices of glasses in the system, Na_2SiO_3–Fe_2O_3–SiO_2 (N. L. Bowen, J. F. Schairer, and H. W. V. Willems, *Amer. Jour. Sci.*, 5th Ser., **20**, 405–55 (1930) (p. 446)).

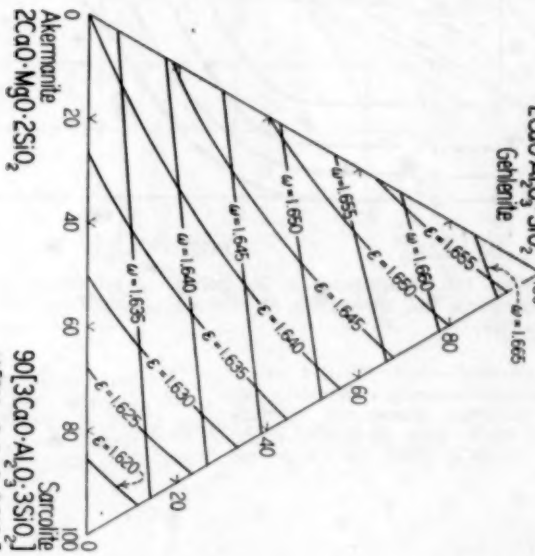

FIG. 139.—Lines connecting similar indices of refraction in the system gehlenite–akermanite–sarcolite plotted for those mixtures which show complete homogeneity within a definite temperature range above 980°C (A. F. Buddington, *Amer. Jour. Sci.*, 5th Ser., **3**, 35–87 (1922) (p. 58)).

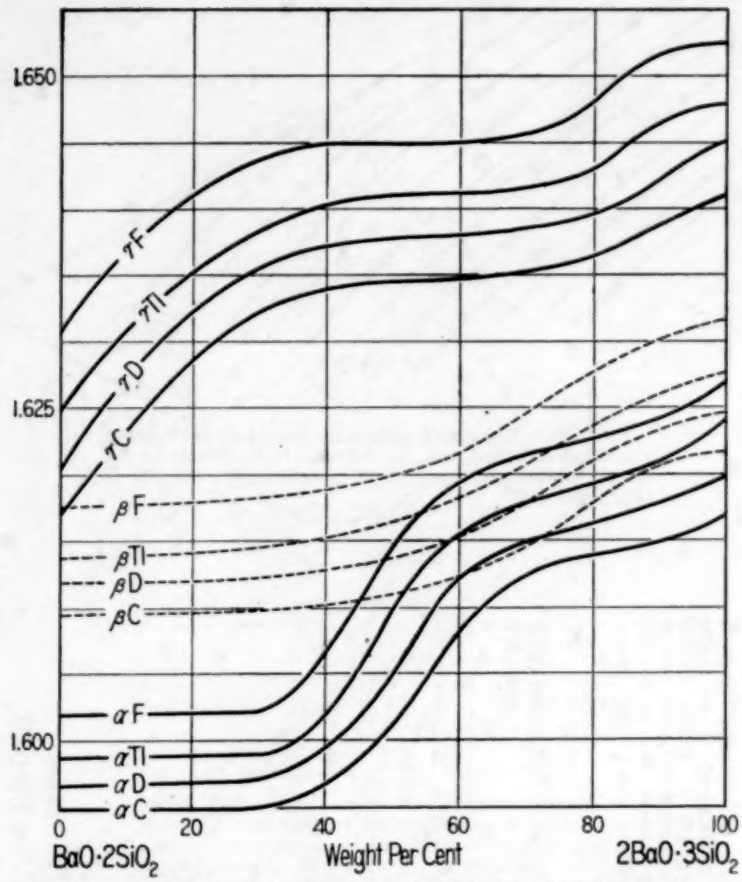

FIG. 140.—Variations in the indices of refraction of solid solutions of $BaO \cdot 2SiO_2$ and $2BaO \cdot 3SiO_2$ (P. Eskola, *Amer. Jour. Sci.*, **4**, 331–75 (1922) (p. 349)).

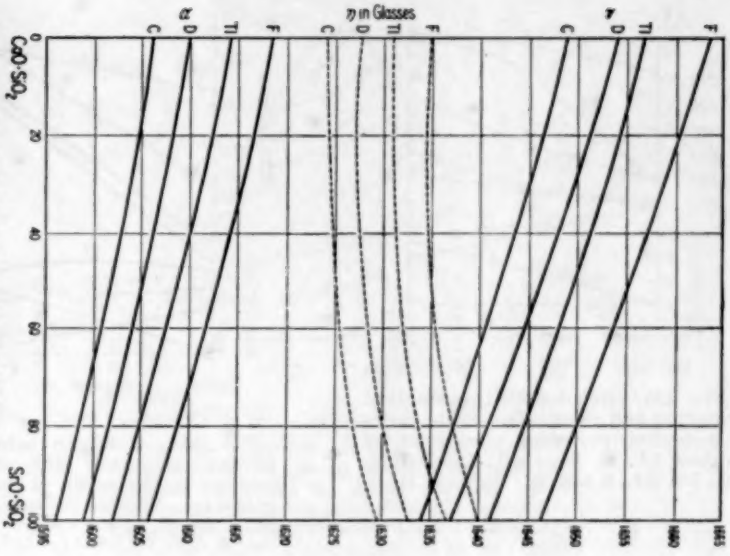

FIG. 141.—Variations in indices of refraction of solid solutions of $CaO{\cdot}SiO_2$ and $SrO{\cdot}SiO_2$ (P. Eskola, *Amer. Jour. Sci.*, 5th Ser., **4**, 331–75 (1922) (p. 355)).

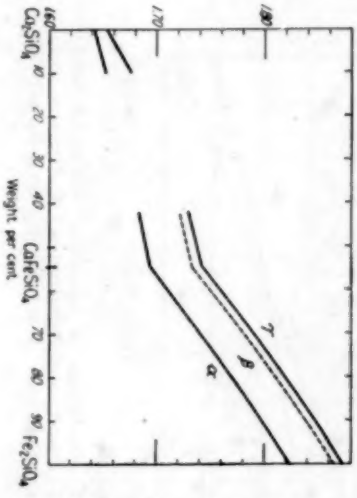

FIG. 142.—Refractive indices of crystalline phases in the system Ca_2SiO_4–Fe_2SiO_4 (N. L. Bowen, J. F. Schairer, and E. Posnjak, *Amer. Jour. Sci.*, 5th Ser., **25**, 273–97 (1933) (p. 286)).

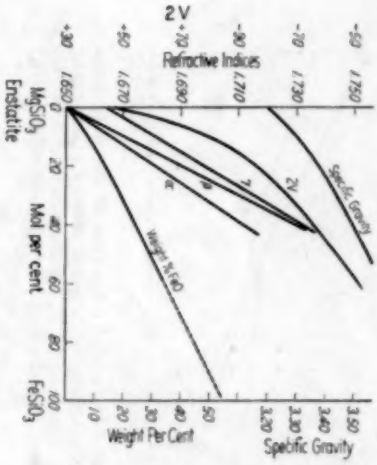

FIG. 143.—Relations between physical properties and compositions in the rhombic pyroxenes, enstatite–$FeSiO_3$ (A. N. Winchell, *Amer. Jour. Sci.*, 5th Ser., **6**, 504–20 (1923) (p. 507)).

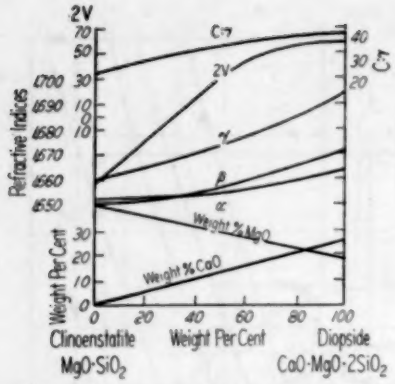

FIG. 144.—Relations between optical properties and composition in the series of monoclinic pyroxenes, clinoenstatite–diopside (A. N. Winchell, *Amer. Jour. Sci.*, 5th Ser., **6**, 504–20 (1923) (p. 513)).

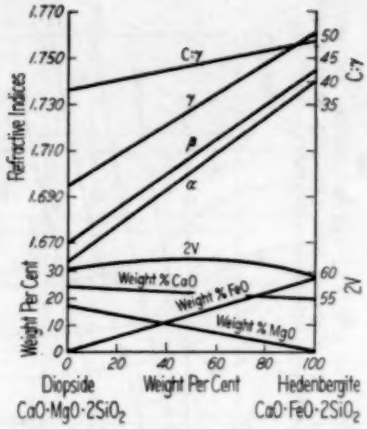

FIG. 145.—Relations between the physical properties and the composition in the series of monoclinic pyroxenes, diopside–hedenbergite (A. N. Winchell, *Amer. Jour. Sci.*, 5th Ser., **6**, 504–20 (1923) (p. 510)).

FIG. 146.—Indices of refraction of the solid solutions of $4CaO{\cdot}Al_2O_3{\cdot}Fe_2O_3$ and $2CaO{\cdot}Fe_2O_3$ (according to W. C. Hansen, L. T. Brownmiller, and R. H. Bogue, *Jour. Amer. Chem. Soc.*, **50**, 396–406 (1928) (p. 400)).

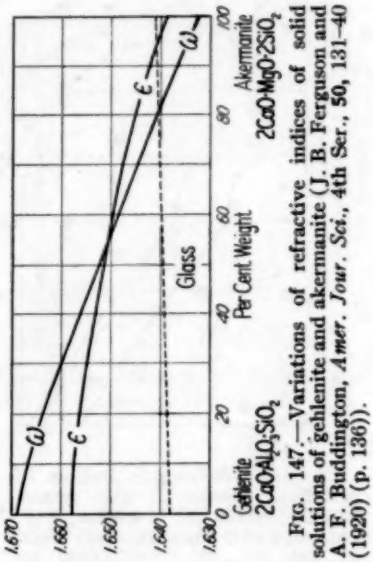

FIG. 147.—Variations of refractive indices of solid solutions of gehlenite and akermanite (J. B. Ferguson and A. F. Buddington, *Amer. Jour. Sci.*, 4th Ser., **50**, 131–40 (1920) (p. 136)).

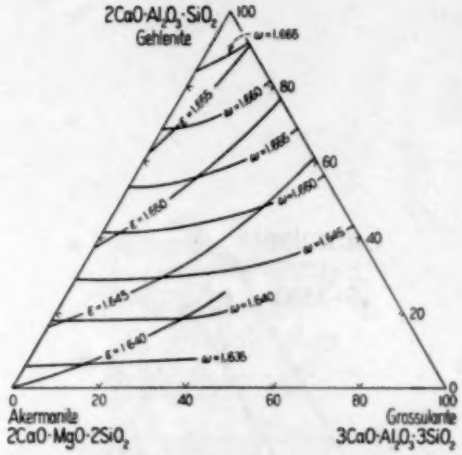

FIG. 148.—Lines connecting equal indices of refraction for the system gehlenite–akermanite–grossularite plotted for those mixtures which show complete homogeneity within a definite comparative range above 980°C (A. F. Buddington, *Amer. Jour. Sci.*, 5th Ser., **3**, 35–87 (1922) (p. 49)).

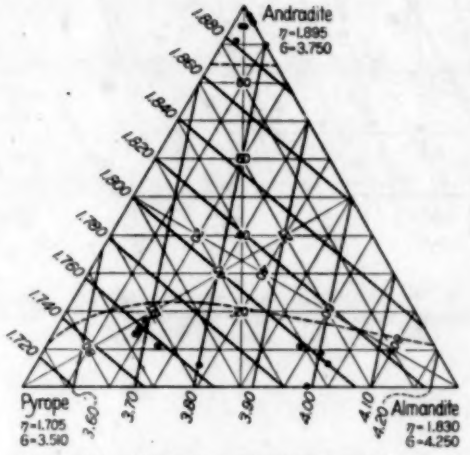

FIG. 149.—Variation of refractive index and specific gravity in the system, pyrope–almandite–andradite (W. E. Ford, *Amer. Jour. Sci.*, 4th Ser., **40**, 33–49 (1915) (p. 44)). The dots represent the position on the chart of the different analyses containing two or three constituents. The broken line indicates the probable limits of the possible mixtures of the series found in natural garnets.

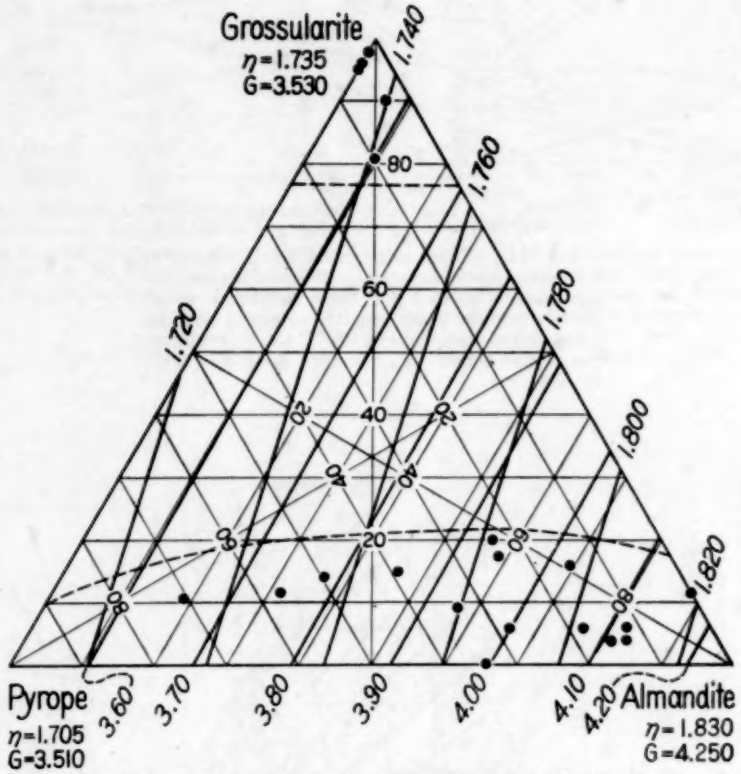

FIG. 150.—System pyrope–almandite–grossularite (W. E. Ford, *op. cit.*, p. 42). See note Fig. 149.

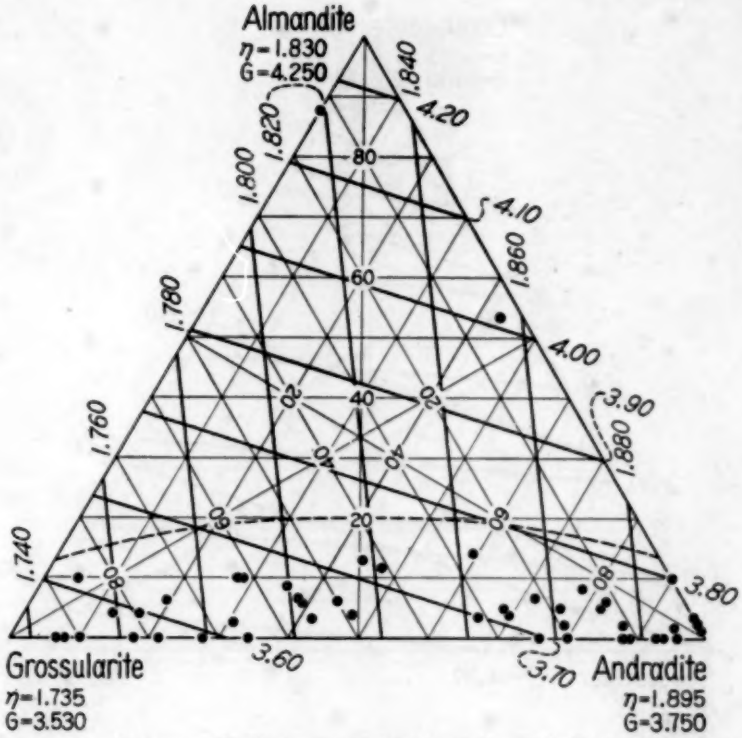

FIG. 151.—System andradite–grossularite–almandite (W. E. Ford, *op. cit.*, p. 41). See note Fig. 149.

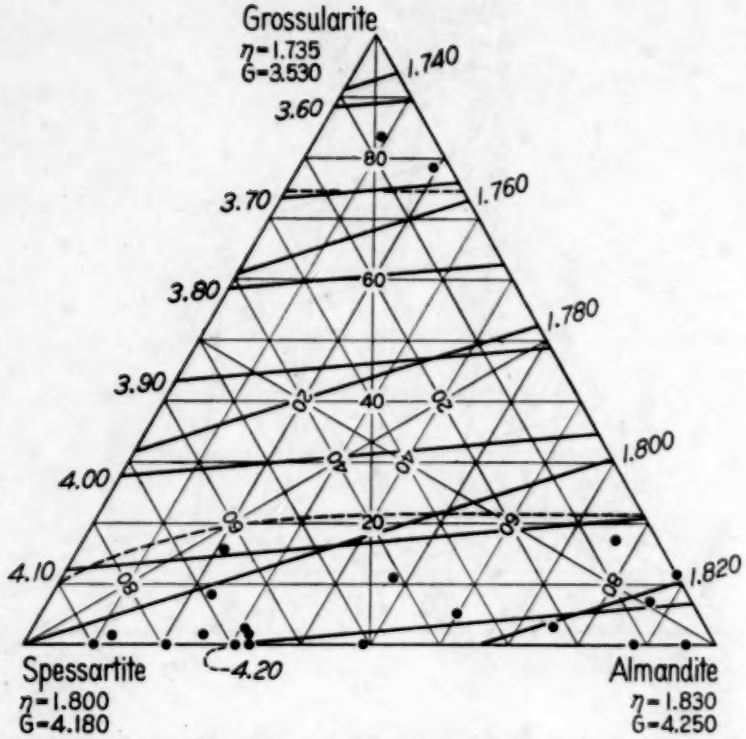

FIG. 152.—System almandite–spessartite–grossularite (W. E. Ford, *op. cit.*, p. 43). See note Fig. 149.

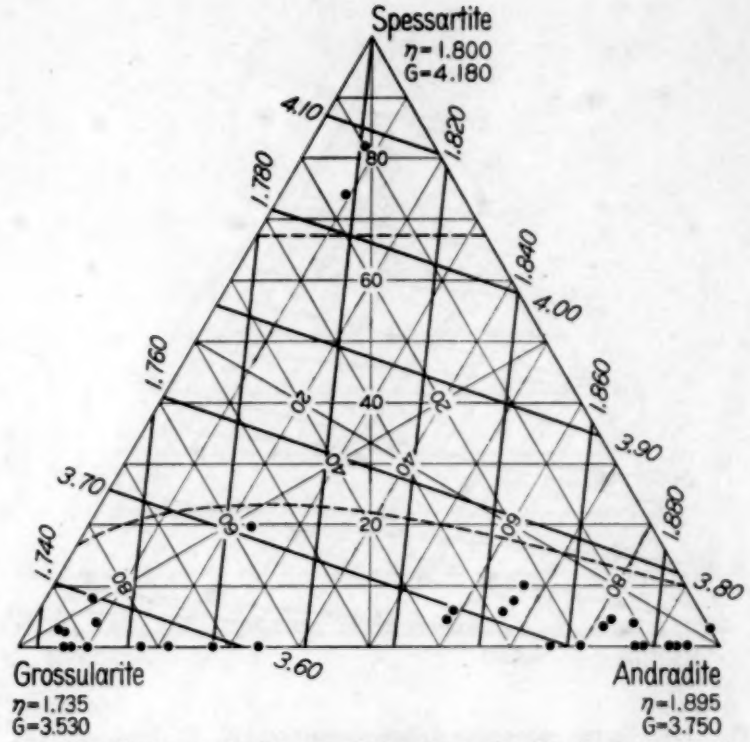

FIG. 153.—System andradite–grossularite–spessartite (W. E. Ford, *op. cit.*, p. 42). See note Fig. 149.

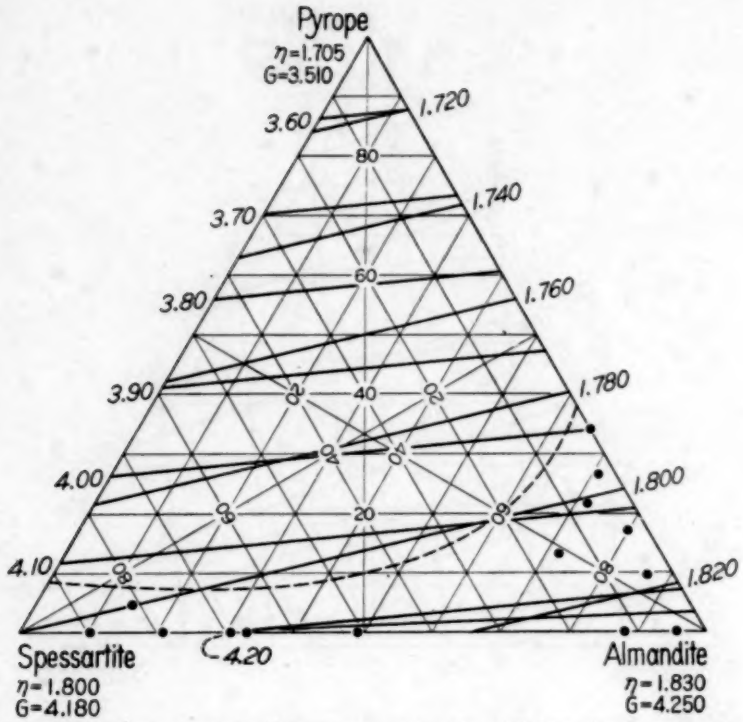

FIG. 154.—System almandite–pyrope–spessartite (W. E. Ford, *op. cit.*, p. 44). See note Fig. 149.

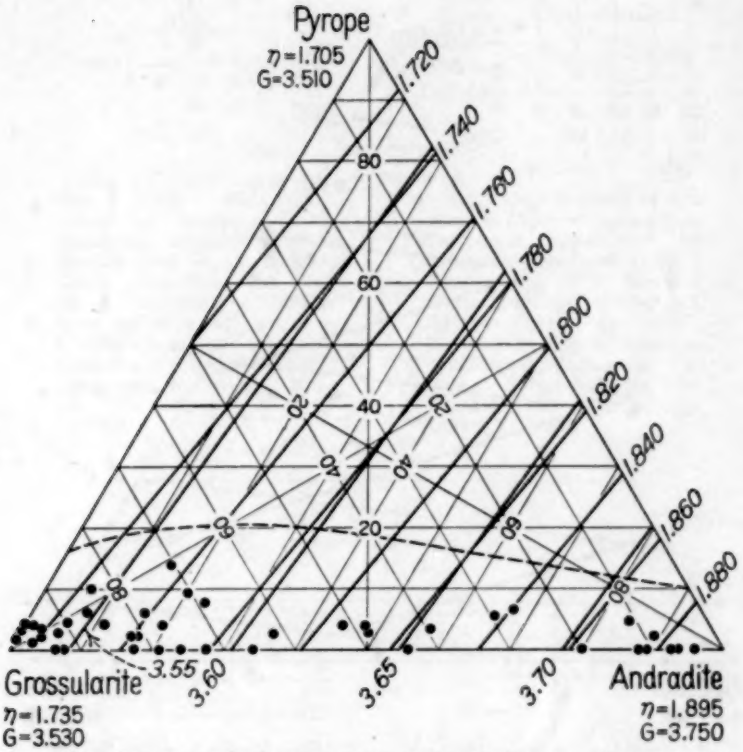

FIG. 155.—System andradite–pyrope–grossularite (W. E. Ford, *op. cit.*, p. 41). See note Fig. 149.

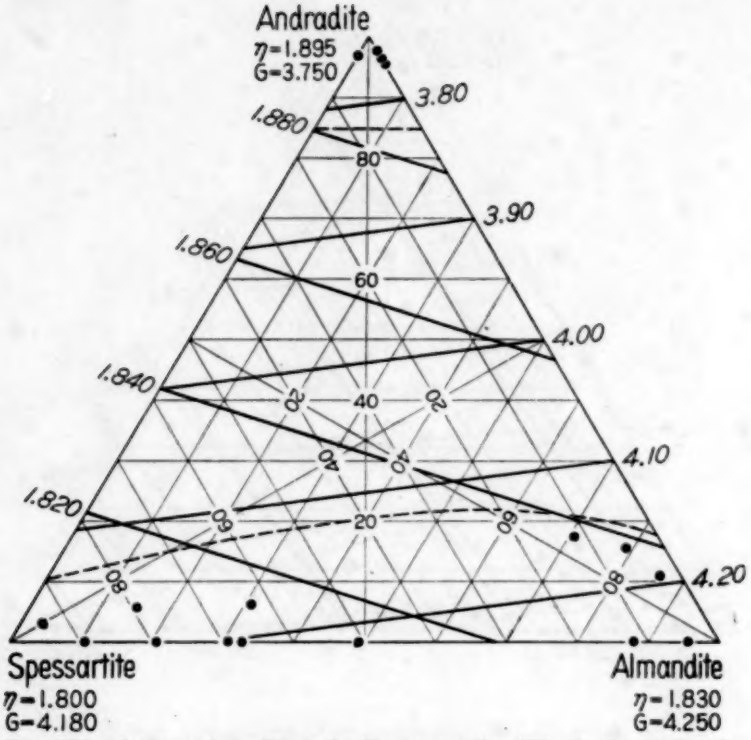

FIG. 156.—System almandite–andradite–spessartite (W. E. Ford, *op. cit.*, p. 43). See note Fig. 149.

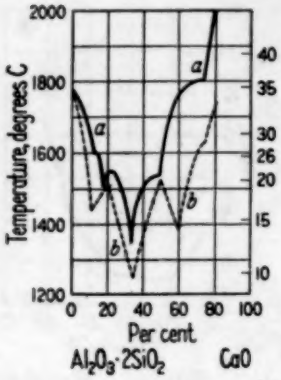

FIG. 157.—Portion of system CaO – $Al_2O_3 \cdot 2SiO_2$. Curve *a* determined by quenching method (G. A. Rankin and F. E. Wright, *Amer. Jour. Sci.*, 4th Ser., **39**, 1–79 (1915); (modified from cut on p. 40)). Curve *b* determined by cone-deformation method (R. Rieke, *Sprechsaal*, No. 37, pp. 1295–97; No. 38, pp. 1313–15 (1906)).

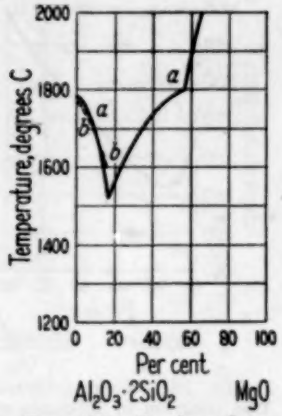

FIG. 158.—Portion of system MgO – $Al_2O_3 \cdot 2SiO_2$. Curve *a* determined by quenching method (G. A. Rankin and H. E. Merwin, *Amer. Jour. Sci.*, 4th Ser., **45**, 301–25 (1918) (p. 322)). Curve *b* is cone-deformation concentration diagram (R. Rieke, *Sprechsaal*, No. 37, pp. 1295–97; No. 38, pp. 1313–15 (1906)).

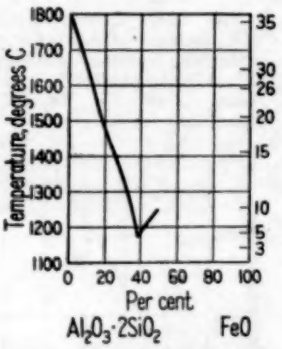

FIG. 159.—Cone-deformation concentration diagram of the system $Al_2O_3 \cdot 2SiO_2$–FeO (R. Rieke, *Sprechsaal*, No. 16, pp. 229–32 (1910)).

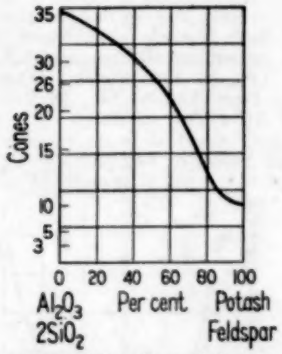

FIG. 160.—Cone-deformation concentration diagram of the system $Al_2O_3 \cdot 2SiO_2$–$K_2O \cdot Al_2O_3 \cdot 6SiO_2$ (adapted from Hewitt Wilson, *Trans. Amer. Ceram. Soc.*, **15**, 217–32 (1913) (p. 229)).

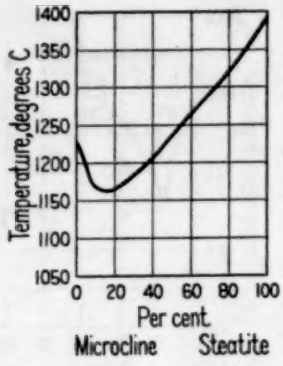

FIG. 161.—Cone-deformation diagram of mixtures of microcline feldspar and steatite (drawn from data by W. L. Howat, *Trans. Amer. Ceram. Soc.*, **18,** 488–91 (1916) (p. 489)).

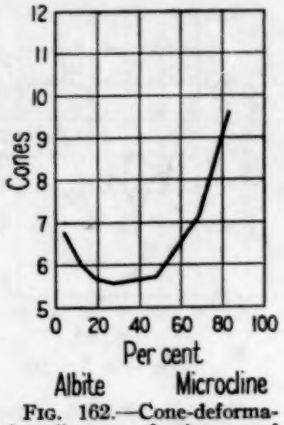

FIG. 162.—Cone-deformation diagram of mixtures of microcline and albite (drawn from data by A. S. Watts, *Trans. Amer. Ceram. Soc.*, **15,** 144–66 (1913) (p. 153)).

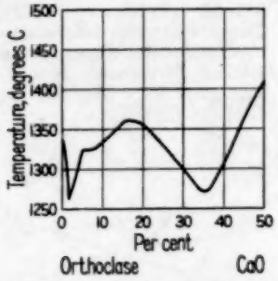

FIG. 163.—Cone-deformation diagram of mixtures of orthoclase feldspar and CaO (F. A. Kirkpatrick, *Trans. Amer. Ceram. Soc.*, **18,** 575–618 (1916) (p. 595)).

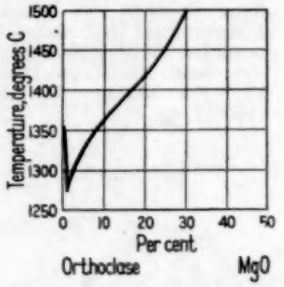

FIG. 164.—Cone-deformation diagram of mixtures of orthoclase feldspar and MgO (F. A. Kirkpatrick, *Trans. Amer. Ceram. Soc.*, **18,** 575–618 (1916) (p. 607)).

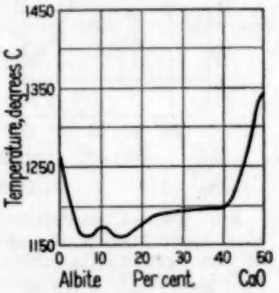

FIG. 165.—Cone-deformation diagram of mixtures of albite feldspar and CaO (F. A. Kirkpatrick, *Trans. Amer. Ceram. Soc.*, **18,** 575–618 (1916) (p. 611)).

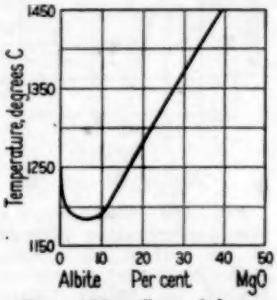

FIG. 166.—Cone-deformation diagam of mixtures of albite feldspar and MgO (F. A. Kirkpatrick, *Trans. Amer. Ceram. Soc.*, **18,** 575–618 (1916) (p. 613)).

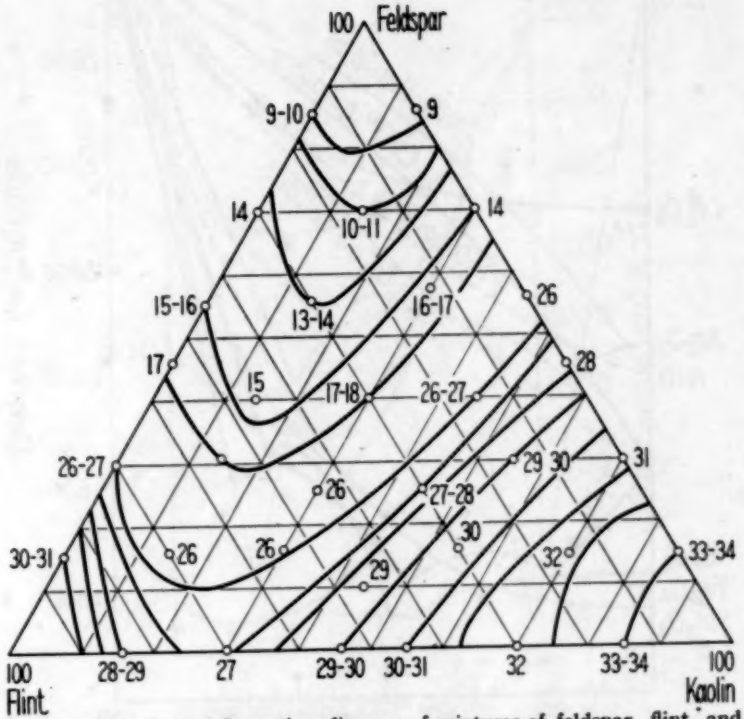

FIG. 167.—Cone-deformation diagram of mixtures of feldspar, flint, and kaolin (Simonis, *Sprechsaal*, No. 40 (1907)). The figures represent the old German pyrometric cones. (Diagram given by Hewitt Wilson, Ceramics—Clay Technology, p. 252.)

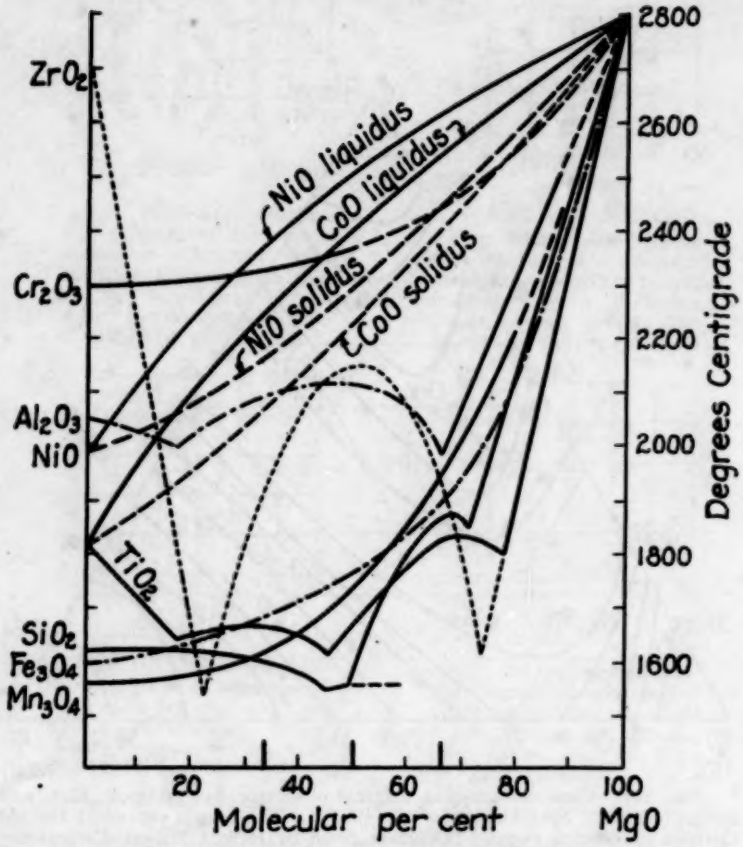

FIG. 168.—Melting curves of MgO with NiO, CoO, Al_2O_3, Cr_2O_3, Fe_3O_4, Mn_3O_4, SiO_2, TiO_2, and ZrO_2 (H. v. Wartenberg and E. Prophet, *Z. anorg. allgem. Chem.*, **208**, 369–79 (1932) (p. 379)).

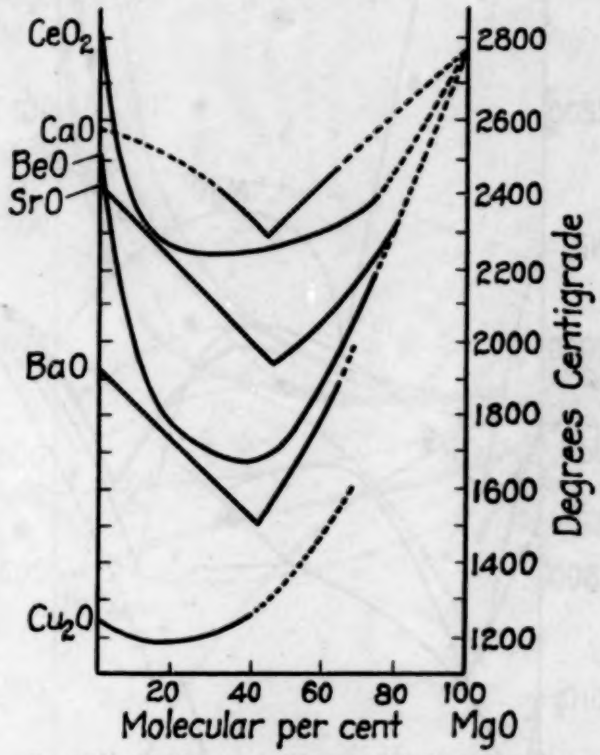

FIG. 169.—Melting curves of MgO with Cu_2O, CaO, BaO, SrO, BeO, and CeO_2 (H. v. Wartenberg and E. Prophet, Part V, *Z. anorg. allgem. Chem.*, **208**, 369–79 (1932) (p. 378)).

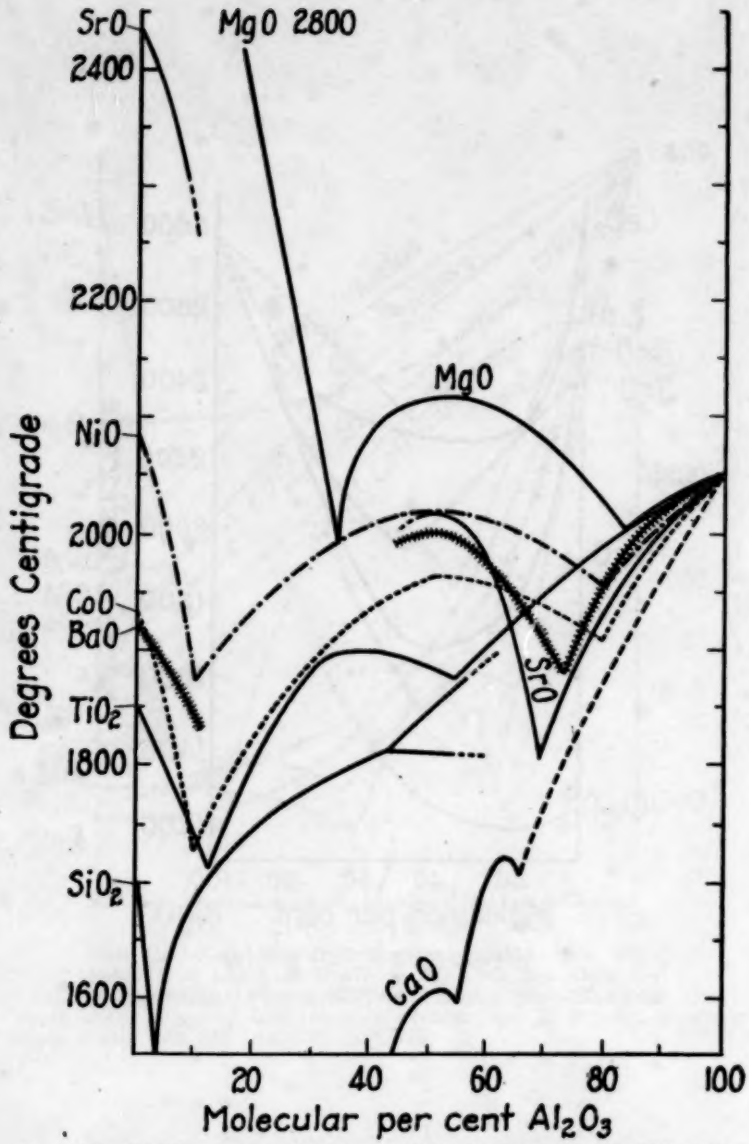

FIG. 170.—Melting curves of Al_2O_3 with CaO, BaO, SrO, MgO, NiO, CoO, TiO_2, and SiO_2 (H. v. Wartenberg and H. J. Reusch, *Z. anorg. allgem. Chem.*, **207**, 1–20 (1932) (p. 18)).

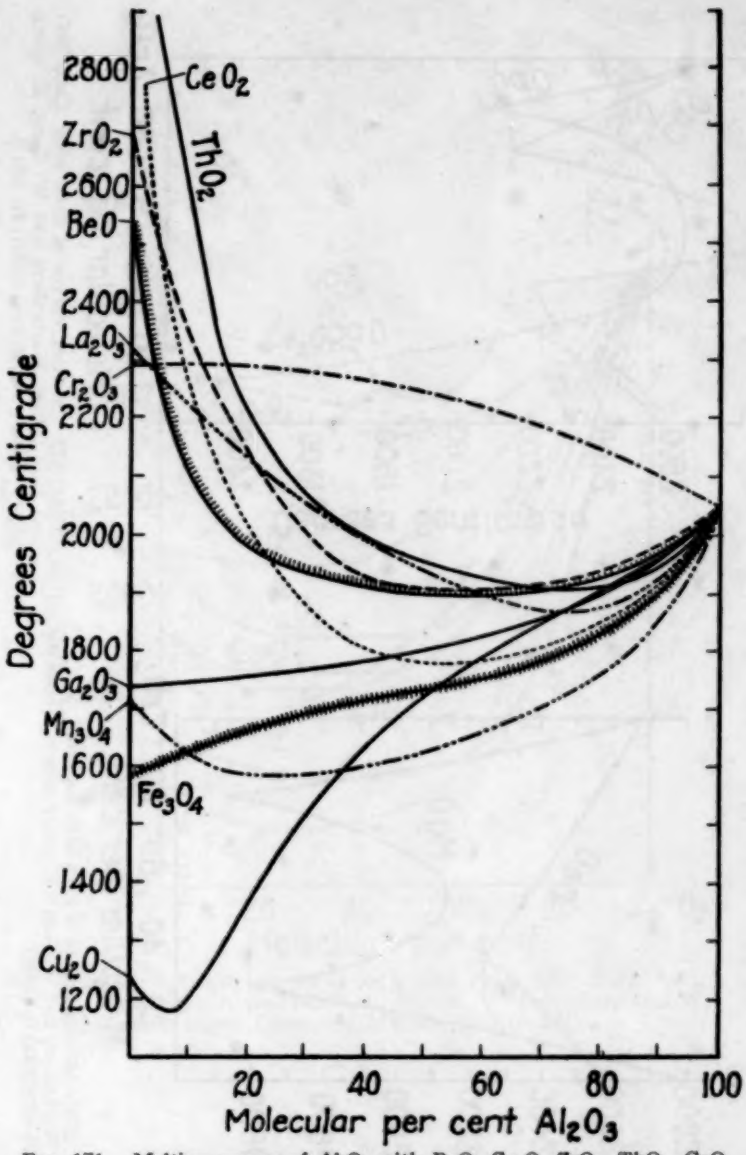

FIG. 171.—Melting curves of Al_2O_3 with BeO, Cu_2O, ZrO_2, ThO_2, CeO_2, La_2O_3, Mn_3O_4, Fe_3O_4, Ga_2O_3, and Cr_2O_3 (H. v. Wartenberg and H. J. Reusch, *Z. anorg. allgem. Chem.*, **207**, 1–20 (1932) (p. 19)).

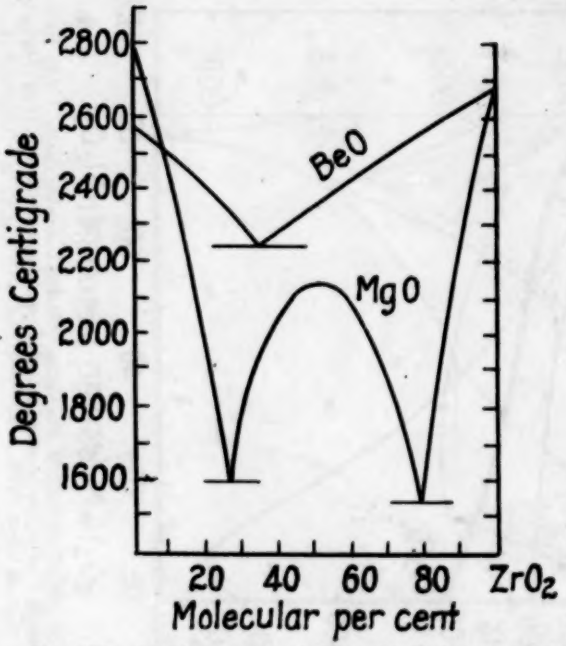

FIG. 173.—Melting curves of ZrO_2 with BeO and MgO (H. v. Wartenberg and W. Gurr), *Z. anorg. allgem. Chem.*, **196**, 374–83 (1931) (p. 381)).

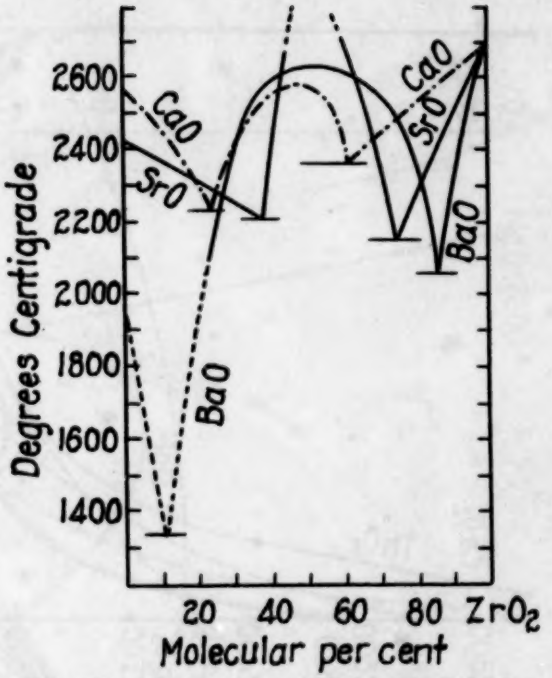

FIG. 172.—Melting curves of ZrO_2 with CaO, SrO, and BaO (H. v. Wartenberg and W. Gurr, *Z. anorg. allgem. Chem.*, **196**, 374–83 (1931) (p. 381)).

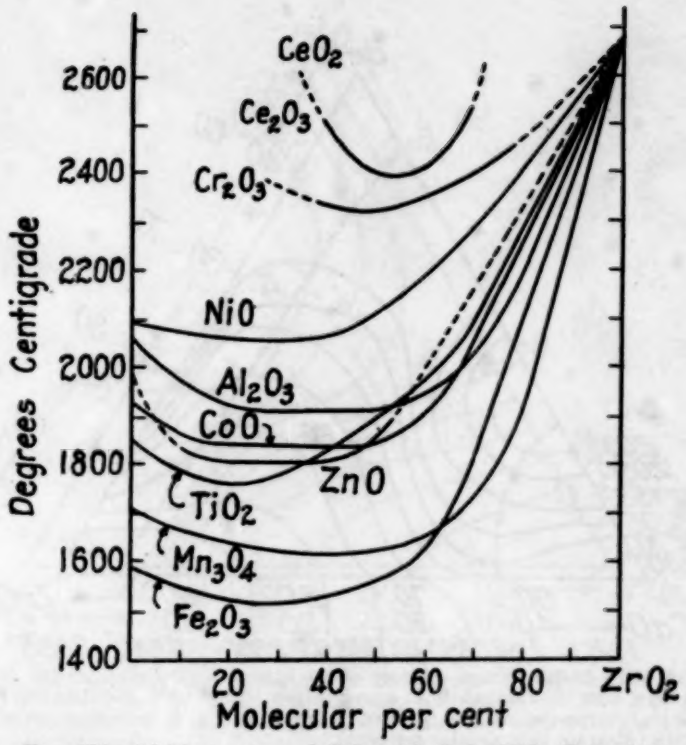

FIG. 174.—Melting curves of ZrO_2 with ZnO, NiO, CoO, Al_2O_3, Cr_2O_3, Fe_2O_3, Mn_3O_4, and (CeO_2, Ce_2O_3) (H. v. Wartenberg and W. Gurr, *Z. anorg. allgem. Chem.*, **196**, 374–83 (1931) (p. 381)).

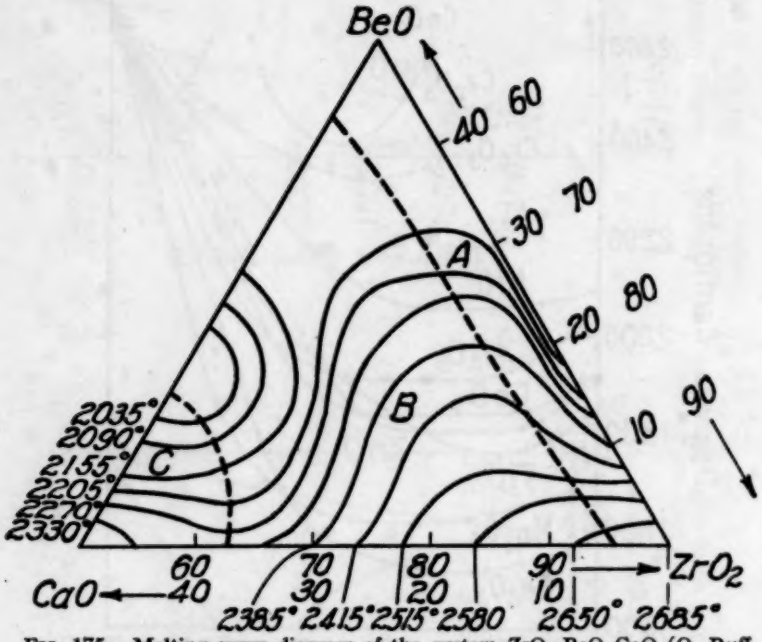

FIG. 175.—Melting curve diagram of the system ZrO_2–BeO–CaO (O. Ruff, F. Ebert, and W. Loerpabel, *Z. anorg. allgem. Chem.*, **207**, 308–12 (1932) (p. 310)). *A* = monoclinic ZrO_2, *B* = cubic mix-crystal, *C* = cubic mix-crystal + $CaZrO_3$ (diagram in molecular per cent).

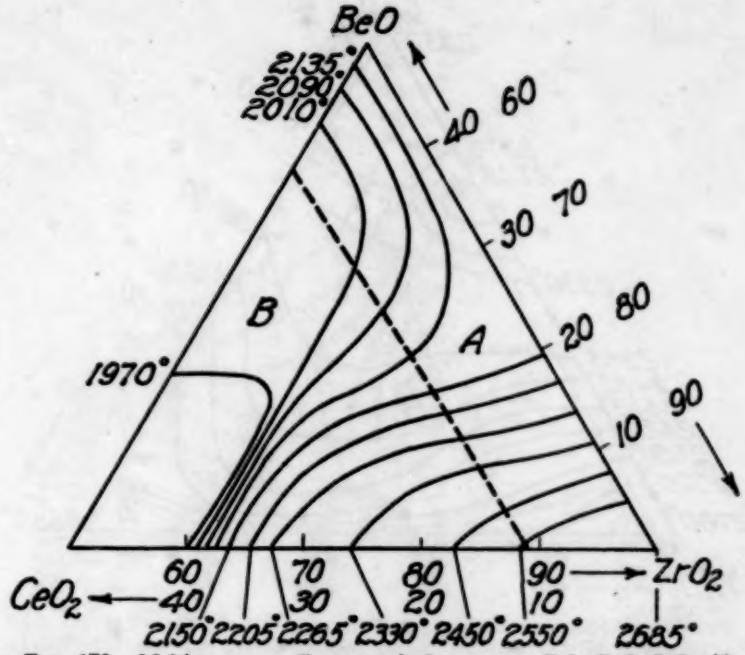

FIG. 176.—Melting curve diagram of the system ZrO_2–BeO–CeO_2 (O. Ruff, F. Ebert, and W. Loerpabel, *Z. anorg. allgem. Chem.*, **207**, 308–12 (1932) (p. 310)). *A* = monoclinic ZrO_2, *B* = cubic mix-crystal (diagram in molecular per cent).

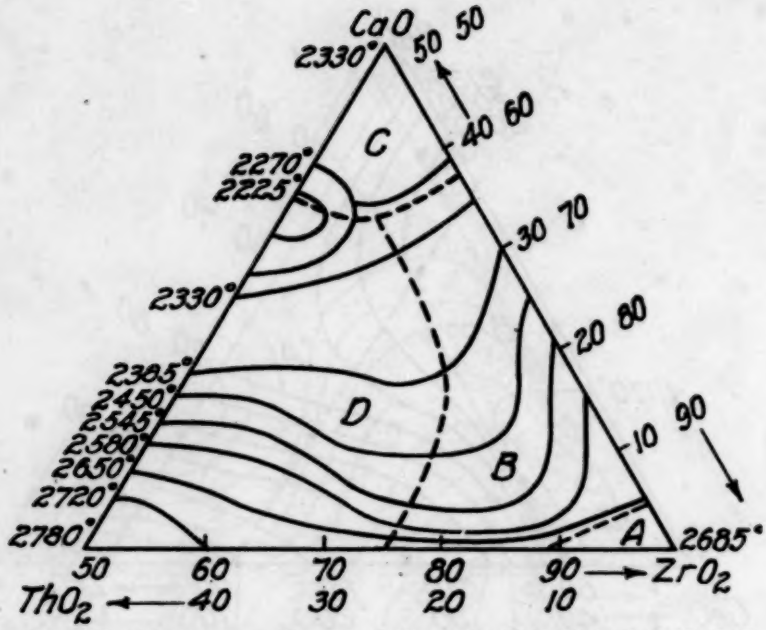

FIG. 177.—Melting curve diagram of the system ZrO_2–ThO_2–CaO (O. Ruff, F. Ebert, and W. Loerpabel, *Z. anorg. allgem. Chem.*, **207**, 308–12 (1932) (p. 309)). *A* = monoclinic ZrO_2, *B* = cubic mix-crystal, *C* = cubic mix-crystal + $CaZrO_3$, *D* = two cubic mix-crystals (miscibility gap) (diagram in molecular per cent).

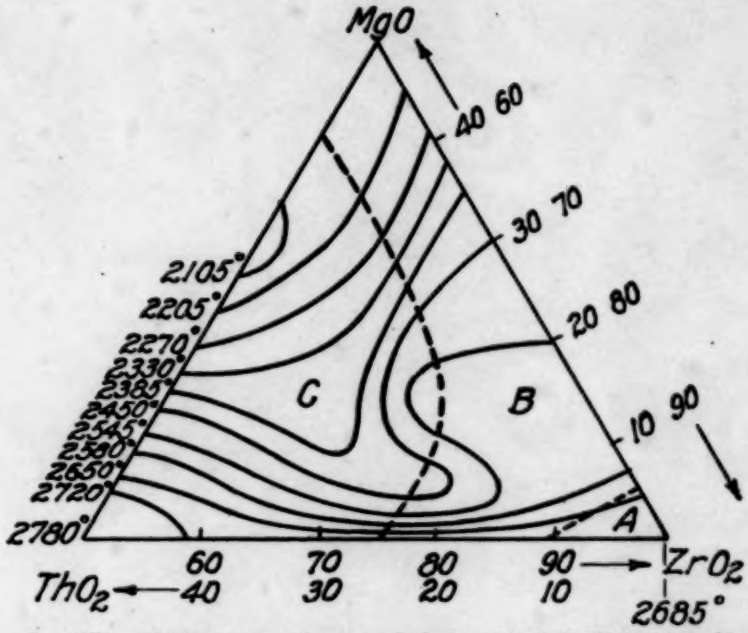

FIG. 178.—Melting curve diagram of the system ZrO_2–ThO_2–MgO (O. Ruff, F. Ebert, and W. Loerpabel, *Z. anorg. allgem. Chem.*, **207**, 308–12 (1932) (p. 309)). *A* = monoclinic ZrO_2, *B* = cubic mix-crystal, *C* = two cubic mix-crystals (diagram in molecular per cent).